UC Riverside

UC Riverside Electronic Theses and Dissertations

Title

Chemical Methods for Detecting Metabolites

Permalink

https://escholarship.org/uc/item/8s4692sf

Author

Guo, Zhili

Publication Date

2021

Peer reviewed|Thesis/dissertation

eScholarship.org Powered by the California Digital Library
University of California

UNIVERSITY OF CALIFORNIA
RIVERSIDE

Chemical Methods for Detecting Metabolites

A Dissertation submitted in partial satisfaction
of the requirements for the degree of

Doctor of Philosophy

in

Chemistry

by

Zhili Guo

June 2021

Dissertation Committee:
Dr. Min Xue, Chairperson
Dr. Ryan R. Julian
Dr. Wenwan Zhong

Copyright by
Zhili Guo
2021

The Dissertation of Zhili Guo is approved:

Committee Chairperson

University of California, Riverside

ACKNOWLEDGEMENT

I would like to thank my advisor, Dr. Min Xue, for his full support in every aspect of my career. He led me through a difficult time and guided me to become a scientist. Also, I would like to show my great appreciation to Dr. Zhonghan Li and Dr. Shiqun Shao for their generous help in the early stage of my graduate school life. Moreover, without the support over the years from my colleagues, I cannot finish my dissertation. In addition, I want to thank my committee members Dr. Ryan Julian, Dr. Wenwan Zhong, Dr. Michael Purring, Dr. Haofei Zhang, and Dr. Jikui Song, for their help with my projects. I also want to thank my collaborators in Dr. Wei Wei's lab at the Institute for Systems Biology (Seattle) for their support.

This dissertation is dedicated to my wife, Yi Huang, who has always supported me in every aspect of life, and my daughter Miyi, who has brought me so much joy when finishing the dissertation.

ABSTRACT OF THE DISSERTATION

Chemical Methods for Detecting Metabolites

by

Zhili Guo

Doctor of Philosophy, Graduate Program in Chemistry
University of California, Riverside, June 2021
Dr. Min Xue, Chairperson

Abnormal metabolism is frequently observed in cancer, where the reprogrammed metabolic activities support cancer cells' malignant processes by altering bioenergetics, enhancing biosynthesis, and maintaining redox balance. Understanding the mechanisms of this metabolic reprogramming calls for novel analytical tools for detecting metabolites. This dissertation presents our efforts in developing chemical methods for detecting metabolites. In the first chapter, we present a chemical approach to profile fatty acid uptake in single cells. We demonstrate a surface-based competition assay using azide-modified analogs to probe the fatty acid influx and surface-immobilized dendrimers with dibenzocyclooctyne (DBCO) groups for detection. By integrating this method onto a microfluidics-based multiplex protein analysis platform, we resolved the relationships between fatty acid influx, oncogenic signaling activities, and cell proliferation in single glioblastoma cells. In the second chapter, we present a

magnetic particle-based high throughput screening protocol to remove resins with strong non-specific binding from a library. This on-resin preclear method can be used to screen metabolites binders from a peptide library. In the third chapter, we showcase the implementation of the library screening approach for identifying cyclic peptide-based probes for several intracellular metabolites.

Table of Contents

Acknowledgment iv

Dedication v

Abstract of the Dissertation vi

Table of Contents viii

List of Figures x

List of Tables xiv

CHAPTER 1 Introduction 1

1.1 Overview of analytical tools for omics studies 1

1.2 Significance of single-cell metabolic studies in cancer 2

1.3 Metabolite surrogates that enable single-cell assays for cellular uptake 3

1.4 Single-cell metabolic assays designed for integration with other single-cell measurements 6

1.5 The scope of this dissertation 11

References 12

CHAPTER 2 Single-cell Profiling of Fatty Acid Uptake Using Surface-Immobilized Dendrimers 15

2.1 Introduction 15

2.2 Materials and Methods 17

2.3 Results and Discussion 26

2.4 Conclusion 49

References 50

CHAPTER 3 A Magnetic Particles-Based Method for Removing Non-Specific Binding Components in On-Bead Screening of Combinatorial Libraries 53

3.1 Introduction 53

3.2 Materials and Methods 56

3.3 Results and Discussion 62

3.4 Conclusion 69

References 70

CHAPTER 4 Screening Metabolites-Binding Peptides from Peptide Libraries 73

4.1 Introduction 73

4.2 Materials and Methods 75

4.3 Results and Discussion 82

4.4 Conclusion 96

4.5 Mass spectroscopy data for hit sequences 97

References 106

List of Figures

Figure 1.1 Metabolite surrogates that enable single-cell assays..... 4

Figure 1.2 Detecting proteins, GSH and cAMP/cGMP on SCBC..... 7

Figure 1.3 Competitive binding assay for profiling glucose uptake 8

Figure 1.4 Competitive binding assay for profiling glutamine uptake..... 9

Figure 1.5 Detection of secreted metabolites..... 10

Figure 2.1 Detecting fatty acid from single cells..... 27

Figure 2.2 UV-Vis spectrum of 10 μM DBCO reacting with 50 μM FA-N_3..... 27

Figure 2.3 The synthesis of DBCO dendrimer conjugated with Cy3-ssDNA..... 29

Figure 2.4 UPLC trace and mass spectrum for the 3rd generation (G-3) dendrimer scaffold..... 30

Figure 2.5 UPLC trace and mass spectrum for the 4th generation (G-4) dendrimer scaffold..... 31

Figure 2.6 FPLC separation of DNA-dendrimer scaffold conjugates 32

Figure 2.7 FPLC separation of DNA-DBCO, G-3 DBCO dendrimer, and G-4 DBCO dendrimer 33

Figure 2.8 The first attempt of conjugating the dendrimer to ssDNA 34

Figure 2.9 The attempt of labeling dendrimer with DBCO 34

Figure 2.10 Another synthetic route to conjugate ssDNA with DBCO dendrimer 35

Figure 2.11 Mass spectrum BHQ2-N_3 (MALDI-TOF) 36

Figure 2.12 Synthesis of BHQ2-N_3 37

Figure 2.13 FA detection scheme 38

Figure 2.14 Detecting FA-N_3 with surface-immobilized DBCO-DNA conjugates 38

Figure 2.15 Surface-based tests 40

Figure 2.16 Cell-based tests 41

Figure 2.17 A picture of the SCBC device 42

Figure 2.18 The operation of the SCBC 43

Figure 2.19 Multiplex single-cell dataset obtained from U87VIII cells 44

Figure 2.20 Agglomerative hierarchical clustering of the single-cell dataset 45

Figure 2.21 PCA analysis loading plots 46

Figure 2.22 The correlation network of the analytes 47

Figure 2.23 Coinhibit P70S6K and FA metabolism 48

Figure 3.1 Colorimetric method to remove non-specific hits 55

Figure 3.2 Fluorescence-activated sorting by the BioSorter®..... 55

Figure 3.3 The proposed method to pull out the non-specific binding resins. 63

Figure 3.4 Results for peptide-biotin incubation..... 63

Figure 3.5 Efforts to pull out positive control TentaGel resins..... 64

Figure 3.6 The proposed method to pull out the non-specific binding resins by antibody-biotin conjugates..... 65

Figure 3.7 Results for antibody incubation..... 66

Figure 3.8 The proposed method to pull out the non-specific binding resins by BSA-biotin conjugates 67

Figure 3.9 Results for BSA-biotin incubation 67

Figure 3.10 Validation of the magnetic particle-based preclear process..... 69

Figure 4.1 The one-bead-two-compounds monocyclic peptide library design ... 83

Figure 4.2 The design of GSH screening target..... 84

Figure 4.3 The screening process of GSH..... 85

Figure 4.4 The linearization of monocyclic peptides 86

Figure 4.5 The results of GSH screening..... 87

Figure 4.6 The design of the bicyclic peptide library. 88

Figure 4.7 Synthesis of the bicyclic peptide library. 89

Figure 4.8 Structures of cAMP, cGMP, cAMP-biotin ,and cGMP-biotin 90

Figure 4.9 The screening procedure for cAMP and cGMP. 91

Figure 4.10 The linearization procedure for the bicyclic peptide libraries. 92

Figure 4.11 Job plot of cAMP and D24 binding..... 95

Figure 4.12 Mass spectrum for D24..... 97

Figure 4.13 Mass spectrum for H13..... 98

Figure 4.14 Mass spectrum for H18..... 99

Figure 4.15 Mass spectrum for H19..... 100

Figure 4.16 Mass spectrum for H7..... 101

Figure 4.17 Mass spectrum for J6. 102

Figure 4.18 Mass spectrum for J11 103

Figure 4.19 Mass spectrum for J23. 104

Figure 4.20 Mass spectrum for K18..... 105

List of Tables

Table 2.1 List of antibodies used in this work. 18

Table 4.1 List of cAMP binding hits 93

Table 4.2 List of cGMP binding hits 94

CHAPTER 1 Introduction

1.1 Overview of analytical tools for omics studies

Omics research is a comprehensive study of a class of molecules, such as DNA, RNA, peptides and proteins, and metabolites.[1] Over the past few decades, technological breakthroughs in omics research have enabled simultaneous analysis of thousands of genes, transcripts, proteins, or metabolites, advancing biology and biomedical science. Moreover, the emerging single-cell analysis technologies have advanced omics research to single-cell resolution.[2]

For the genomic and transcriptomic studies, the dominant analytical tools have been the next-generation sequencing (NGS) platforms. The NGS technology has been implemented at the single-cell level, and large amounts of single cells have been analyzed simultaneously, supported by numerous pieces of literature and several commercially available platforms.[3-8]

As for the proteomic and metabolomic study, the predominant technique has been mass spectrometry. With the development of the target acquisition methods such as selected ion monitoring (SIM), selected reaction monitoring (SRM), and parallel reaction monitoring (PRM), it is possible to target multiple selected peptides with a single data acquisition[9]. With the advance in nanoscale liquid chromatography (LC) and progress in software development, it is possible to quantify the order of 10^2-10^3 proteins at the same time at bulk level.[10, 11] However, mass spectrometry methods have not routinely reached the single-cell level. On the contrary, single-cell quantification of proteins has heavily relied on

immunorecognition, which inherently has limited throughput. Nevertheless, devices that allow parallel quantification of up to 40 proteins in single cells are already commercially available.

For metabolites detection at the bulk level, separation techniques coupled with mass spectrometry, including gas chromatography-mass spectrometry (GC-MS), liquid chromatography-MS (LC-MS) and capillary electrophoresis-MS (CE-MS), nuclear magnetic resonance (NMR), Raman microscopy detect a broad range of metabolites, e.g., lipids, sugars, amino acids, etc.[12] These methods, however, are challenging to implement at the single-cell level. [13-15] In addition, these methods cannot provide access to a multiplex quantitation of different analyte categories.

1.2 Significance of single-cell metabolic studies in cancer

Cancer cells often display altered metabolic activities. In order to proliferate and survive, malignant cells need to meet three basic metabolic demands - bioenergetics, biosynthesis, and redox balance.[16] For example, elevated glucose uptake is widely observed among cancer cells. Consequently, ^{18}F-fluorodeoxyglucose (FDG) positron emission tomography (PET) is a primary clinical tool in cancer diagnosis. Six metabolic hallmarks of cancer have been recently reviewed[17], including deregulated glucose and amino acid consumptions, use of opportunistic modes of nutrient acquisition, and use of glycolysis/ tricarboxylic acid (TCA) cycle intermediates for biosynthesis. However, each cancer cell often presents different metabolic hallmarks or even does not show any

metabolic hallmarks depending on the cellular states and microenvironment. [18] Solving this metabolic heterogeneity calls for single-cell metabolomic profiling.

1.3 Metabolite surrogates that enable single-cell assays for cellular uptake

Antibodies have been widely used in targeted single-cell proteomics. However, they are not suitable for studying single-cell metabolomics, as metabolites typically do not generate an immune response. However, a few metabolite-specific antibodies do exist. An example is the glutathione antibody.[19] Antibodies which capture cyclic adenosine monophosphate (cAMP) and cyclic guanosine monophosphate (cGMP) are also available. Nevertheless, in general, antibodies are not suitable for profiling metabolites, let alone in single cells. Thus, the current strategies for investigating metabolites mainly rely on metabolite surrogates, which directly compete with native metabolites and provide readout.

Glucose is a major energy source of cells as well as an essential carbon source for biosynthesis. Therefore, its cellular uptake behavior is most widely studied. Owing to its connection to diabetes, the analytical methods for detecting blood glucose levels are well developed. However, despite great success in blood glucose detection, it is hard to apply these methods to single-cell analysis due to lack of sensitivity. In addition, the influx (uptake), rather than the concentration, is more critical in single-cell analysis. Therefore, molecular surrogates are more useful here.

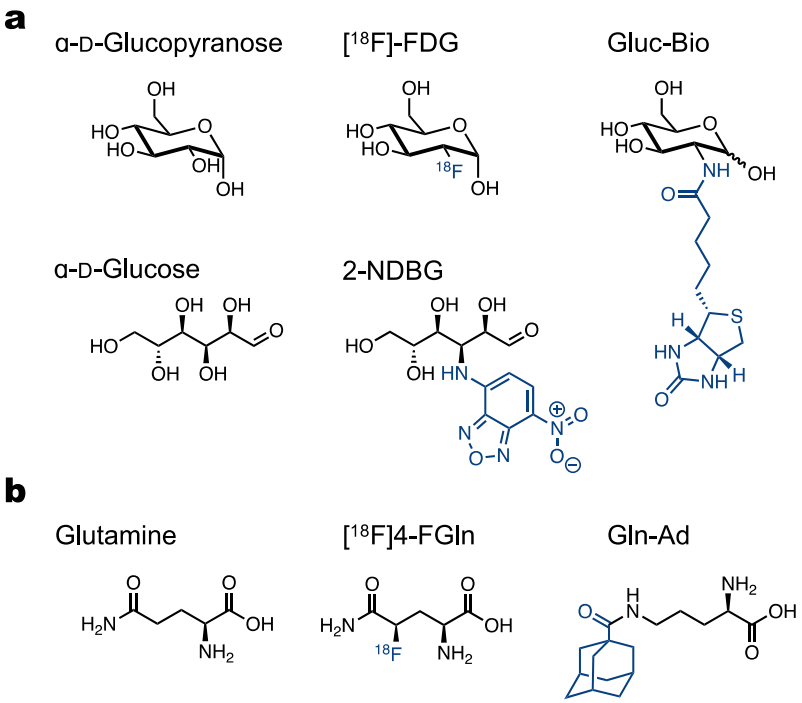

Figure 1.1 Metabolite surrogates that enable single-cell assays for cellular uptake.

Figure 1a lists the glucose structure, together with a popular fluorescent D-glucose analog, 2-[*N*-(7-nitrobenz-2-oxa-1,3-diazol-4-yl)amino]-2-deoxy-D-glucose (2-NBDG)[20] and two surrogates of the cyclic hexamer, ^{18}F-FDG, and a biotin-labeled glucose[21]. To faithfully preserve metabolite bioactivities, the surrogates have to be carefully designed and validated. 2-NBDG is such a representative compound that has been validated by several different assays.[22] In mammalian cells, glucose is transported into cells mainly through glucose transporter 2 (GLUT2) in an active transport manner. Therefore, the uptake of glucose is temperature-dependent, and 2-NBDG uptake was found influenced by temperature. Moreover, manipulation of the GLUT2 affects the 2-NBDG transport efficiency as well. Engineered cells that overexpress and repress GLUT2 show

different 2-NBDG uptake rates, similar to glucose. In addition, by blocking the transporter GLUT2, the 2-NBDG uptake activity can be inhibited as well.

Like 2-NBDG, the biotinylated glucose surrogate (Gluc-Bio) is another suitable probe to investigate glucose uptake.[21] Gluc-Bio can be uptaken in the cells through the glucose transporter. Moreover, the Gluc-Bio uptake efficiency negatively correlated with native glucose concentration. Furthermore, the transportation of Gluc-Bio can be affected by temperature as well, consistent with an active transportation process. Finally, Gluc-Bio is proven to be a substrate for hexokinase, making it suitable for evaluating the influx.

Like glucose, amino acids also play critical roles in cellular energy production. Amino acids can directly enter the TCA cycle and relieve cells from metabolic stress[23]. Among the 20 canonical amino acids, glutamine is the most abundant in blood and serves as the primary nitrogen source for biosynthesis. As it plays such an essential role in cellular metabolism, it has been a target for in vivo PET imaging[24, 25] and single-cell analysis[26]. Figure 1.1b presents well-established glutamine surrogates: an ^{18}F-labeled glutamine analog ([^{18}F]4-FGln) PET probe and an adamantane-labeled glutamine surrogate (Gln-Ad) [26]. Gln-Ad is a glutamine surrogate screened out from a glutamine analog library, which competes for cellular uptake with glutamine, and whose uptake process responds to temperature change. The Gln-Ad can be used to access the glutamine uptake behavior via a supermolecule interaction with cyclodextrin. Moreover, the Gln-Ad

uptake was proven to go through the SLC1A5 sodium-dependent neutral amino acid transporter, the major pathway for the glutamine uptake process.

1.4 Single-cell metabolic assays designed for integration with other single-cell measurements

Developing multi-omics single-cell assays could reveal complex biologic activities, such as signaling network activities. However, such a task is extremely challenging because assays for different classes of molecules are often not compatible with each other. The recent development of the single-cell barcode chip (SCBC) platform provided a solution to this problem and has demonstrated its applications in the simultaneous analysis of proteins and metabolites. In the SCBC platform, an addressable immunofluorescence microarray was employed for targeted proteome analysis, and orthogonal chemical methods have been developed for metabolic assays. It is worth emphasizing that these chemical approaches targeting each metabolite can be integrated into the SCBC platform in the same manner as assays targeting proteins.

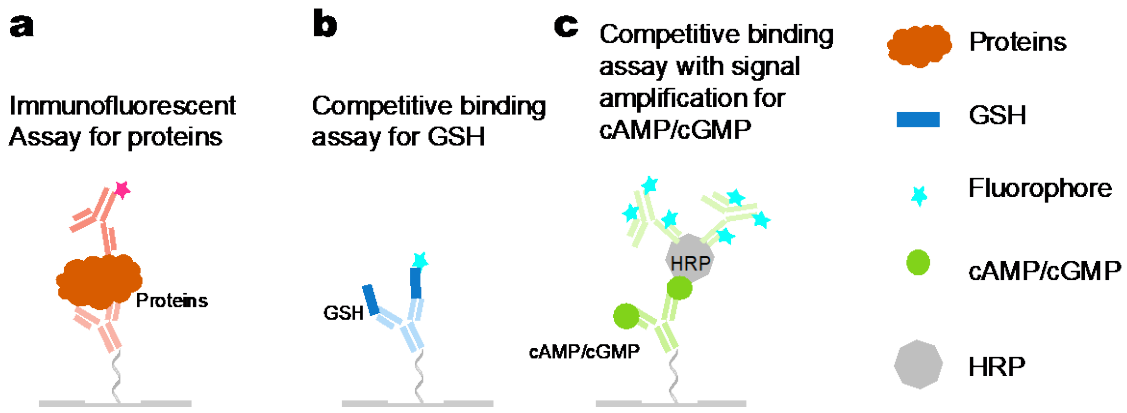

Figure 1.2 Detecting proteins, GSH and cAMP/cGMP on SCBC.

As shown in Figure 1.2a, antibodies are immobilized on the SCBC, and proteins can be analyzed by immunofluorescence assays. Since antibodies against glutathione (GSH), cyclic adenosine monophosphate (cAMP), and cyclic guanosine monophosphate (cGMP) are available, competitive-binding assays can be readily developed. For example, GSH competes with Alexa647-tagged GSH for the binding sites on anti-GSH antibodies and therefore generating a concentration-dependent readout (Figure 1.2b). As for cAMP and cGMP quantification, a signal amplification method was developed because of the low abundance of the second messengers. Specifically, the native cAMP/cGMP competes with the horseradish peroxidase(HRP)-labeled cAMP/cGMP, and the signal was generated through polyclonal anti-HRP antibodies labeled with multiple Alexa Fluor 647 groups (Figure 1.2c).

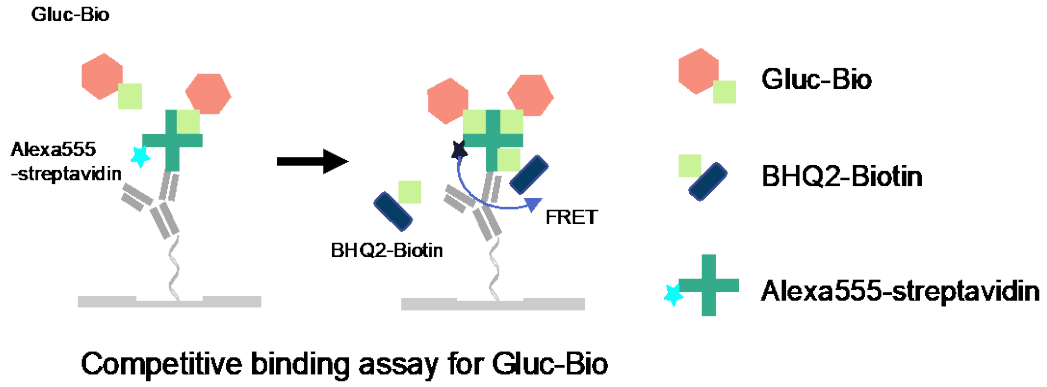

Figure 1.3 Competitive binding assay for profiling glucose uptake

As mentioned before, the Gluc-Bio probe was proven to be a suitable surrogate. To quantify glucose uptake, Gluc-Bio was incubated with cells, allowing uptake. Later, the excess probes were thoroughly washed away. Upon cell lysis, the Gluc-Bio was released to the surface and captured by the surface-immobilized fluorescent-labeled streptavidin. Subsequentially, a known concentration of biotinylated BHQ2 was introduced to the surface and bond to the unoccupied streptavidin sites. BHQ2 is an effective quencher, and it quenches fluorescent signals from streptavidin through the Föster resonance energy transfer (FRET) mechanism. Therefore, the glucose uptake activities are negatively correlated with the amount of biotinylated BHQ2 attached to the fluorescent-labeled streptavidin and positively correlated with the fluorescent signal from streptavidin (Figure 1.3). The dynamic range of this assay can be adjusted by the concentration of streptavidin as well as the Gluc-Bio incubation duration. This assay achieves a low nanomolar sensitivity. As a result, there is no need to remove the glucose in the cell media, which minimizes the unnecessary perturbation to the cells.

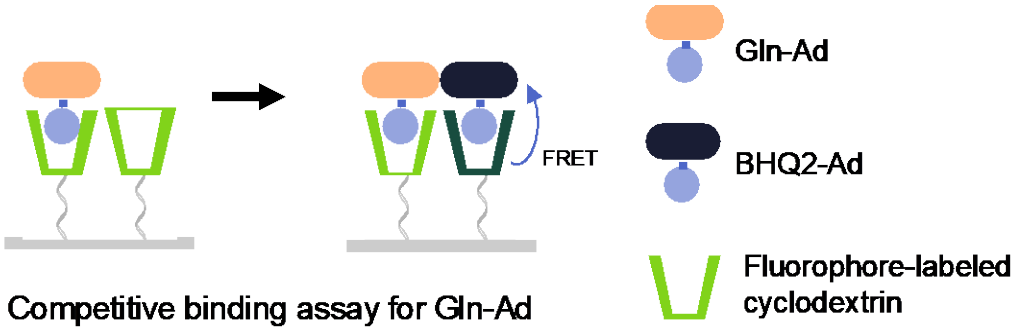

Figure 1.4 Competitive binding assay for profiling glutamine uptake

Similarly, the detection of glutamine uptake was based on Gln-Ad, as described in section 1.3. A competitive binding scheme can be developed on the SCBC utilizing cyclodextrin (Figure 1.4), a well-known host for adamantane. However, the binding affinity between adamantane and β-cyclodextrin is far weaker than that of streptavidin-biotin. As a result, it is necessary to increase the local concentration of the surface-immobilized cyclodextrin. Based on high-density DNA patterning, cyclodextrin was immobilized on the surface at a high density suitable for capturing Gln-Ad from single cells. Similar to glucose uptake assay, upon cell lysis, the Gln-Ad was released and captured onto the surface by a Cy3-labeled cyclodextrin. A positively correlated concentration-dependent curve can be generated when competing with a known concentration of quencher, BHQ2-adamantane.

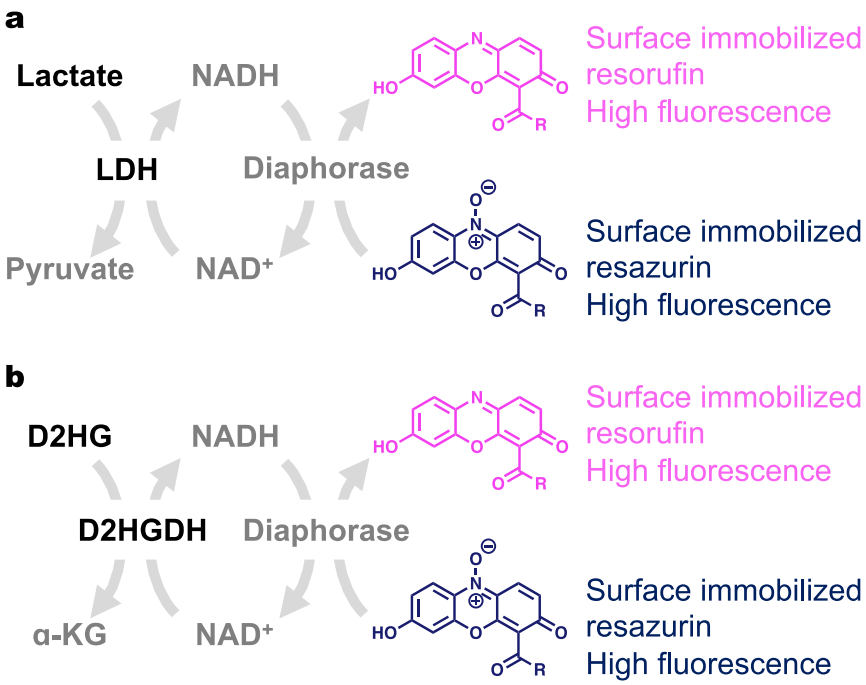

Figure 1.5 Detection of secreted metabolites based on coupled enzyme reactions.

A chemical method detecting lactate at the single-cell level was reported by our group[27] (Figure 1.5a). Unlike glucose and glutamine, lactate is a secreted molecule instead of an influx metabolite. As a result, we cannot apply a similar competitive binding strategy to lactate detection. Instead, we utilized coupled enzyme reactions and fluorescent substrates. Specifically, we immobilized resazurin to a barcoded surface via single-stranded DNA molecules. In the presence of excess lactate dehydrogenase and NAD^+, the lactate quantity was translated to fluorescence readouts. Moreover, we adapted this strategy to detect other redox-active metabolites like D-2-Hydroxyglutarate (D2HG) with different sets of enzymes (Figure 1.5b)[28].

1.5 The scope of this dissertation

The main focus of this dissertation is to expand the analytical toolbox for targeted metabolites detection. Specifically, I aim to complete the repertoire of single-cell analysis of major energy source molecules (Chapter 2).

Despite its success, utilizing specific chemical reactions to detect metabolites will hit the multiplexing limits easily. For example, the detecting methods for lactate and D2HG share a similar strategy and cannot be implemented simultaneously. Therefore, carrying out massively parallel targeted metabolites detection calls for a more generic detection scheme. In Chapter 3 and chapter 4, I tested the feasibility of screening peptide binders to capture metabolites from a peptide library. Presumably, the metabolite-binding peptides would allow the development of orthogonal assays for different metabolites and lead the way towards a true single-cell metabolic analysis.

References

1. Akiyama, M., Multi-omics study for interpretation of genome-wide association study. *Journal of Human Genetics* **2021,** *66* (1), 3-10.

2. Heath, J. R.; Ribas, A.; Mischel, P. S., Single-cell analysis tools for drug discovery and development. *Nat Rev Drug Discov* **2016,** *15* (3), 204-216.

3. Chen, K. H.; Boettiger, A. N.; Moffitt, J. R.; Wang, S.; Zhuang, X., Spatially resolved, highly multiplexed RNA profiling in single cells. *Science* **2015,** *348* (6233).

4. Islam, S.; U., K.; Moliner, A.; Zajac, P.; Fan, J.-B.; Lonnerberg, P.; Linnarsson, S., Characterization of the single-cell transcriptional landscape by highly multiples RNA-seq. *Genome Res* **2011,** *21*, 1160-1167.

5. Macosko, Evan Z.; Basu, A.; Satija, R.; Nemesh, J.; Shekhar, K.; Goldman, M.; Tirosh, I.; Bialas, Allison R.; Kamitaki, N.; Martersteck, Emily M.; Trombetta, John J.; Weitz, David A.; Sanes, Joshua R.; Shalek, Alex K.; Regev, A.; McCarroll, Steven A., Highly Parallel Genome-wide Expression Profiling of Individual Cells Using Nanoliter Droplets. *Cell* **2015,** *161* (5), 1202-1214.

6. Picelli, S.; Faridani, O. R.; Björklund, Å. K.; Winberg, G.; Sagasser, S.; Sandberg, R., Full-length RNA-seq from single cells using Smart-seq2. *Nat. Protocols* **2014,** *9* (1), 171-181.

7. Tang, F.; Barbacioru, C.; Wang, Y.; Nordman, E.; Lee, C.; Xu, N.; Wang, X.; Bodeau, J.; Tuch, B. B.; Siddiqui, A.; Lao, K.; Surani, M. A., mRNA-Seq whole-transcriptome analysis of a single cell. *Nat Meth* **2009,** *6* (5), 377-382.

8. Wu, A. R.; Neff, N. F.; Kalisky, T.; Dalerba, P.; Treutlein, B.; Rothenberg, M. E.; Mburu, F. M.; Mantalas, G. L.; Sim, S.; Clarke, M. F.; Quake, S. R., Quantitative assessment of single-cell RNA-sequencing methods. *Nat Meth* **2014,** *11* (1), 41-46.

9. Borràs, E.; Sabidó, E., What is targeted proteomics? A concise revision of targeted acquisition and targeted data analysis in mass spectrometry. *PROTEOMICS* **2017,** *17* (17-18), 1700180.

10. Nikolov, M.; Schmidt, C.; Urlaub, H., Quantitative mass spectrometry-based proteomics: an overview. *Quantitative methods in proteomics* **2012**, 85-100.

11. Percy, A. J.; Yang, J.; Chambers, A. G.; Borchers, C. H., Increased Depth and Breadth of Plasma Protein Quantitation via Two-Dimensional Liquid Chromatography/Multiple Reaction Monitoring-Mass Spectrometry with Labeled Peptide Standards. In *Quantitative Proteomics by Mass Spectrometry*, Sechi, S., Ed. Springer New York: New York, NY, 2016; pp 1-21.

12. Wishart, D. S., Emerging applications of metabolomics in drug discovery and precision medicine. *Nature Reviews Drug Discovery* **2016,** *15*, 473.

13. Ibáñez, A. J.; Fagerer, S. R.; Schmidt, A. M.; Urban, P. L.; Jefimovs, K.; Geiger, P.; Dechant, R.; Heinemann, M.; Zenobi, R., Mass spectrometry-based metabolomics of single yeast cells. *Proceedings of the National Academy of Sciences* **2013,** *110* (22), 8790-8794.

14. Fessenden, M., Metabolomics: Small molecules, single cells. *Nature* **2016,** *540*, 153.

15. Comi, T. J.; Do, T. D.; Rubakhin, S. S.; Sweedler, J. V., Categorizing Cells on the Basis of their Chemical Profiles: Progress in Single-Cell Mass Spectrometry. *Journal of the American Chemical Society* **2017,** *139* (11), 3920-3929.

16. DeBerardinis, R. J.; Chandel, N. S., Fundamentals of cancer metabolism. *Science advances* **2016,** *2* (5), e1600200.

17. Pavlova, N. N.; Thompson, C. B., The Emerging Hallmarks of Cancer Metabolism. *Cell Metab* **2016,** *23* (1), 27-47.

18. Fouad, Y. A.; Aanei, C., Revisiting the hallmarks of cancer. *American journal of cancer research* **2017,** *7* (5), 1016.

19. Blokhina, O.; Virolainen, E.; Fagerstedt, K. V., Antioxidants, Oxidative Damage and Oxygen Deprivation Stress: a Review. *Annals of Botany* **2003,** *91* (2), 179-194.

20. Yamada, K.; Saito, M.; Matsuoka, H.; Inagaki, N., A real-time method of imaging glucose uptake in single, living mammalian cells. *Nature Protocols* **2007,** *2*, 753.

21. Xue, M.; Wei, W.; Su, Y.; Kim, J.; Shin, Y. S.; Mai, W. X.; Nathanson, D. A.; Heath, J. R., Chemical Methods for the Simultaneous Quantitation of

Metabolites and Proteins from Single Cells. *Journal of the American Chemical Society* **2015,** *137* (12), 4066-4069.

22. Yamada, K.; Nakata, M.; Horimoto, N.; Saito, M.; Matsuoka, H.; Inagaki, N., Measurement of Glucose Uptake and Intracellular Calcium Concentration in Single, Living Pancreatic β-Cells. *Journal of Biological Chemistry* **2000,** *275* (29), 22278-22283.

23. Yang, C.; Ko, B.; Hensley, Christopher T.; Jiang, L.; Wasti, Ajla T.; Kim, J.; Sudderth, J.; Calvaruso, Maria A.; Lumata, L.; Mitsche, M.; Rutter, J.; Merritt, Matthew E.; DeBerardinis, Ralph J., Glutamine Oxidation Maintains the TCA Cycle and Cell Survival during Impaired Mitochondrial Pyruvate Transport. *Molecular Cell 56* (3), 414-424.

24. Qu, W.; Zha, Z.; Ploessl, K.; Lieberman, B. P.; Zhu, L.; Wise, D. R.; B. Thompson, C.; Kung, H. F., Synthesis of Optically Pure 4-Fluoro-Glutamines as Potential Metabolic Imaging Agents for Tumors. *Journal of the American Chemical Society* **2011,** *133* (4), 1122-1133.

25. Lieberman, B. P.; Ploessl, K.; Wang, L.; Qu, W.; Zha, Z.; Wise, D. R.; Chodosh, L. A.; Belka, G.; Thompson, C. B.; Kung, H. F., PET Imaging of Glutaminolysis in Tumors by 18F-(2S,4R)4-Fluoroglutamine. *Journal of Nuclear Medicine* **2011,** *52* (12), 1947-1955.

26. Xue, M.; Wei, W.; Su, Y.; Johnson, D.; Heath, J. R., Supramolecular Probes for Assessing Glutamine Uptake Enable Semi-Quantitative Metabolic Models in Single Cells. *J Am Chem Soc* **2016,** *138* (9), 3085-93.

27. Li, Z.; Cheng, H.; Shao, S.; Lu, X.; Mo, L.; Tsang, J.; Zeng, P.; Guo, Z.; Wang, S.; Nathanson, D. A.; Heath, J. R.; Wei, W.; Xue, M., Surface Immobilization of Redox-Labile Fluorescent Probes: Enabling Single-Cell Co-Profiling of Aerobic Glycolysis and Oncogenic Protein Signaling Activities. *Angewandte Chemie International Edition* **2018,** *57* (36), 11554-11558.

28. Cheng, H.; Li, Z.; Guo, Z.; Shao, S.; Mo, L.; Wei, W.; Xue, M., Single-cell profiling of D-2-hydroxyglutarate using surface-immobilized resazurin analogs. *Biosensors and Bioelectronics* **2021,** *190*, 113368.

CHAPTER 2 Single-cell Profiling of Fatty Acid Uptake Using Surface-Immobilized Dendrimers

2.1 Introduction

Similar to glucose and amino acids, fatty acids are a major energy source required for sustaining cellular growth and proliferation.[1] Abnormal fatty acid metabolism is frequently observed in cancer, but its regulatory mechanisms and therapeutic implications are unclear. Compared with the well-studied glucose and amino acid metabolic patterns in cancer cells[2, 3], altered fatty acid metabolism received less attention, and current research primarily focuses on the *de novo* fatty acid synthesis pathway[4]. However, increasing evidence demonstrates that cancer cells' survival and metastatic spreading often require exogenous fatty acid uptake and consumption, even in cells exhibiting high lipogenic activities[5-10]. In addition, fatty acid metabolism in tumor cells exhibits significant plasticity - even the same set of cells can alter their fatty acid dependence in response to drug or environmental stress.[9, 11] These studies highlight the relevance and complexity of fatty acid metabolism in cancer and necessitate more comprehensive research.

The study of cancer cell metabolism can be confounded by prominent cellular heterogeneity. The causes of this heterogeneity include genetic diversity, signaling and metabolic pathway redundancy, and local microenvironment variations. Such heterogeneity enables metabolic flexibility and promotes tumor progression. On the other hand, these metabolic abnormalities also render tumor

cells more vulnerable to metabolic perturbations, which may be exploited therapeutically[9, 12, 13]. Therefore, deciphering cancer cell metabolism, especially in the context of oncogenic signaling heterogeneity, promises the rational design of combinatory therapies for synergistic intervention. Such a task calls for a multiplex single-cell analytical assay that can simultaneously profile metabolic activity and protein levels.

To address this need, we have previously implemented the single-cell barcode chip (SCBC) technology to perform simultaneous analysis of glycolysis, glutamine metabolism, and oncogenic signaling activities at single-cell resolution.[14-16] Nevertheless, a single-cell method to study fatty acid influx on the SCBC platform remains elusive. The technological challenge is the lack of an appropriate fatty acid surrogate that can faithfully report the fatty acid influx while being easy to detect at low concentrations. Fluorescence-labeled fatty acid analogs, such as the BODIPY-fatty acids,[17] are widely used and straightforward to detect. However, they may not faithfully resemble the natural fatty acids in complex biological systems. Isotope-labeled fatty acid surrogates, such as ^{18}F-fluoro-pivalic acid, can perfectly mimic natural fatty acids[18], but their single-cell implementation is challenging. Herein, we choose azide-modified fatty acids (FA-N_3) as surrogates and demonstrate a surface-based chemical method for detecting fatty acid uptake. The azide group is chemically inert, and its small size promises a better mimicry to natural fatty acids. We further adapt this method to the SCBC platform to achieve

the multiplex analysis of fatty acid uptake with critical signaling proteins from the same single cancer cells.

2.2 Materials and Methods

Materials:

Rink amide MBHA resin (loading capacity 0.68 mmol/g) was purchased from Aapptec (Louisville, KY). All the Fmoc-protected amino acids were purchased from Anaspec (Fremont, CA) except Fmoc-l-Lys (Fmoc)-OH and Fmoc-Lys(N_3)-OH (Azido-lysine), which were purchased from Chem-Impex (Wood Dale, IL). BHQ2 carboxyl acid and Fmoc-PEG5-OH were purchased from Biosearch Technologies (Petaluma, CA) and BroadPharm (San Diego, CA), respectively. S-HyNic and S-4FB were purchased from TriLink BioTechnologies (San Diego, CA). The coupling reagent 2-(1H-benzotriazol-1-yl)-1,1,3,3-tetramethyluronium hexafluorophosphate (HBTU, 99.6%) was obtained from Chem-Impex (Wood Dale, IL). Diisopropylethylamine (DIEA, 99.5%) was purchased from ACROS (Germany). Triisopropylsilane (TIPS) was obtained from TCI (Portland, OR). Piperidine was purchased from Alfa Aesar (Ward Hill, MA). α-cyano-4-hydroxycinnamic acid (CHCA) was obtained from Sigma-Aldrich (St. Louis, MO). Tris base, sodium phosphate dibasic anhydrous (Na_2HPO_4, 99.6%), sodium phosphate monobasic monohydrate (NaH_2PO_4, 99.4%), sodium chloride (NaCl), ascorbic acid, Tween 20, sodium dodecyl sulfate (SDS), bovine serum albumin (BSA), acetonitrile (CH_3CN), diethyl ether (Et_2O), ethyl acetate (EA), N,N'-dimethylformamide (DMF), and dichloromethane (DCM) were purchased from

Thermo Fisher Scientific (Waltham, MA). DNA-Cy3-NH_2 (5'- /5AmMC6/AAA AAA AAA AAA /iCy3/TGC TCG GGA AGG CTA CTC -3') was ordered from Integrated DNA Technologies, Inc. (Coralville, IA). DBCO-C6-Sulfo-NHS was purchased from Click Chemistry Tools (Scottsdale, AZ).

Table 2.1 List of antibodies used in this work.

Capture antibody name	Manufacture
Phospho-p70 S6 Kinase (T389) DuoSet	R&D Systems, DYC896
Human EGFR Antibody, Goat Polyclonal	R&D Systems, AF231
Human/Mouse/Rat Phospho-ERK1 (T202/Y204) DuoSet	R&D Systems, DYC1825
Human NDRG1, Goat Polyclonal	R&D Systems, AF5209
Human Phospho-Src (Y419) DuoSet	R&D Systems, DYC2685
Human/Mouse 4EBP1 antibody, Goat Polyclonal	R&D Systems, AF3227
Human/Mouse Phospho-Akt1 (S473) DuoSet	R&D Systems, DYC2289C
Human Ki-67/MKI67, Sheep Polyclonal	R&D Systems, AF7617

Detection antibody name	Manufacture
Phospho-p70 S6 Kinase (T389) DuoSet	R&D Systems, DYC896
Phospho-EGF Receptor (Tyr1173) Antibody, Rabbit Monoclonal	Cell Signaling, 4407S
Human/Mouse/Rat Phospho-ERK1 (T202/Y204) DuoSet	R&D Systems, DYC1825
Phospho-NDRG1 (Thr346) Antibody, Rabbit Monoclonal	Cell Signaling, 7497S
Human Phospho-Src (Y419) DuoSet	R&D Systems, DYC2685
Phospho-4E-BP1 (Thr37/46) Antibody, Rabbit Monoclonal	Cell Signaling, 5132S
Human/Mouse Phospho-Akt1 (S473) DuoSet	R&D Systems, DYC2289C
Ki-67 Antibody, Rabbit Monoclonal	Cell Signaling, 12075S

Experiments:

Solid-phase peptide synthesis. Peptides were synthesized on Rink Amide MBHA resin via the standard Fmoc solid-phase peptide synthesis (SPPS) chemistry. For Fmoc deprotection, the resin was agitated with piperidine (20% v/v in DMF, 3x5 min) and washed with DMF 5 times. To couple amino acids to the resin, a DMF solution of Fmoc-AA(protection group)-OH (5 eq.), HBTU (4.75 eq.), and DIEA (15 eq.) was mixed for 3 minutes, and then the mixture was added to the resin and agitated at room temperature for 1 hour. For peptide side-chain global deprotection and cleavage, the resin was washed with DCM and dried with compressed airflow. The beads were then cleaved in a TFA cleavage solution (TFA: TIPS: ddH_2O; 95: 2.5: 2.5) for 2 hours. All peptides were purified on the RP-HPLC (DIONEX Ultimate 3000; Thermo Scientific, Germany) using a C18 reversed-phase preparative column (Kinetex. 5 μm EVO, 250 Å~ 21.2 mm) or a C18 reversed-phase semi-preparative column (Kinetex. 5 μm EVO, 250 Å~ 10 mm). The product was validated using MALDI-TOF MS (AB SCIEX TOF/TOF 5800, Framingham, MA) and lyophilized for long-term storage at -20 ºC.

Synthesis of azide-attached poly-lysine dendrimers. The azide-attached poly-lysine dendrimer scaffolds were synthesized on rink amide MBHA resin following standard SPPS protocols. The synthetic scheme is shown in Figure 2a. Fmoc-l-Lys(N_3)-OH and Fmoc-PEG5-OH were attached to the resin first, followed by 3 or 4 rounds of Fmoc-l-Lys(Fmoc)-OH coupling. Before the cleavage, the Fmoc protecting groups were removed by piperidine. After the cleavage and

purification, the dendrimer scaffolds were characterized by MALDI-TOF MS and lyophilized for storage.

Conjugation of DBCO to ssDNA-Cy3-NH_2. 50 µL of ssDNA-Cy3-DBCO solution (250 µM, in 1× PBS, pH 7.4) was mixed with 10 µL of DBCO-Sulfo-NHS solution (12.5 µL, 10 mM in 1× PBS) for 4 hours. After incubation, the mixture was purified by an SEC column on FPLC to remove unreacted small molecules. ssDNA-Cy3-DBCO was collected. The concentration of ssDNA-Cy3-DBCO was determined by UV-Vis absorbance at 550 nm.

Conjugation of the poly-lysine dendrimers (1 and 2) to ssDNA. 50 µL of ssDNA-Cy3-DBCO solution (200 µM, in 1× PBS, pH 7.4) was mixed with 10 µL of poly-lysine dendrimer scaffold (10 mM, in 1× PBS, pH 7.4) at 37 ºC for 6 hours. After incubation, the mixture was purified by an SEC column on FPLC to remove unreacted small dendrimer scaffolds. The ssDNA-dendrimer scaffold conjugates were collected. The concentrations of the conjugates were determined by their UV-Vis absorbance at 550 nm.

Labeling the ssDNA-dendrimer conjugates (3 and 4) with DBCO. 50 µL of ssDNA-dendrimer scaffold conjugates (100 µM in 1× PBS) was mixed with 20 µL of DBCO-Sulfo-NHS ester solution (10 mM for 3^{rd} generation**,** 20 mM for 4^{th} generation, in 5× PBS, pH 7.4). The mixture was incubated at room temperature overnight. The final products were purified by an SEC column on FPLC, and stored at 4 ºC. The concentrations of the DBCO dendrimers and the number of DBCO on

each dendrimer were determined by UV-Vis absorbance at 550 nm and 310 nm, respectfully.

Immobilization of the dendrimer on a glass surface. A 16-well (50 µL each) PDMS slab was placed onto a microscope glass slide patterned with ssDNA strands that are complementary to the oligonucleotide sequence on DBCO dendrimers**.** Each well was blocked with 50 µL of 1% BSA in 1× PBST at room temperature for 1 hour. Afterward, the blocking solution was removed, and 45 µL of dendrimer (100 nM in 1% BSA, 1× PBST) was added to each well. After 1 hour of incubation at room temperature, each well was washed with 1× PBST three times. At this point, the dendrimer was immobilized on the device and ready to use.

Generation of the FA-N_3 response curve via a surface-based competition assay. The 3rd or 4th generation dendrimer was immobilized on the glass slide surface (described above). To generate a working curve of FA-N_3, 45 µL of FA-N_3 (various concentrations in 1× PBST) was added to each well. The slide was incubated at 37 ºC for 2 hours, allowing FA-N_3 to react with the DBCO groups on the dendrimer. The FA-N_3 solution was then removed, and each well was washed with 1× PBST three times. 45 µL of BHQ2-N_3 solution (25 µM in 1× PBST) was added to each well, and the slide/PDMS device was incubated at 37 ºC for 1 hour, allowing BHQ2-N_3 to react with unoccupied DBCO sites. After removing the BHQ2-N_3 solution, and the device was washed with 1× PBST three times. The PDMS slab was then removed, and the slide was washed with 1× PBS, 50% 1× PBS/water, and water. The slide was then air-dried, and the fluorescence

intensities were obtained using a Genepix microarray scanner. Experiments were run in quadruplets to get the error bar.

BHQ2-N_3 optimization on the surface platform. The 3rd generation dendrimer was first immobilized on the glass slide as described above. To scan for an optimal BHQ2-N_3 concentration, 45 μL of FA-N_3 (100 μM in 1× PBST) was added to each well. The device was left at 37 ºC for 2 hours. The FA-N_3 solution was taken out, and each well was washed with 1× PBST three times. 45 μL of BHQ2-N_3 (various concentrations in 1× PBST) was then added to each well, and the device was kept at 37 ºC for 1 hour, allowing BHQ2-N_3 to react with unoccupied DBCO sites. Afterward, the solution was removed, and the device was washed with 1× PBST three times. After the 16-well PDMS slab was removed from the device, the glass chip was washed with 1× PBS, 50% 1×PBS/water, and water. The chip was air-dried, and the fluorescence intensities were obtained using a Genepix microarray scanner. Experiments were run in quadruplets to obtain the error bar.

Cell culture. U87vIII cell line was provided as a gift by Prof. Paul Mischel (UCSD, San Diego, U.S.A.). Cells were cultured in Dulbecco's Modified Eagle Media with high glucose, pyruvate (DMEM, Thermo), heat-inactivated fetal bovine serum (FBS), 100 U/mL of penicillin-streptomycin, and 250ng/mL Amphotericin B (Thermo) in a humidified 5% CO_2 (v/v) incubator at 37 ◦C.

FA-N_3 tolerance experiment. A 96-well plate was seeded with U87 cells (10k/well), and the cells were allowed to grow overnight. Then the FA-N_3 solution

was added (100 μL per well, various concentrations) to the cells and incubated for 24 hours. After the incubation, the cell media was removed, and a resazurin solution (10 μg/mL, in cell media) was added to the plate and incubated for 2 hours. The fluorescence was read by a plate reader (Biotek, 540 nm excitation/ 590 nm emission).

FA-N_3 uptake experiment at the bulk level. The U87 cells were collected via centrifugation at 500 g for 5 min. The media was removed, and the cells were resuspended in FBS-free DMEM, resulting in a 4 M cells/mL suspension. 250 μL of the cell suspension was dispensed into Eppendorf tubes and mixed with 250 μL of the FA-N_3 solution (various concentrations, in FBS free DMEM). After 30 min incubation in the cell incubator, the cells were centrifuged at 500 g for 5 min, and the resulting pellet was washed 3 times to remove any excess FA-N_3. Then, 100 μL cell lysis buffer was added to each tube and kept on ice for 15 min. The tubes were then sonicated and vortexed for 5 min. Finally, the tubes were centrifuged at maximum speed for 10 min. The supernatant was collected and subjected to surface-based FA-N_3 detection.

Single-cell suspension preparation. To harvest the cells, the culture media was gently aspirated without disturbing the cells. The cells were then washed with PBS and further treated with 0.05% trypsin for 5 min at 37 °C, followed by the addition of an equal volume of culture media to terminate the trypsinization process. The collected cells were then pelleted via centrifugation at 500 g for 5

min. After discarding the supernatant, the cells were then disassociated as single cells and ready for tests.

For SCBC measurements, the as-prepared single cells were resuspended in warm FBS-free media supplemented with 10 mM FA-N_3 at 2 M cells/mL. After being incubated at 37°C for 30 min and washed with FBS-free media 3 times, the collected cell pellet was resuspended in serum-free, biotin-free media. The concentration of the as-prepared single-cell suspension was 2 M cells/mL.

Single-cell metabolic/proteomic measurements. The single-cell barcode chips (SCBC) were fabricated according to well-established procedures.[14] DNA-encoded antibody library (DEAL) was grafted onto the surface through DNA hybridization to enable capture antibody arrays. The FA surface probe was also incorporated into the surface barcode through the same procedure. The devices were operated following previously established protocols.

Statistical analysis. The single-cell data was obtained as a matrix, where each row represented a single cell, and each column was the intensity of one analyte. Statistical analysis of this dataset was performed in OriginPro 2019b® software. The dataset was first standardized on each column to obtain the Z score of each value. The Euclidean distance values between data points were calculated and tabulated as a matrix. This distance matrix was then used as the input for agglomerative hierarchical clustering using Ward's method. To perform principal component analysis, the standardized single-cell dataset was used as input. The

correlation coefficient was directly calculated from the data set by Spearman's rank method. Analyte-analyte correlation networks were generated by running the calculation through all the analyte pairs in the panel, and only those significant correlations (with Bonferroni correction) were shown in the networks. The network was presented as a Circos plot.[19]

Drug synergy measurements. To ensure optimal cell attachment, 100 µL of 10 µg/mL laminin was added into each well of a 96-well plate, and the plate was incubated at 4°C overnight. Afterward, the plate was washed with PBS three times. 100 µL of U87vIII cell suspension at 50k/mL was then added into each well, and the plate was incubated at 37 °C overnight. On the second day, the media was changed to 200 µL of fresh media containing various concentrations of trimetazidine and LY2584702. The cells were cultured for another 48 hrs. Subsequently, 20 µL of 0.2 mg/mL resazurin PBS solution was added to each well, followed by incubation at 37 °C for 3 hrs. The resulting fluorescent signals were recorded by a plate reader (560 nm excitation / 590 nm emission).

The synergy scores of the two drugs were calculated by using the following equation:

$$S_{A,B} = I_{A,B} - (I_A + I_B - I_A \times I_B)$$

where $S_{A,B}$ is the synergy effect between drugs A and B, $I_{A,B}$ is the cell-killing efficiency by using the combination of drug A and B, while I_A and I_B are the cell-killing efficiencies from independent doses of drug A or B, respectively.

2.3 Results and Discussion

Our fatty acid uptake analysis design is shown in Figure 2.1. Cells take up the FA-N_3 and then release them upon lysis. The released analogs can then be quantified through a surface-based competitive binding assay. A straightforward method for detecting these azide-bearing analogs is to use the azide-alkyne click chemistry. Because we aimed to multiplex the fatty acid uptake analysis with protein profiling, we cannot use Cu to catalyze the click reaction due to its incompatibility with our immunofluorescence-based SCBC platform. Consequently, we must resort to Cu-free click chemistry, i.e., strain-promoted azide-alkyne cycloaddition (SPAAC). However, azide-based SPAAC chemistry is limited by its low reaction rate. Even with the best reactant – dibenzocyclooctyne (DBCO), the rate constant is only 0.31 M^{-1} S^{-1}.[20] Such a reaction rate is not suitable for detecting the low amount of fatty acids in single cells. For instance, 50 μM azide-fatty acid and 10 μM DBCO-COOH lead to negligible changes after 3 hours of incubation (Figure 2.2).

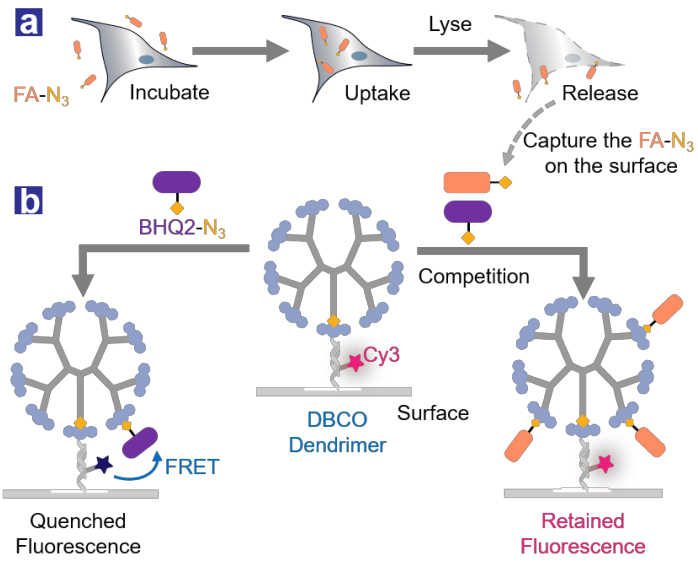

Figure 2.1 Detecting fatty acid from single cells. (a) Cells take up the azide-modified fatty acid (FA-N_3) molecules and subsequently release them upon lysis. (b) Cy3-modified dibenzocyclooctyne (DBCO) dendrimers capture the released FA-N_3 molecules. The FA-N_3 competes with the BHQ2-N_3 quencher and rescues the Cy3 fluorescence.

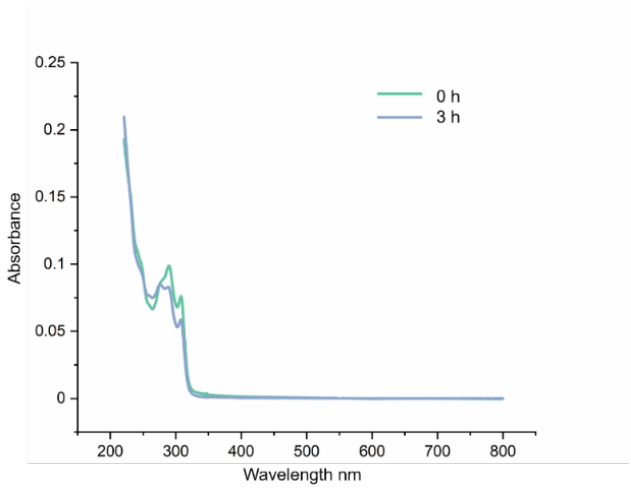

Figure 2.2 UV-Vis spectrum of 10 μM DBCO reacting with 50 μM FA-N_3. After 3 hours, no significant absorbance decrease at 310 nm was observed.

In order to improve the SPAAC reaction rate, we proposed to increase the local DBCO concentration. We hypothesized that a dendritic structure terminated with densely packed DBCO groups could effectively capture the azide-modified fatty acids (Figure 2.1 b). Nevertheless, this prominent hydrophobicity also makes it challenging to implement this detection in an aqueous detection environment.

To overcome the hydrophobicity problem, we proposed to conjugate the dendrimer to a single-strand DNA oligomer (ssDNA). This conjugation also helps to make the SPAAC-based detection compatible with the SCBC platform. We first synthesized G-3 and G-4 DBCO dendrimers using lysine as building blocks and appended azido-lysine polyethylene glycol [Lys(N_3)-PEG] linkers. We then conjugated the dendrimers to ssDNA through a SPAAC reaction. Lastly, we installed DBCO groups on the dendrimer and obtained the dendrimer-DNA conjugate (Figure 2.3 – Figure 2.6). The numbers of DBCO on each dendrimer structure are calculated by the ratio of 310 nm/550 nm on the FPLC traces, 8.25 DBCO on G-3 DBCO dendrimer, and 17.0 DBCO on G-4 DBCO dendrimer (Figure 2.7), which are close to the theory value 8 and 16.

It is worth pointing out that it was critical not to introduce DBCO groups until the very last step, or the strong hydrophobicity of DBCO groups would prevent further conjugation to DNA (Figure 2.8 – Figure 2.10).

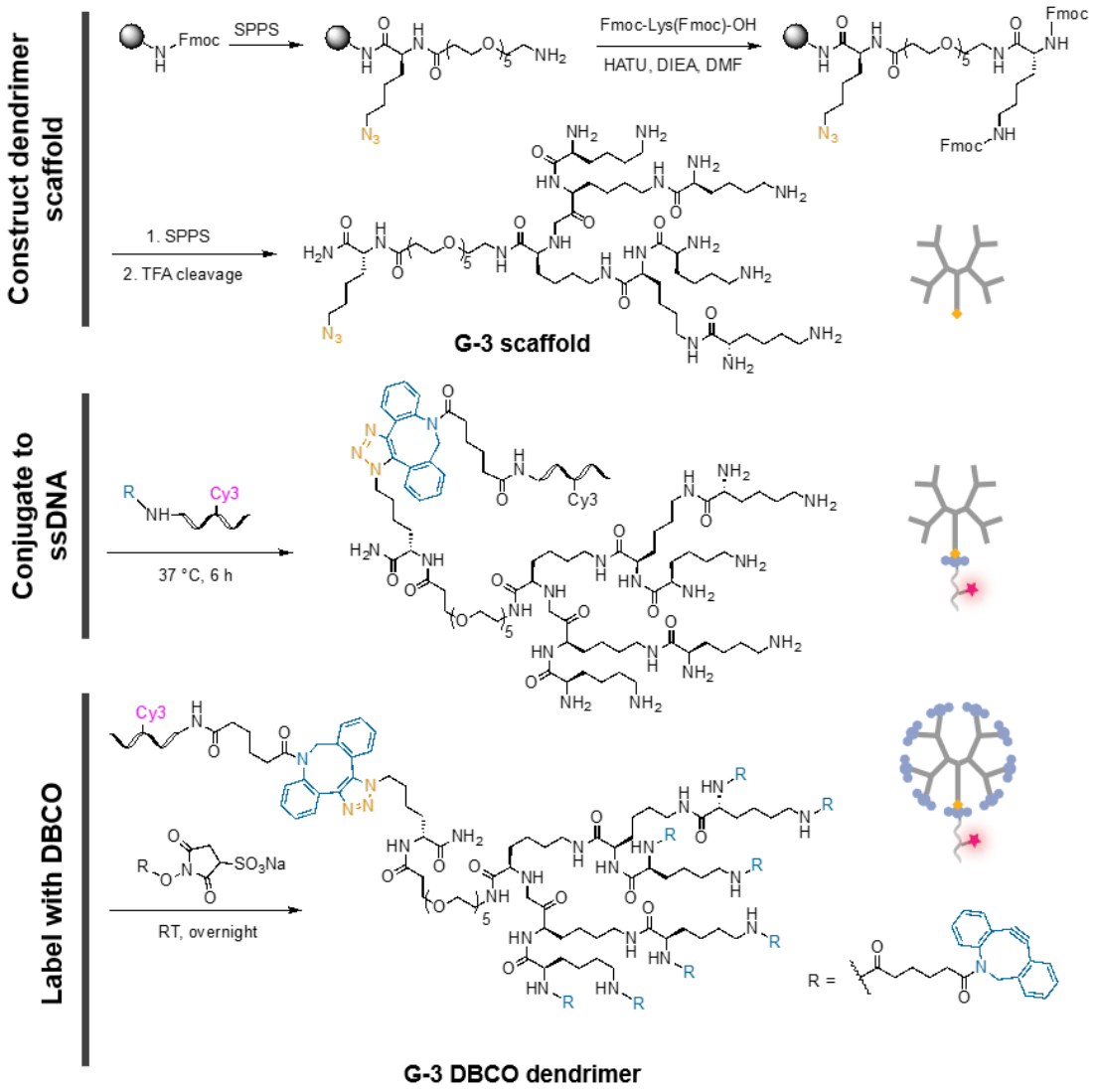

Figure 2.3 The synthesis of DBCO dendrimer conjugated with Cy3-ssDNA. The dendritic scaffold was constructed and cleaved off from the resin. It was later conjugated with ssDNA via SPAAC. Finally, all of the primary amines on the dendrimer scaffold were terminated by DBCO-sulfo-NHS ester. G-4 DBCO dendrimer was prepared in a similar manner with an additional round of lysine conjugation.

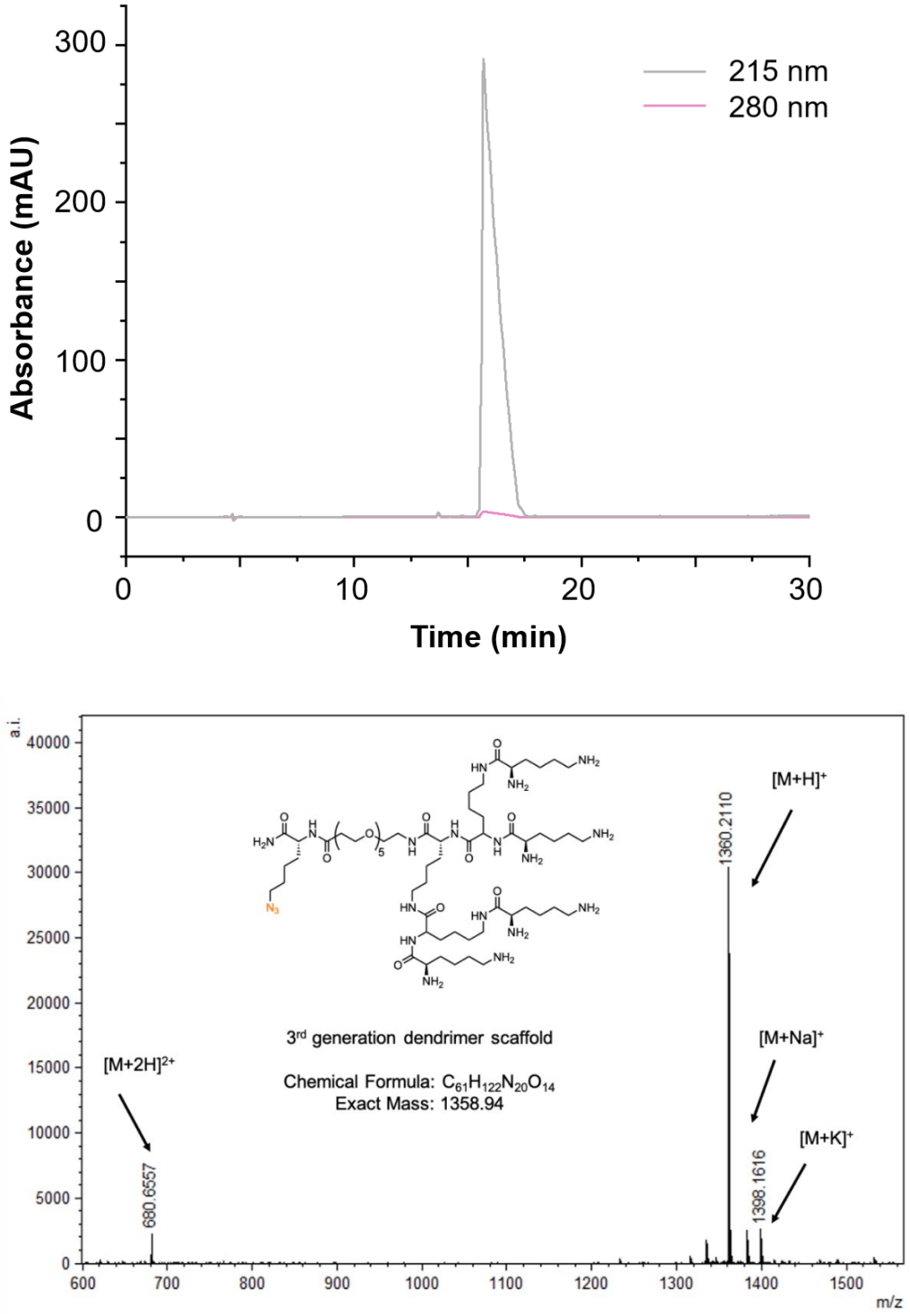

Figure 2.4 UPLC trace and mass spectrum for the 3rd generation (G-3) dendrimer scaffold (MALDI-TOF). $[M+H]^+$ calculated: 1359.94, found 1360.21.

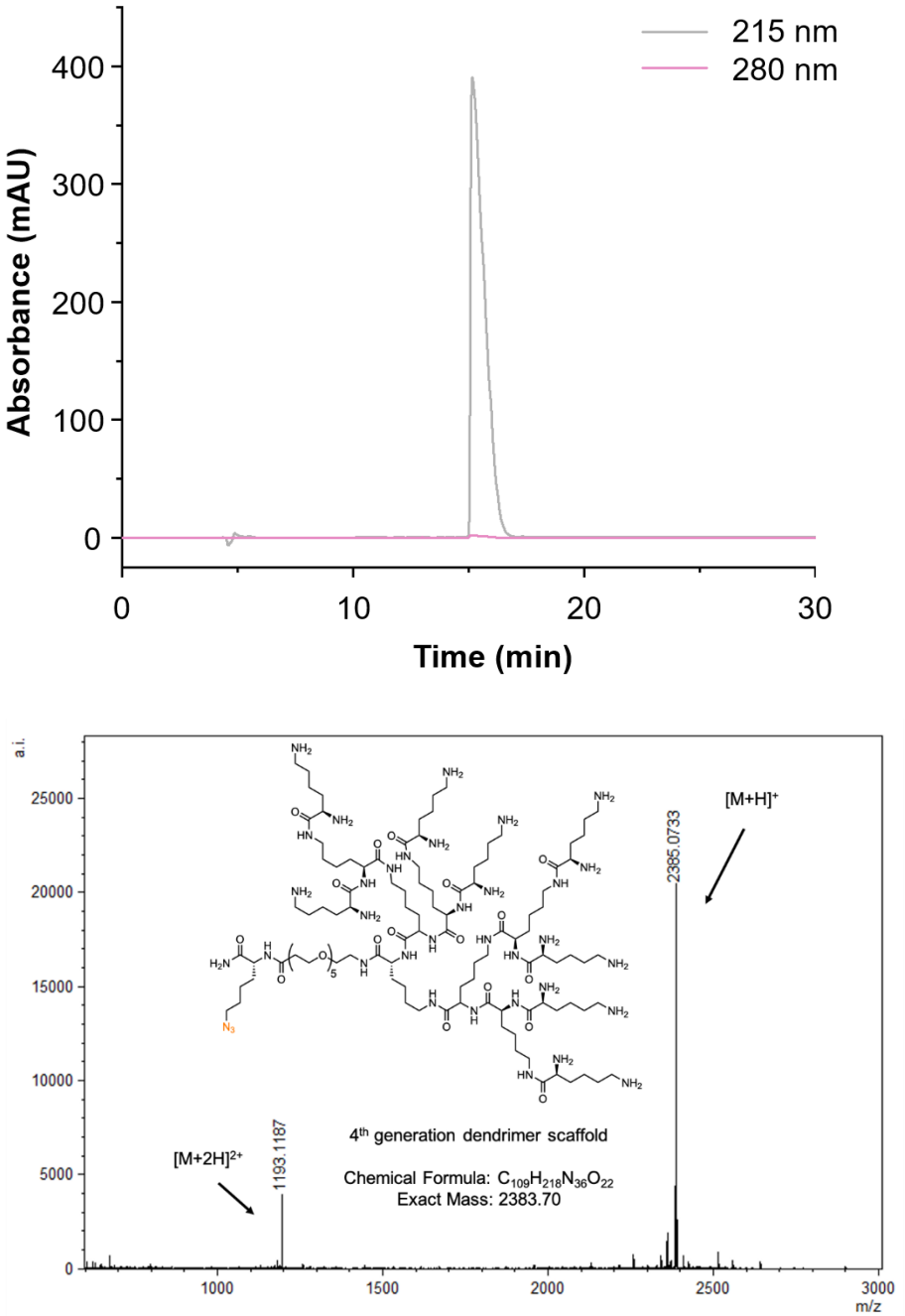

Figure 2.5 UPLC trace and mass spectrum for the 4th generation (G-4) dendrimer scaffold (MALDI-TOF). $[M+H]^+$ calculated: 2384.70, found 2385.07.

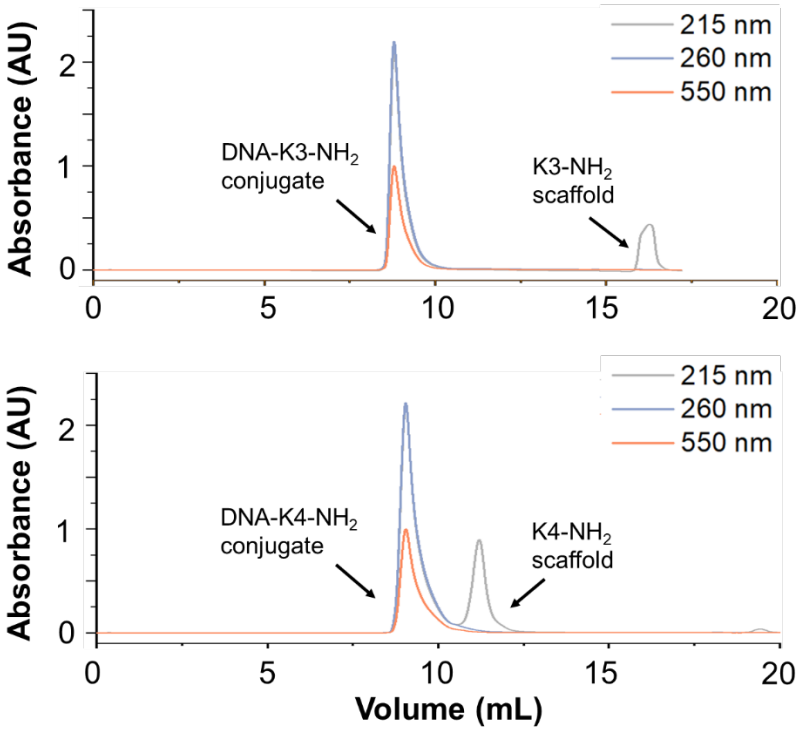

Figure 2.6 FPLC separation of DNA-dendrimer scaffold conjugates. After SPAAC conjugation of dendrimer scaffold and DNA-DBCO, the resulting solution was separated through Size Exclusion Chromatography (SEC). The eluting condition is 3x PBS with 450 mM of NaCl. It is essential to maintain relatively high ionic strength, or aggregation will be formed.

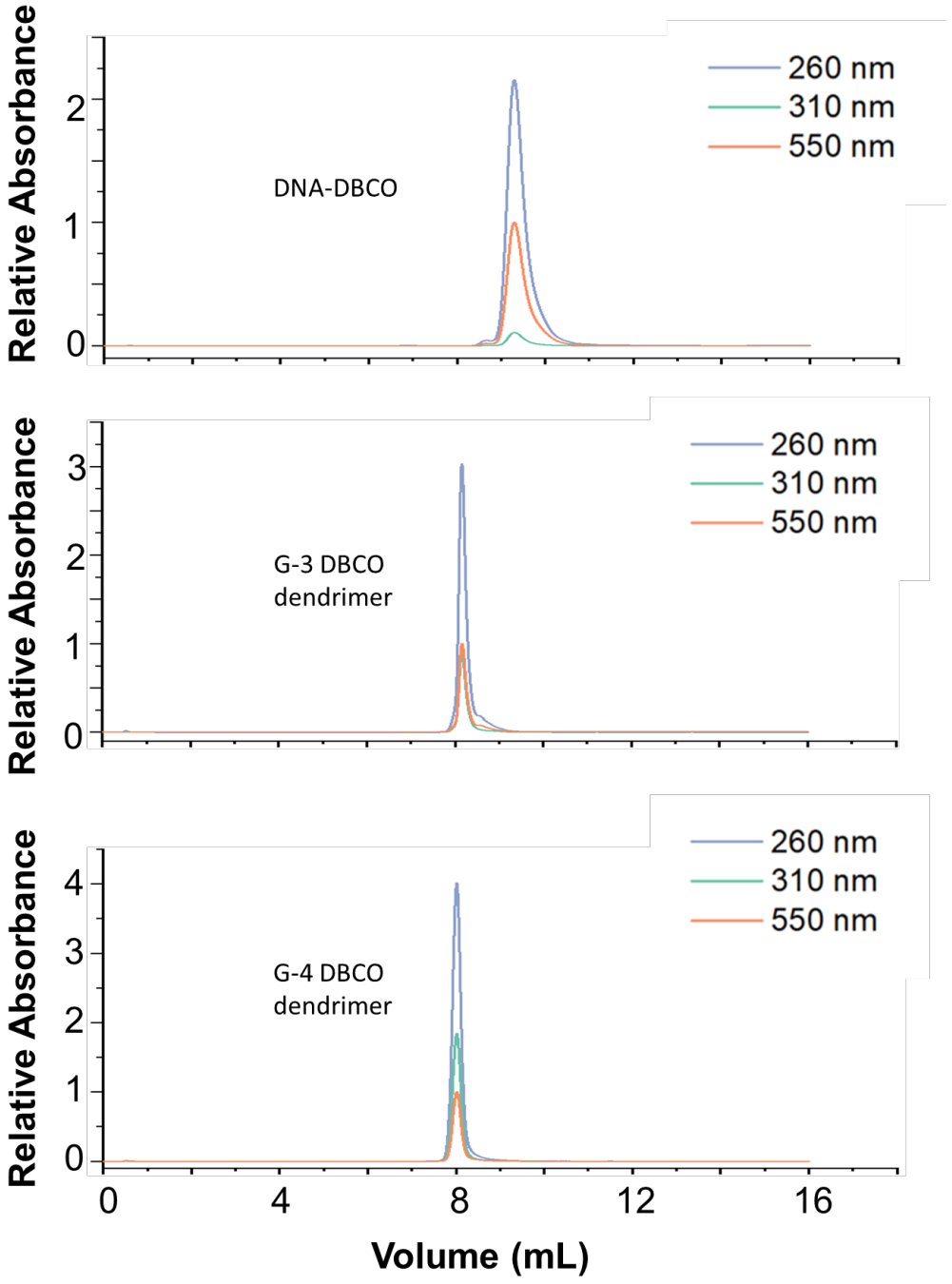

Figure 2.7 FPLC separation of DNA-DBCO, G-3 DBCO dendrimer, and G-4 DBCO dendrimer. All FPLC traces are obtained by SEC. All traces are normalized by the peak of 550 nm channel.

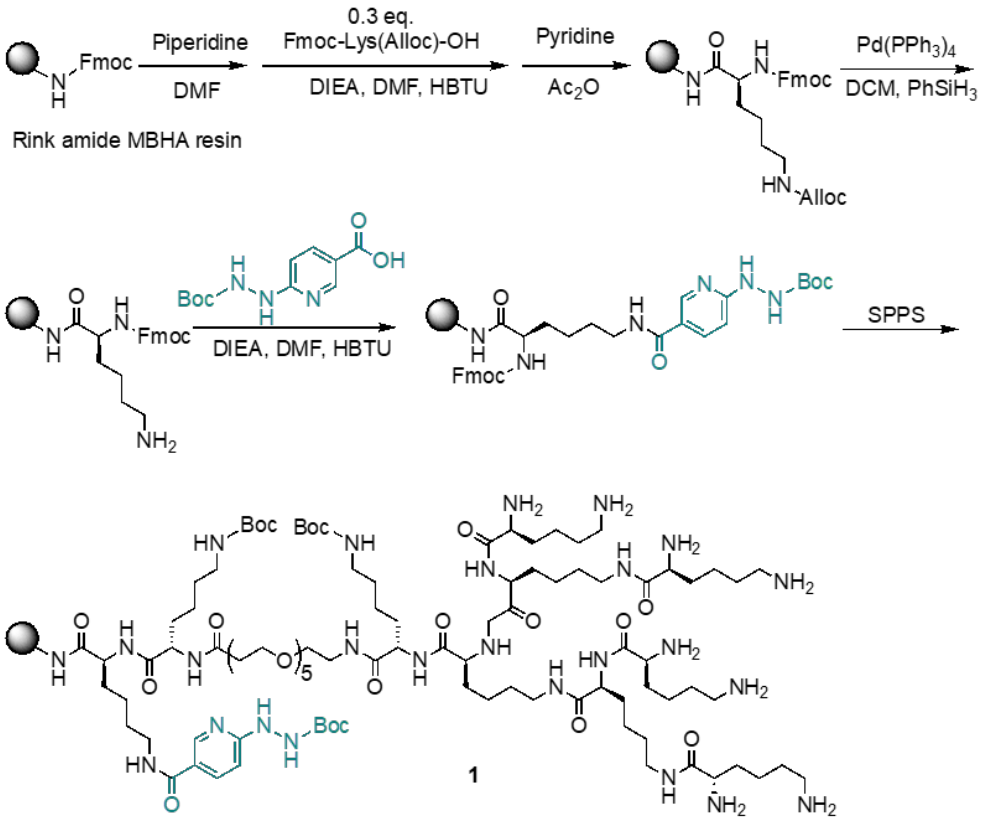

Figure 2.8 The first attempt to conjugate the dendrimer to ssDNA through a hydrazone linkage. G-3 and G-4 scaffolds were synthesized on Rink amide and later conjugated to Boc-HNA, which would link to ssDNA. The loading capacity of rink amide MBHA was reduced to 0.2 mmol/g at the beginning of the synthesis to allow more room for the DBCO-dendrimer.

Method A:

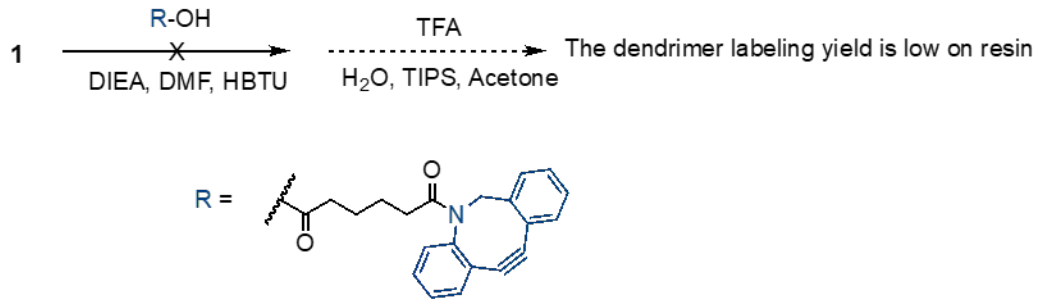

Figure 2.9 The attempt of labeling dendrimer with DBCO on resin led to a very low yield.

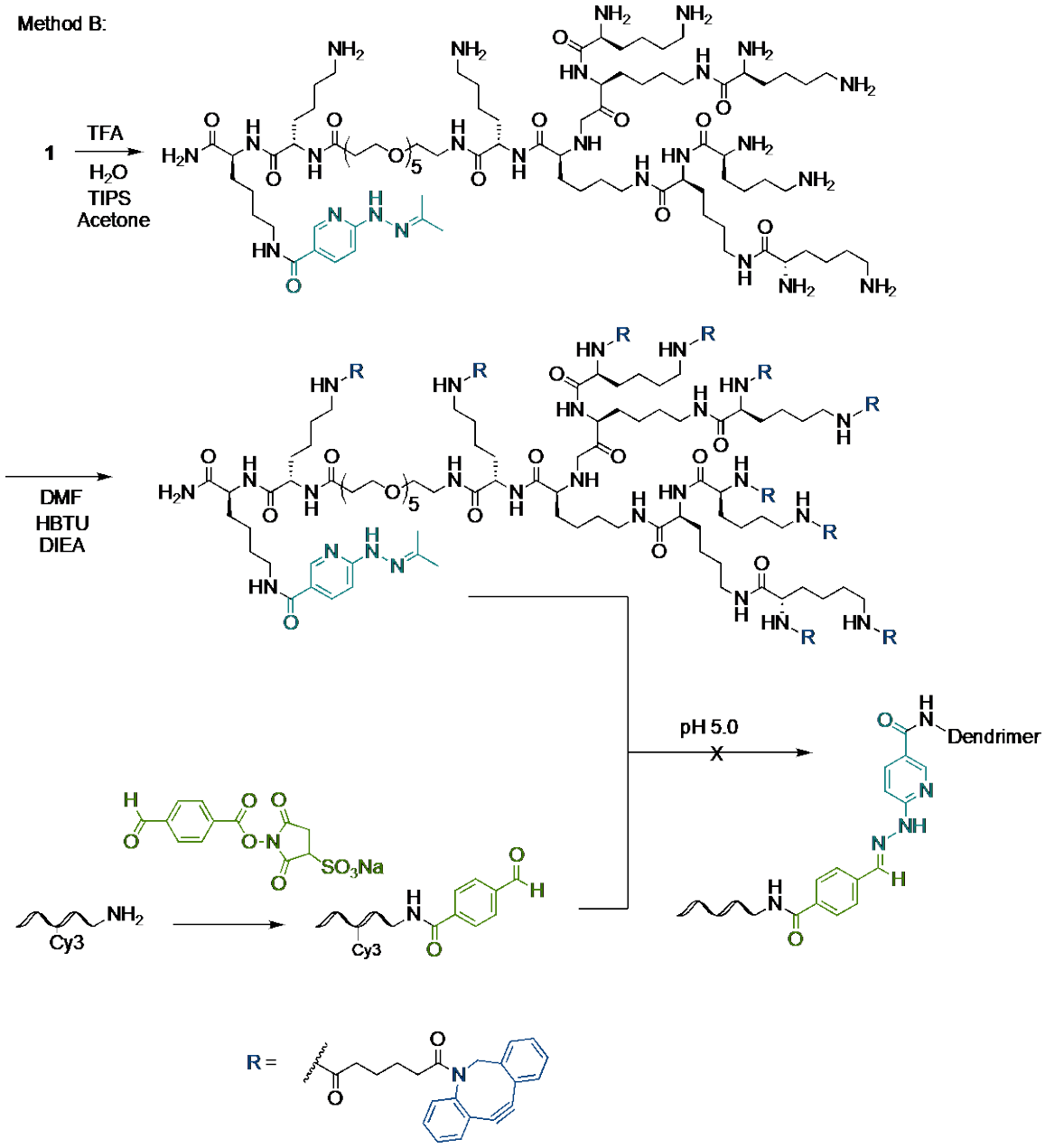

Figure 2.10 Another synthetic route to conjugate ssDNA with DBCO dendrimer. After labeling the dendrimer scaffold with DBCO in solution, the dendrimer became very hydrophobic and could not couple with ssDNA in any common solvents.

In our proposed detection scheme (Figure 2.1), the dendrimer-ssDNA conjugate has an embedded Cy3 group that provides a fluorescence signal. This signal is later quenched by a BHQ2-N_3 molecule (Figure 2.11 – Figure 2.12) through the Föster resonance energy transfer (FRET) mechanism, and the presence of FA-N_3 rescues the Cy3 fluorescence. In this manner, the amount of FA-N_3 correlates with the retained fluorescence. We validated our design by confirming both the quenching (Figure 2.13a) and the rescuing parts. We found that both G-3 and G-4 DBCO dendrimers successfully rescued fluorescence in a concentration-dependent manner (Figure 2.13b) while immobilizing DBCO alone failed to generate any signal (Figure 2.14). This result proved that the dendritic structure was effective and necessary. Since the third-generation dendrimer was easier to synthesize, we carried out our subsequent studies using the G-3 DBCO dendrimer.

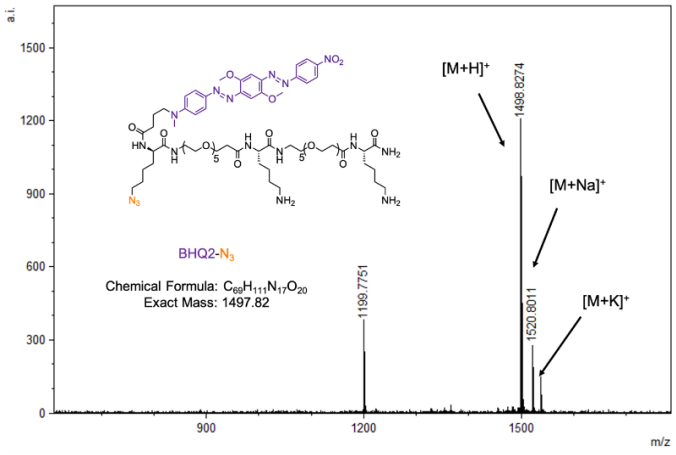

Figure 2.11 Mass spectrum BHQ2-N_3 (MALDI-TOF). $[M+H]^+$ calculated: 1498.82, found 1498.83. The 1199 peak corresponds to the photolytic cleavage of the azo bond. [21]

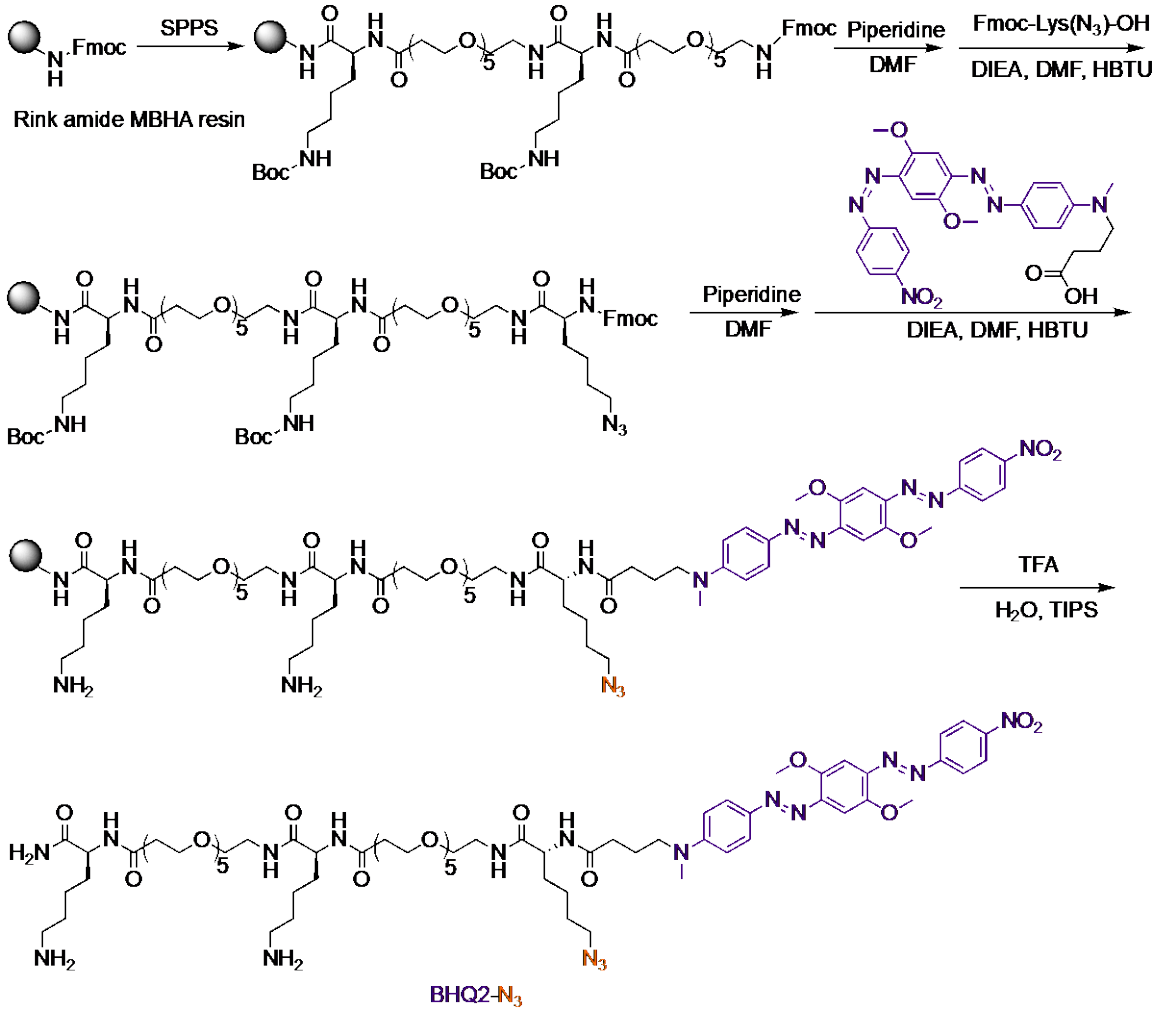

Figure 2.12 Synthesis of BHQ2-N_3. Lysine and polyethylene glycol residues were necessary to increase the aqueous solubility.

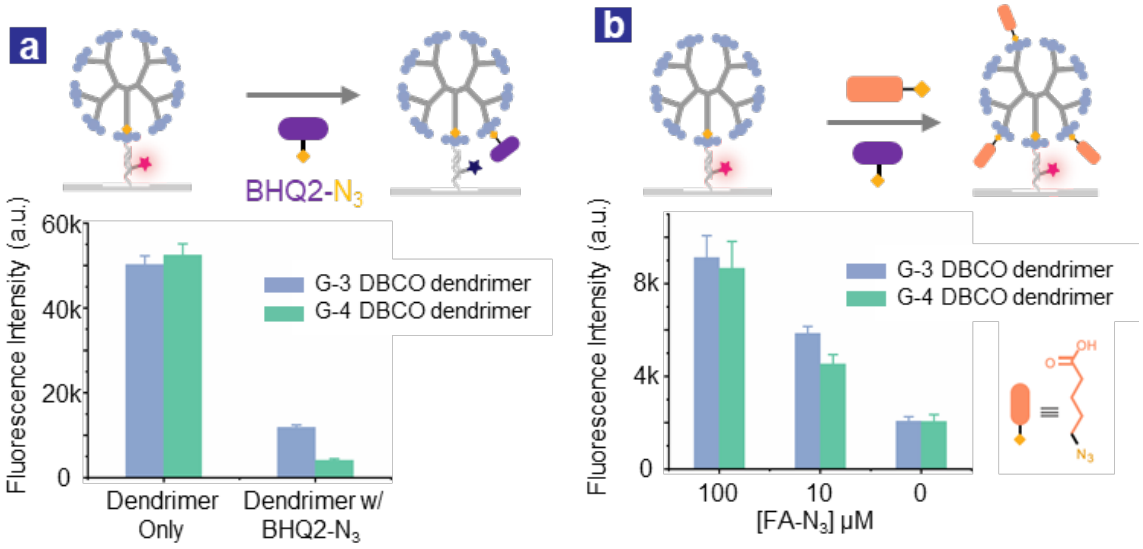

Figure 2.13 FA detection scheme (a) BHQ2-N_3 effectively reacted with the DBCO dendrimer and quenched the Cy3 fluorescence. (b) Azidopentanoic acid rescued the Cy3 fluorescence in a concentration-dependent manner.

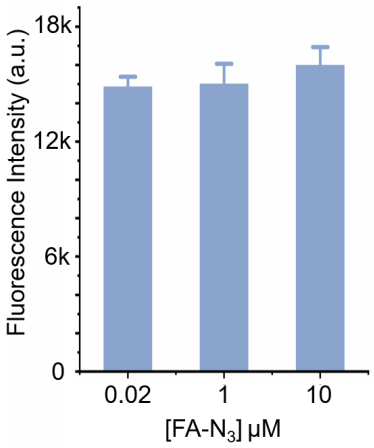

Figure 2.14 Detecting FA-N_3 with surface-immobilized DBCO-DNA conjugates. No dendrimer structure was involved here, and each ssDNA was conjugated to a single DBCO group. No significant changes were observed with varying concentrations of FA-N_3.

Because of the competitive binding nature of the detection method, the fluorescence readouts can be adjusted by changing the concentrations of BHQ2-N_3. To identify an optimal quencher concentration, we evaluated how different concentrations of BHQ2-N_3 compete with 100 μM of FA-N_3 (Figure 2.15a). We chose 0.5 μM as the best BHQ2-N_3 concentration because it led to significant, but not complete, quenching of the Cy3 signal, and that would allow the detection of lower FA-N_3 concentrations. We then generated a fluorescence response curve by varying the concentrations of azidopentanoic acid (Figure 2.15b). We confirmed that this method could detect FA-N_3 at the μM-level, which is the expected concentration range for single-cell analysis.

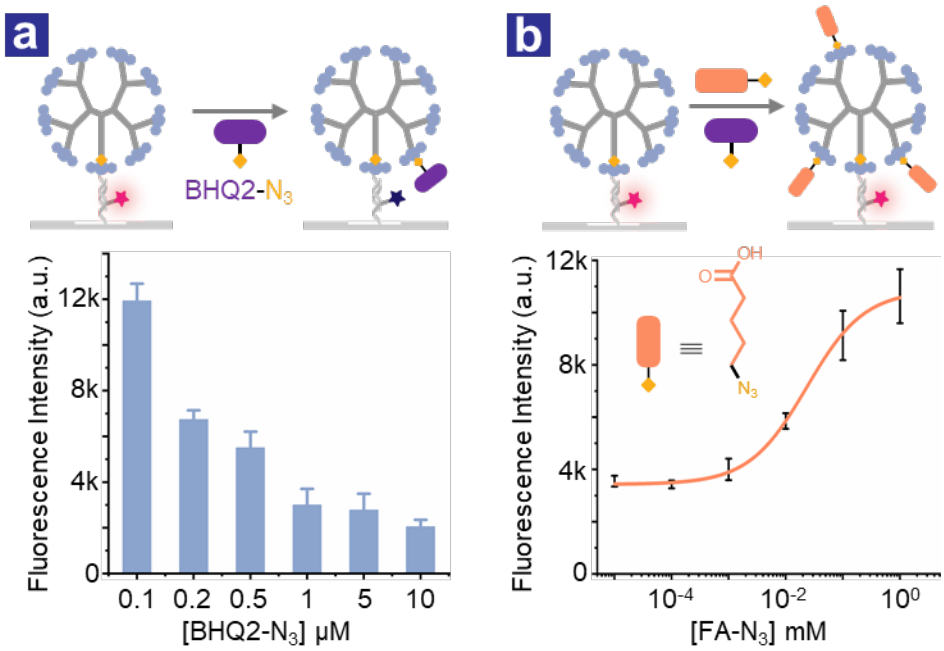

Figure 2.15 Surface-based tests (a) Different concentrations of BHQ2-N_3 competing with 100 μM of FA-N_3 for the DBCO dendrimer binding sites. The attachment of BHQ2-N_3 caused quenching of the Cy3 fluorescence. (b) The fluorescence response curve was generated by using varying concentrations of the FA-N_3.

We tested our detection scheme using U87VIII cells as our model system. These are human glioblastoma cells that exhibit constitutively amplified oncogenic signaling activities and harbor prominent metabolic plasticity. We incubated these cells with varying concentrations of the Azidopentanoic acid probe and used our dendrimer-DNA conjugate / BHQ2-N3 system to evaluate the surrogate uptake at the bulk level. The results (Figure 2.16a) show that the detection scheme was compatible with cell lysates, and that cells took up the fatty acid surrogate in a con-

centration-dependent manner. In addition, we found that the fatty acid analog was well-tolerated by the cells (Figure 2.16b).

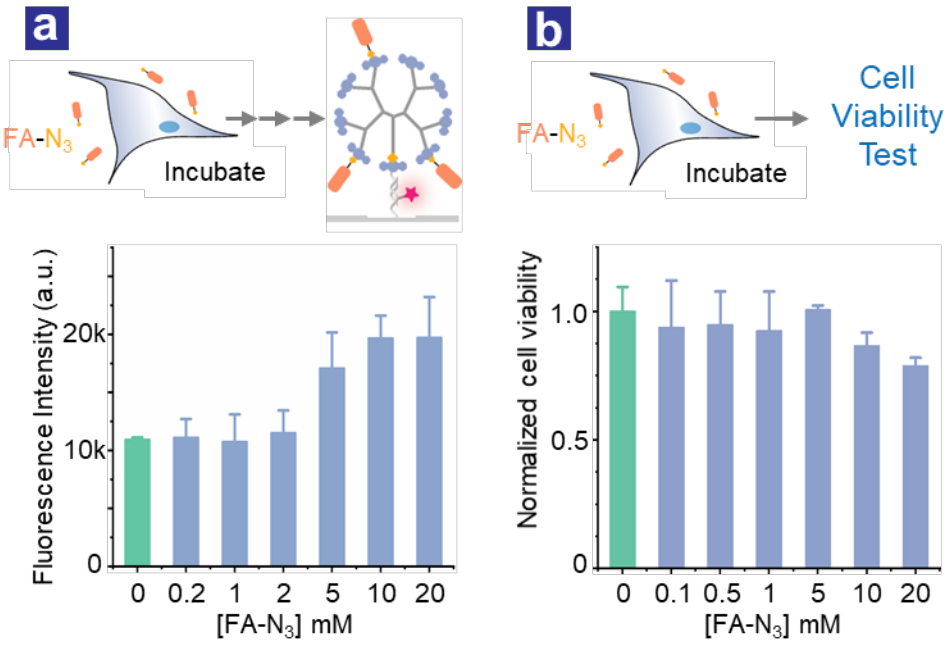

Figure 2.16 Cell-based tests (a) Incubating U87VIII cells with varying concentrations of FA-N_3 led to different fluorescence intensities on the dendrimer-based detection platform. (b) FA-N_3 (up to 20 mM) was not toxic to U87VIII cells.

We then incorporated the fatty acid uptake assay onto the SCBC platform.[14] The SCBC is a two-layer microfluidic device coupled with a DNA-barcoded glass slide. Single cells can be loaded onto the SCBC device and segregated in 416 programmable chambers. These chambers allow on-chip cell culture and cell lysis, and they are equipped with pre-patterned DNA barcode stripes that enable multiplex fluorescence measurements (Figure 2.17 – Figure 2.18). Here, we quantified the azidopentanoic acid uptake, critical signaling protein levels, and cell proliferation marker (Ki67) in U87VIII single cells.

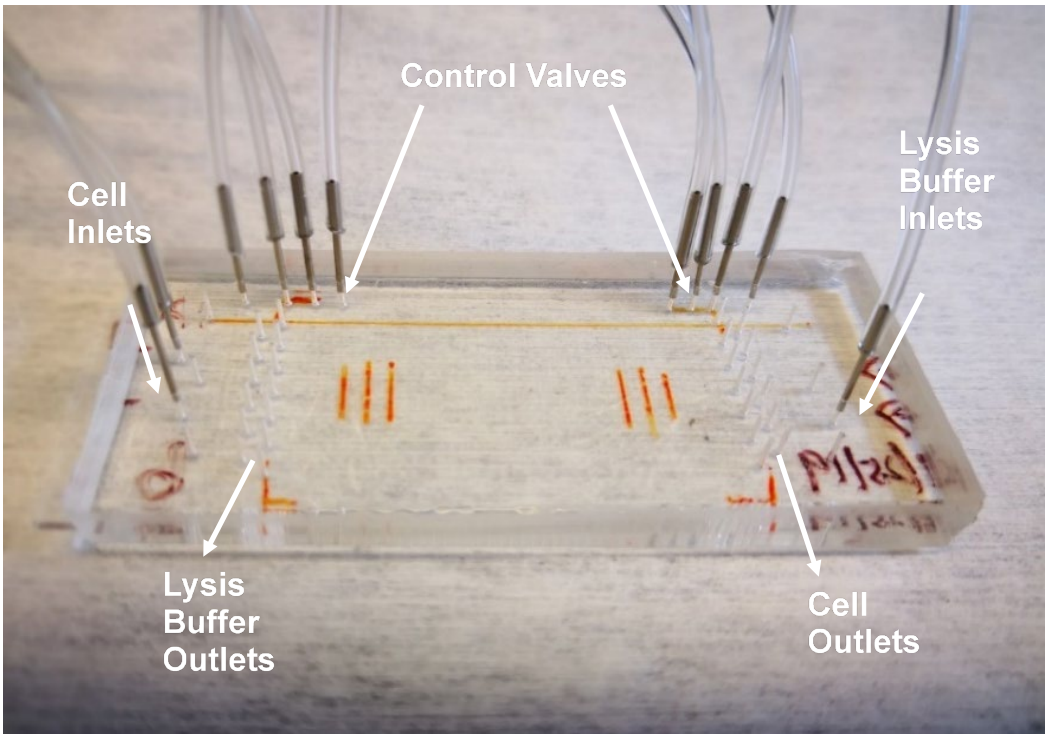

Figure 2.17 A picture of the SCBC device. The SCBC device consists of a DNA barcoded microarray glass chip and two layers of PDMS slabs that control the microfluid circuits. The fabrication of SCBC is well documented in our previous paper. [14]

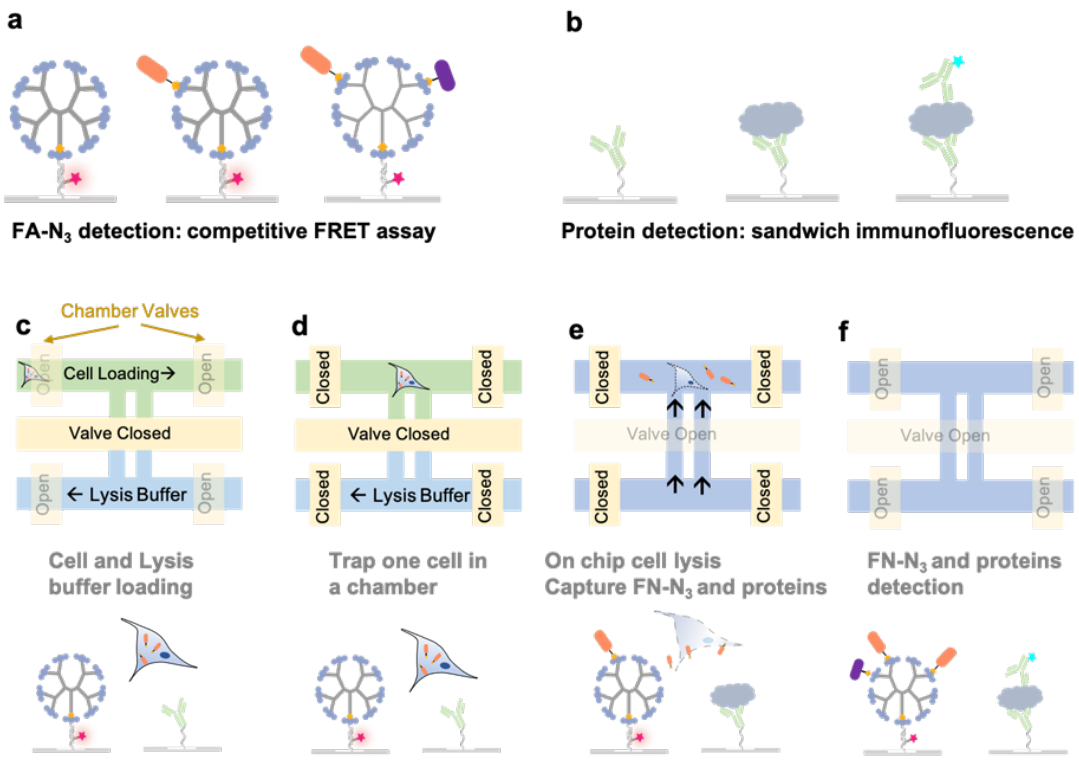

Figure 2.18 The operation of the SCBC. a) FA-N_3 detection was achieved by a surface-based competitive assay. b) Protein detection was carried out by a sandwich immunofluorescence assay. c-f). Schematic representation of microchamber on the SCBC and the operation protocols. The cells were loaded in the SCBC with FA-N_3 first. Then each cell was isolated and lysed on each chamber. Upon cell lysing, FA-N_3 and other analytes were released from the cell and captured on the surface. Subsequently, the detection cocktail containing BHQ2-N_3 and antibodies was added to the chamber, and the fluorescence readout was recorded. The operation of SCBC, except for the fatty acid detection, is well documented in our previous paper. [14]

As shown in Figure 2.19, fatty acid uptake abilities varied significantly among cells. The degree of heterogeneity of this fatty acid uptake was also different from those associated with signaling proteins. Most notably, fatty acid uptake had no outliers (|Z| > 2), while all the protein levels showed outliers, many of which even extended beyond Z = 4. The distribution of fatty acid uptake also exhibited two subpopulations corresponding to low (Z < -1) and high (Z > 0) uptake activities. Such a clear population separation was not observed in the protein levels. Moreover, this fatty acid uptake distribution is different from the glucose and glutamine uptakes from our previous studies on the same cell line.[14, 15]

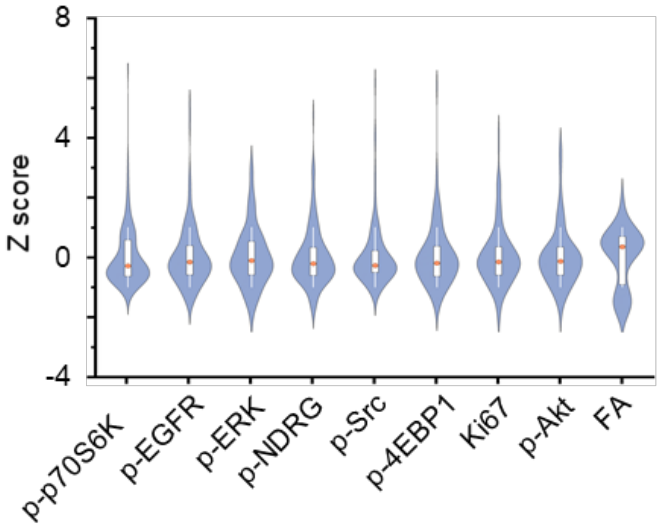

Figure 2.19 Multiplex single-cell dataset obtained from U87VIII cells. The violin plots represent the standardized analyte level distributions. The boxes depict the 25%-75% data ranges, and the whiskers show the standard deviations. The orange dots label the median values.

To further investigate the subpopulations, we performed agglomerative hierarchical clustering analysis (Figure 2.20a). Based on the clusters' analyte levels (Figure 2.20), we found that cells with high fatty acid uptake exhibited low oncogenic signaling activities (p-EGFR, p-ERK, p-Src, and p-Akt). This divergence pointed to a compensatory relationship between glycolysis and fatty acid metabolism. We also noticed that the levels of the cell proliferation marker, Ki67, did not vary between the two subpopulations. This result indicated that neither oncogenic signaling nor fatty acid metabolism was strongly associated with cell proliferation. Such an observation was consistent with our previous studies.[14, 15]

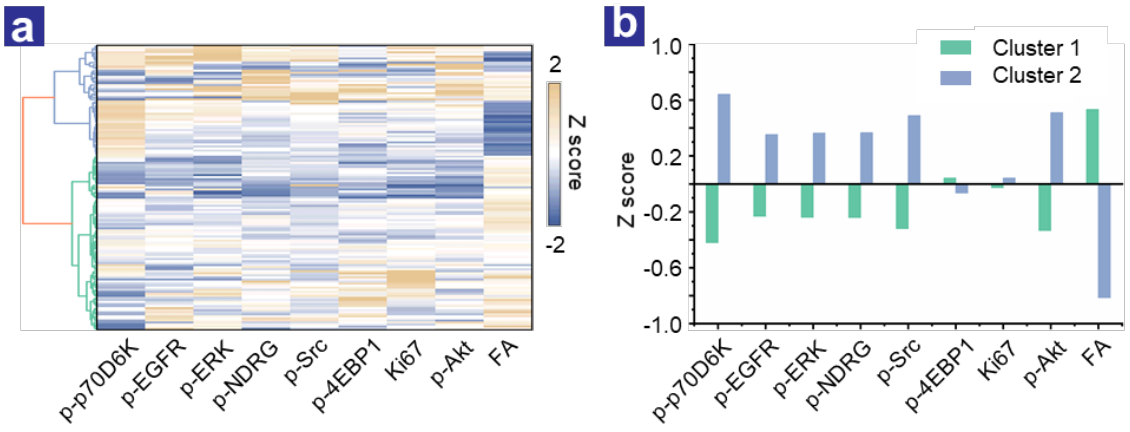

Figure 2.20 (a) Agglomerative hierarchical clustering of the single-cell dataset identified two distinct clusters. (b) Analytes levels of the cluster centroids.

In order to better evaluate how each analyte contributed to the global cellular heterogeneity, we performed principal component analysis (Figure 2.21a). We found that PC1 was primarily populated by oncogenic phosphoproteins, including p-Akt, p-ERK, p-Src, etc, while fatty acid uptake was aligned along PC2 with minimal contribution to PC1. This orthogonality between fatty acid uptake and

critical oncogenic signaling matched our clustering results. Moreover, we observed a strong divergence between fatty acid uptake and p-p70S6K, as well as a corporative relationship between fatty acid uptake and p-4EBP1. Because p70S6K and 4EBP1 are two main effectors downstream of mTOR,[22] these findings hinted that fatty acid uptake was regulated by mTOR signaling, possibly differentially controlled by the 4EBP1 and S6K axes. These results were consistent with the critical role of mTOR signaling in lipid homeostasis and fatty acid metabolism.[23-25] Nevertheless, PC1 and PC2 only collectively captured half of the global cellular heterogeneity variance (Figure 2.21b). Therefore, the conclusions drawn from analyzing PC1 and PC2 required further support.

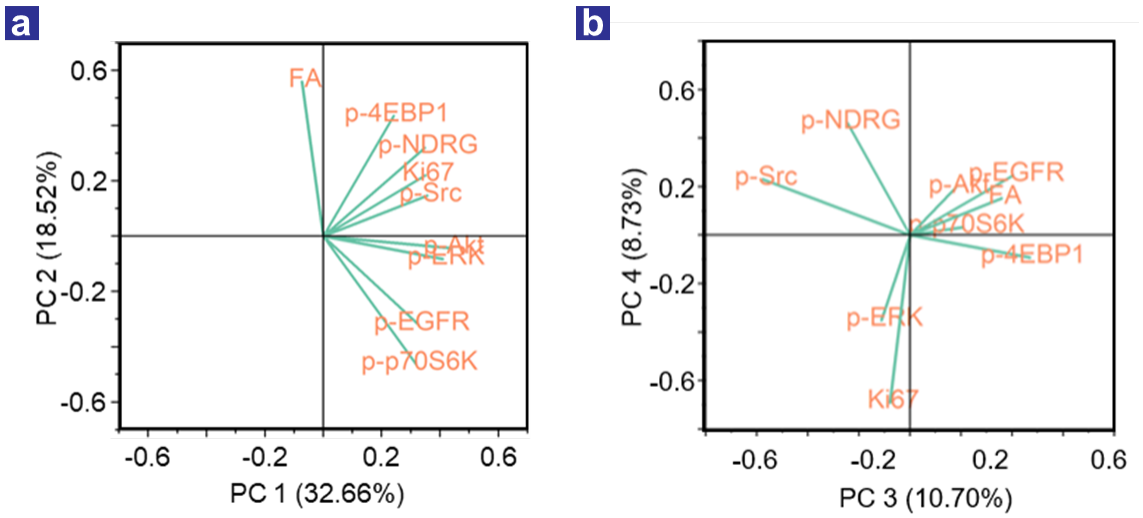

Figure 2.21 (a) The loading plot showing the first two principal components of the single-cell dataset. (b) PC 3 and PC 4 loading plot. The relationship between p-Akt and p-70S6K was not consistent with the PC1/PC2 result.

We then sought to scrutinize the interactions between analytes. We calculated the pairwise Spearman correlation values among all analytes, and the result is shown in Figure 2.22. We found strong correlations between signaling proteins, which were indicative of highly coordinated oncogenic signaling network activities and consistent with our previous studies on U87VIII cells. Notably, fatty acid showed a positive correlation with p-4EBP1 and negative correlations with p-p70S6K and p-EGFR. These correlations dovetailed the principal component analysis results and further supported our hypothesis that the p-4EBP1 and p-p70S6K signaling axes differentially regulated fatty acid uptake. Based on the strong anticorrelation between fatty acid uptake and p-p70S6K, we further hypothesized that co-inhibiting p70S6K and fatty acid metabolism would synergistically inhibit cell proliferation.

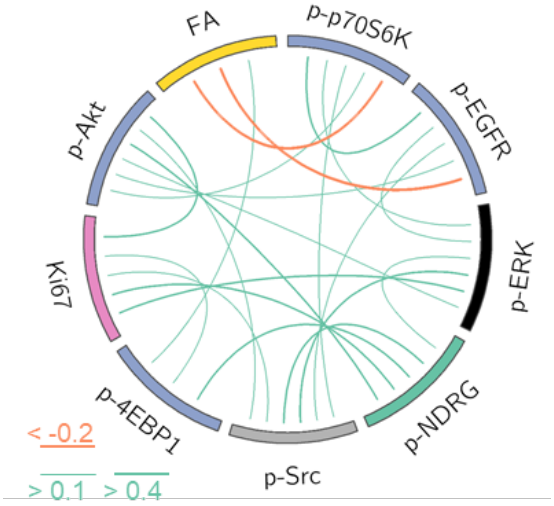

Figure 2.22 The correlation network of the analytes. Orange and green lines represent negative and positive correlations, respectively. The line thickness corresponds to the correlation level.

To test our hypothesis, we treated U87VIII cells with LY2584702 (a p70S6K inhibitor), trimetazidine (a fatty acid metabolism inhibitor), and a combination of them. It was evident that the combination synergistically inhibited cell proliferation (Figure 2.23a). To quantitatively evaluate this synergy, we treated the cells with drugs under a concentration titration and calculated the synergy score using the BLISS definition of independence. As shown in Figure 2.23b, we observed strong synergy between the two drugs across a wide range of concentrations. This result supported our hypothesis that p70S6K negatively regulated fatty acid metabolism in U87VIII cells.

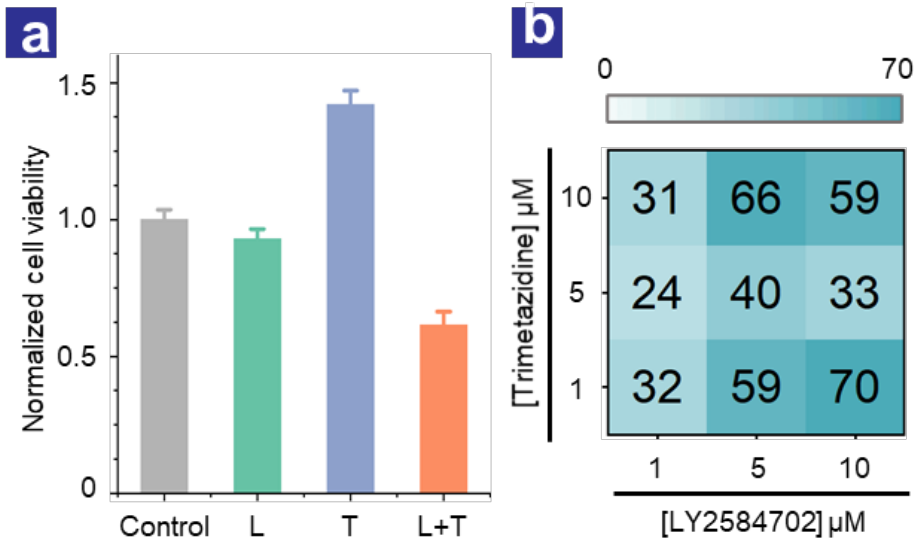

Figure 2.23 (a)U87VIII cell viabilities as results of LY2584702 (p70S6K inhibitor, 10 µM) and trimetazidine (fatty acid metabolism inhibitor, 1 µM) treatments. (b) Synergy scores calculated from the BLISS method across different concentrations of trimetazidine and LY2584702 combinations.

2.4 Conclusion

In conclusion, we established a dendrimer-based detection scheme for profiling fatty acid uptake in single cells. When integrated into the multiplex single-cell barcode chip platform, we were able to perform simultaneous analysis of fatty acid uptake and critical oncogenic signaling proteins in single cells. Using this technology, we identified 4EBP1 and p70S6K as potential regulators of fatty acid metabolism. We found that co-targeting p70S6K and fatty acid metabolism could synergistically inhibit U87VIII proliferation. The technology presented here can be extended to identify other potential regulatory mechanisms of fatty acid metabolism by including additional proteins into the panel, given that the appropriate antibody pairs are available. In addition, the dendrimer-based platform can be easily adapted to detect other azide-modified small molecules.

References

1. Currie, E.; Schulze, A.; Zechner, R.; Walther, T. C.; Farese Jr, R. V., Cellular fatty acid metabolism and cancer. *Cell metabolism* **2013,** *18* (2), 153-161.

2. Pavlova, N. N.; Thompson, C. B., The Emerging Hallmarks of Cancer Metabolism. *Cell Metab* **2016,** *23* (1), 27-47.

3. Martinez-Outschoorn, U. E.; Peiris-Pages, M.; Pestell, R. G.; Sotgia, F.; Lisanti, M. P., Cancer metabolism: a therapeutic perspective. *Nat Rev Clin Oncol* **2017,** *14* (1), 11-31.

4. Carracedo, A.; Cantley, L. C.; Pandolfi, P. P., Cancer metabolism: fatty acid oxidation in the limelight. *Nat Rev Cancer* **2013,** *13* (4), 227-32.

5. Kamphorst, J. J.; Cross, J. R.; Fan, J.; de Stanchina, E.; Mathew, R.; White, E. P.; Thompson, C. B.; Rabinowitz, J. D., Hypoxic and Ras-transformed cells support growth by scavenging unsaturated fatty acids from lysophospholipids. *Proc Natl Acad Sci U S A* **2013,** *110* (22), 8882-7.

6. Raynor, A.; Jantscheff, P.; Ross, T.; Schlesinger, M.; Wilde, M.; Haasis, S.; Dreckmann, T.; Bendas, G.; Massing, U., Saturated and mono-unsaturated lysophosphatidylcholine metabolism in tumour cells: a potential therapeutic target for preventing metastases. *Lipids Health Dis* **2015,** *14*, 69.

7. Beloribi-Djefaflia, S.; Vasseur, S.; Guillaumond, F., Lipid metabolic reprogramming in cancer cells. *Oncogenesis* **2016,** *5*, e189.

8. Liu, Y.; Zuckier, L. S.; Ghesani, N. V., Dominant uptake of fatty acid over glucose by prostate cells: a potential new diagnostic and therapeutic approach. *Anticancer Res* **2010,** *30* (2), 369-74.

9. Bensaad, K.; Favaro, E.; Lewis, C. A.; Peck, B.; Lord, S.; Collins, J. M.; Pinnick, K. E.; Wigfield, S.; Buffa, F. M.; Li, J. L.; Zhang, Q.; Wakelam, M. J.; Karpe, F.; Schulze, A.; Harris, A. L., Fatty acid uptake and lipid storage induced by HIF-1alpha contribute to cell growth and survival after hypoxia-reoxygenation. *Cell Rep* **2014,** *9* (1), 349-65.

10. Camarda, R.; Zhou, A. Y.; Kohnz, R. A.; Balakrishnan, S.; Mahieu, C.; Anderton, B.; Eyob, H.; Kajimura, S.; Tward, A.; Krings, G.; Nomura, D. K.;

Goga, A., Inhibition of fatty acid oxidation as a therapy for MYC-overexpressing triple-negative breast cancer. *Nat Med* **2016,** *22* (4), 427-32.

11. Du, J.; Su, Y.; Qian, C.; Yuan, D.; Miao, K.; Lee, D.; Ng, A. H. C.; Wijker, R. S.; Ribas, A.; Levine, R. D.; Heath, J. R.; Wei, L., Raman-guided subcellular pharmaco-metabolomics for metastatic melanoma cells. *Nat Commun* **2020,** *11* (1), 4830-4830.

12. Tateishi, K.; Iafrate, A. J.; Ho, Q.; Curry, W. T.; Batchelor, T. T.; Flaherty, K. T.; Onozato, M. L.; Lelic, N.; Sundaram, S.; Cahill, D. P.; Chi, A. S.; Wakimoto, H., Myc-Driven Glycolysis Is a Therapeutic Target in Glioblastoma. *Clin Cancer Res* **2016,** *22* (17), 4452-65.

13. Hensley, C. T.; Faubert, B.; Yuan, Q.; Lev-Cohain, N.; Jin, E.; Kim, J.; Jiang, L.; Ko, B.; Skelton, R.; Loudat, L.; Wodzak, M.; Klimko, C.; McMillan, E.; Butt, Y.; Ni, M.; Oliver, D.; Torrealba, J.; Malloy, C. R.; Kernstine, K.; Lenkinski, R. E.; DeBerardinis, R. J., Metabolic Heterogeneity in Human Lung Tumors. *Cell* **2016,** *164* (4), 681-694.

14. Xue, M.; Wei, W.; Su, Y.; Kim, J.; Shin, Y. S.; Mai, W. X.; Nathanson, D. A.; Heath, J. R., Chemical methods for the simultaneous quantitation of metabolites and proteins from single cells. *J Am Chem Soc* **2015,** *137* (12), 4066-9.

15. Xue, M.; Wei, W.; Su, Y.; Johnson, D.; Heath, J. R., Supramolecular Probes for Assessing Glutamine Uptake Enable Semi-Quantitative Metabolic Models in Single Cells. *J Am Chem Soc* **2016,** *138* (9), 3085-93.

16. Li, Z.; Cheng, H.; Shao, S.; Lu, X.; Mo, L.; Tsang, J.; Zeng, P.; Guo, Z.; Wang, S.; Nathanson, D. A.; Heath, J. R.; Wei, W.; Xue, M., Surface Immobilization of Redox-Labile Fluorescent Probes: Enabling Single-Cell Co-Profiling of Aerobic Glycolysis and Oncogenic Protein Signaling Activities. *Angewandte Chemie International Edition* **2018,** *57* (36), 11554-11558.

17. Huang, H.; Starodub, O.; McIntosh, A.; Kier, A. B.; Schroeder, F., Liver fatty acid-binding protein targets fatty acids to the nucleus. Real time confocal and multiphoton fluorescence imaging in living cells. *J Biol Chem* **2002,** *277* (32), 29139-51.

18. Witney, T. H.; Pisaneschi, F.; Alam, I. S.; Trousil, S.; Kaliszczak, M.; Twyman, F.; Brickute, D.; Nguyen, Q. D.; Schug, Z.; Gottlieb, E.; Aboagye, E. O., Preclinical evaluation of 3-18F-fluoro-2,2-dimethylpropionic acid as an imaging agent for tumor detection. *J Nucl Med* **2014,** *55* (9), 1506-12.

19. Krzywinski, M.; Schein, J.; Birol, I.; Connors, J.; Gascoyne, R.; Horsman, D.; Jones, S. J.; Marra, M. A., Circos: an information aesthetic for comparative genomics. *Genome Res* **2009,** *19* (9), 1639-1645.

20. Debets, M. F.; van Berkel, S. S.; Schoffelen, S.; Rutjes, F. P. J. T.; van Hest, J. C. M.; van Delft, F. L., Aza-dibenzocyclooctynes for fast and efficient enzyme PEGylation via copper-free (3+2) cycloaddition. *Chemical Communications* **2010,** *46* (1), 97-99.

21. Wyplosz, N. Laser desorption mass spectrometric studies of artists' organic pigments. University of Amsterdam, 2003.

22. Liu, G. Y.; Sabatini, D. M., mTOR at the nexus of nutrition, growth, ageing and disease. *Nature Reviews Molecular Cell Biology* **2020,** *21* (4), 183-203.

23. Tsai, S.-Y.; Rodriguez, Ariana A.; Dastidar, Somasish G.; Del Greco, E.; Carr, Kaili L.; Sitzmann, Joanna M.; Academia, Emmeline C.; Viray, Christian M.; Martinez, Lizbeth L.; Kaplowitz, Brian S.; Ashe, Travis D.; La Spada, Albert R.; Kennedy, Brian K., Increased 4E-BP1 Expression Protects against Diet-Induced Obesity and Insulin Resistance in Male Mice. *Cell Reports* **2016,** *16* (7), 1903-1914.

24. Koundouros, N.; Poulogiannis, G., Reprogramming of fatty acid metabolism in cancer. *British Journal of Cancer* **2020,** *122* (1), 4-22.

25. Ricoult, S. J. H.; Manning, B. D., The multifaceted role of mTORC1 in the control of lipid metabolism. *EMBO Rep* **2013,** *14* (3), 242-251.

CHAPTER 3 A Magnetic Particles-Based Method for Removing Non-Specific Binding Components in On-Bead Screening of Combinatorial Libraries

3.1 Introduction

Combinatorial chemistry allows rapid preparation of peptide libraries. There are two major types of combinatorial peptide libraries, biological peptide libraries and chemical peptide libraries. Biological peptide libraries are typically much more diverse than chemical peptide libraries. For example, the diversity of DNA-encoded libraries[1-4], mRNA display libraries[5], and phage display libraries[6, 7] can be as high as 10^{11} -10^{13}. In contrast, the diversity of a typical chemical peptide library is only around ~10^{6}.[8] Nevertheless, chemical peptide libraries are more tolerant to intensive chemical modification, such as head-to-tail cyclization[9], incorporation noncanonical amino acids[10], and chemical stapling[11, 12]. Such modifications confer unique advantages to these peptides, including the resistance to proteolytic enzymes[10], increased cell permeabilities[13], and better binding affinities[14].

One-bead-one-compound (OBOC) peptide libraries are a prominent type of chemical peptide libraries. OBOC libraries can be prepared by combinatorial processes using the "split-and-pool" method to generate million-scale chemical diversity. Screening campaigns using these OBOC libraries have facilitated the development of many ligands, including imaging agents[15] and protein-protein interaction inhibitors[16, 17].

Despite the great success in OBOC peptide library screening, non-specific interactions during the on-bead screening have posed significant technical challenges, which often lead to false-positive results and pan-assay interference compounds (PAINS).[16-18] This non-specific binding usually roots from the interaction between the screening target and the solid support,[19] and multivalent interactions can further worsen the scenario.[20] Therefore, it is critical to remove, or at least significantly reduce, these non-specific binding components from the screening process.

A common approach to eliminate the non-specific hits is through a preclear screening process before the actual screening of the target of interest.[21, 22] Currently, several preclear strategies exist, and our lab has adopted and relied on two methods. In the colorimetric method[21], OBOC libraries are screened against scrambled targets with biotin. After an enzymatic assay, the non-specific binding resins will be colored and manually removed (Figure 3.1). This method eliminates a variety of non-specific interactions effectively, yet it is time-consuming and tedious, and it lacks efficiency. The other approach is to use a fluorescence-activated BioSorter®.[17] Here, the library is incubated with a panel of fluorophores and fluorescently labeled proteins. Beads with strong non-specific interactions exhibit high fluorescent intensities, which will be sorted out by the BioSorter® (Figure 3.2). This method is quantitative and automated, but it is low-throughput (10 beads/s) and expensive. Herein, we aim to develop another method to remove those non-specific hits efficiently and cost-effectively.

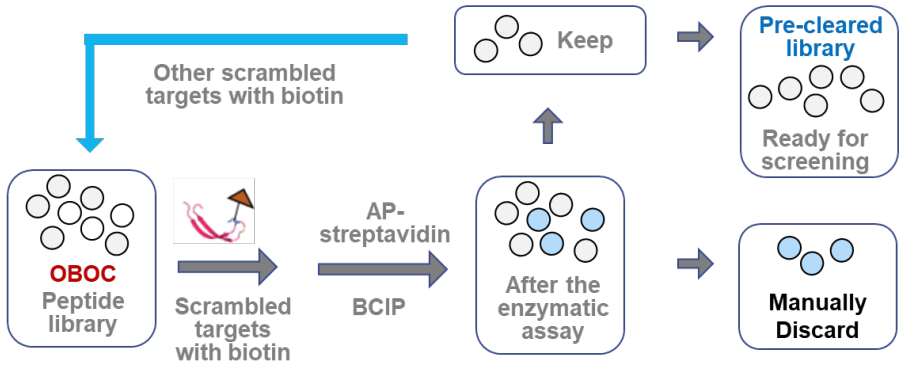

Figure 3.1 Colorimetric method to remove non-specific hits. The library is incubated with scrambled targets with biotin. After being washed, the resins are incubated with alkaline phosphatase-streptavidin and stained with BCIP. The colored beads are picked out manually under a microscope.

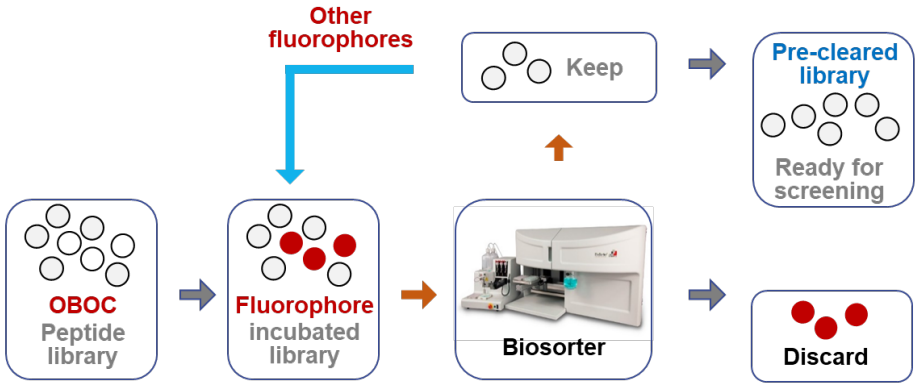

Figure 3.2 Fluorescence-activated sorting. The library is incubated with a panel of fluorophores and fluorescently labeled proteins, and beads with high fluorescent intensity are removed by the BioSorter®.

3.2 Materials and Methods

Materials:

M280 streptavidin-coated Dynabeads was purchased from Thermo Fisher (Vilnius, LT). Biotinylated goat anti-rabbit IgG antibody and normal rabbit IgG control were purchase from Vector Laboratories and R&D system respectfully. Rink amide MBHA resin (loading capacity 0.68 mmol/g) was purchased from Aapptec (Louisville, KY). TentaGel S-NH_2 resin (0.28 mmol/g) was purchased from Rapp Polymere GmbH (Tübingen, Germany). All the Fmoc-protected amino acids were purchased from Anaspec (Fremont, CA) except Fmoc-Lys(N_3)-OH (azido-lysine), which were purchased from Chem-Impex (Wood Dale, IL). Fmoc-Glu(OAll)-OH was purchased from Novabiochem (Latvia). Fmoc-L-propargylglycine was ordered from Matrix Scientific (Columbia, SC). Hoveyda-Grubbs Catalyst™ 2nd Generation (97%) was purchased from Sigma-Aldrich. Tetrakis(triphenylphosphine)palladium(0) (99%) was ordered from STREM CHEMICALS (Newburyport, MA). Cuprous Iodide (98.0%) was ordered from Spectrum (New Brunswick, NJ). Fmoc-PEG5-OH was purchased from BroadPharm (San Diego, CA). The coupling reagent 2-(1H-benzotriazol-1-yl)-1,1,3,3-tetramethyluronium hexafluorophosphate (HBTU, 99.6%) was obtained from Chem-Impex (Wood Dale, IL). Diisopropylethylamine (DIEA, 99.5%) was purchased from ACROS (Germany). Triisopropylsilane (TIPS) was obtained from TCI (Portland, OR). Piperidine was purchased from Alfa Aesar (Ward Hill, MA). α-cyano-4-hydroxycinnamic acid (CHCA) was obtained from Sigma-Aldrich (St.

Louis, MO). Tris base, sodium phosphate dibasic anhydrous (Na_2HPO_4, 99.6%), sodium phosphate monobasic monohydrate (NaH_2PO_4, 99.4%), sodium chloride (NaCl), ascorbic acid, Tween 20, bovine serum albumin (BSA), acetonitrile (CH_3CN), diethyl ether (Et_2O), ethyl acetate (EA), N,N′-dimethylformamide (DMF), and dichloromethane (DCM) were purchased from Thermo Fisher Scientific (Waltham, MA).

Buffers:

1× TBS: 20 mM Tris and 150 mM NaCl, pH 7.6; 1× TBST: TBS, 0.05% Tween20; 1× PBS: 150 mM NaCl, 10mM phosphate buffer, pH 7.4; AP buffer: 100 mM Tris, 150 mM NaCl, 1 mM $MgCl_2$, pH 9.0.

Methods:

Construction of NT-A library. The NT-A library was synthesized as described in J. Am. Chem. Soc. 2018, 140, 44, 14552–14556.[23] Specifically, three stages were involved in NT-A library synthesis, including linear peptide precursor synthesis, Cu(I)-catalyzed azide-alkyne cycloaddition CuAAC click reaction, and ring-closing metathesis (RCM) reaction, and global deprotection. For linear peptide precursor synthesis, the library was synthesized based on well-established protocols on TentaGel S NH_2 resin (loading capacity 0.29 mmol/g). In a typical synthesis, the pre-swelled resin (2 g, 0.58 mmol) was firstly coupled with ANP linker (1.25 g, 2.9 mmol), HATU (1.06 g, 2.78 mmol), DIEA (1.2 mL, 7.25 mmol) in DMF (20 mL), the mixture was agitated at room temperature for 2 hours and washed with DMF (5× 20 mL); followed by deprotection of Fmoc (20 mL, 20% v/v

in DMF, 3×10 min) and washing with DMF (5× 20 mL). Then the ANP linked resin was coupled with Fmoc-Glu-(OAll)-OH (1.19 g, 2.9 mmol), HATU (1.06 g, 2.78 mmol), DIEA (1.2 mL, 7.25 mmol) in DMF (20 mL), the mixture was agitated at room temperature for 2 hours and washed with DMF (5× 20 mL); followed by deprotection of Fmoc (20 mL, 20% v/v in DMF, 3×10 min) and washed with DMF (5× 20 mL). Then the 2 g resin was split evenly into 18 fractions. Each fraction was coupled to a designated amino acid (Arg, His, Lys, Asp, Glu, Ser, Thr, Asn, Gln, Gly, Pro, Ala, Val, Ile, Leu, Phe, Tyr, Trp) using the following recipe: amino acid (0.16 mmol), HATU (0.15 mmol, 0.2 M in DMF, 768 uL), DIEA (0.4 mmol, 66 uL) in DMF (1.0 mL). The resins were agitated at room temperature for 2 hours to allow sufficient coupling. Later, all 18 fractions were washed with DMF and pooled together and undergone Fmoc deprotection. These split-pool processes were repeated for another 4 cycles. For the shared sequences involving Fmoc-Pro-OH, Fmoc-Glu(OAll)-OH, Fmoc-L-Lys(N_3)-OH, Fmoc-propargylglycine, the coupling was performed in one pot with the same method as the ANP coupling.

After the linear peptide precursor was obtained, the first ring was cyclized by CuAAC reaction. The resins were mixed with CuI (552 mg, 2.9 mmol) and ascorbic acid (1.53 g, 8.7 mmol) in DMF (20% v/v 2,6-lutidine, 44 mL) and agitated overnight. The excess copper was removed from the resins by washing extensively with a Cu chelating solution (Sodium diethyldithiocarbamate 5% w/v, DIEA 5% v/v in DMF). Then the second ring was cyclized by RCM reaction. The resins were first dried under vacuum and then mixed with Hoveyda-Grubbs 2nd generation

catalyst (HG-II) (73 mg, 0.12 mmol) in a 100 mL flask, charged with argon 3 times. De-oxygenated 1,2-dichloroethane (20 mL) was added, and the mixture was stirred gently at 70 °C overnight. Another batch of HG-II catalyst (73 mg, 0.12 mmol) was added, and the reaction continued for additional 16 hours. The resin was washed with DCM (20 mL×5) and incubated with tris(hydroxymethyl)phosphine (0.2 M in isopropanol, 20 mL) at 80 °C for at least 12 hours. Then the resin was washed with (50% DMF in H_2O 20 mL×3), DMF (20 mL×3).

Finally, after removing the Fmoc protecting group at the N-terminal of the peptide, global deprotection was performed using a mixture of trifluoroacetic acid, triisopropylsilane and water (95:2.5:2.5 v/v, 20 mL) for 2 hours. The library was then washed with DMF (20 mL×3) and was ready to use.

Positive control - biotinylated TentaGel S-NH_2 resin preparation. The pre-swelled resin (200 mg, 0.058 mmol) was coupled with biotin (70.8 mg, 0.29 mmol), HATU (0.106 g, 0.278 mmol), DIEA (0.2 mL, 0.725 mmol) in DMF (5 mL), the mixture was agitated at room temperature for 2 hours and washed with DMF (5× 10 mL).

Screening process with the magnetic particles. There were generally 4 steps for magnetic particles screening, including library preparation, incubation with biotinylated molecules, pulling out resins with the magnetic particles, and the library recovery.

Preparation of the NT-1 library: 100 mg of the NT-1 library was washed with DCM (3 × 6 mL), DMF (3 × 6 mL), methanol (3 × 6 mL), water (10 × 6 mL), and 1×

PBS (5 × 6 mL) in a syringe with the filtrate. The NT-1 library was swelled in 1×PBS for 2 hours.

Incubation with biotinylated molecules: For the rabbit IgG-based experiment, the library was incubated with normal rabbit IgG control (1.5 μM in 1× PBS) overnight at 4 °C. Later, the library was washed with (3 × 3 mL) and incubated with biotinylated goat anti-rabbit IgG (1.5 μM in 1× PBS). For other screening processes, the prepared library was incubated with biotinylated molecules (biotinylated scrambled peptide/BSA) (1.5 μM in 1× PBS) overnight at 4 °C.

Pulling out resins with the magnetic particles: After the incubation with biotinylated molecules, the library was washed with 1× PBS (3 × 3 mL) and transferred to a 2 mL Eppendorf tube with 1 mL 1× PBS. 2 μL of M280 streptavidin-coated Dynabeads was added to the system and was incubated with the library for 1 hour with gentle shaking. The resins could be transferred to a petri dish, allowing for observation under a microscope. Otherwise, the 2 mL Eppendorf tube was placed on a magnetic rack and the library was gently pipetted up and down. The beads with a positive response to the magnet would attach to the wall of the Eppendorf tube, while the others would be settled at the bottom of the tube. Transfer out the unattached beads and repeat the process 3-5 times until no beads/magnetic particles could be attracted to the Eppendorf tube wall.

Recovery of the library: After the separation, the positive and negative resins are transferred into proper size syringes with filtrate, respectfully. The resins were washed with 6 M guanidine chloride, pH 8, for 2 hours and then washed with

1× PBS intensively. Later, the syringes were centrifuged at maximum speed to remove all the magnetic particles. Finally, the beads were washed with 1× PBS, water, methanol, DMF, and DCM. The library was air-dried and stored at 4 °C.

Colorimetric validation experiment. The library was swelled in TBS buffer for 2 hours and incubated with biotinylated BSA (1.5 μM in 1× TBS) overnight at 4 °C. Later, the library was washed with 1× TBS (3 × 3 mL) and incubated with Avidin-AP (1/10000 dilution) at 4 °C for 1 hour. Finally, 10 μL BCIP substrate (50 mg/mL) was introduced to the systems with 1 mL of AP buffer. The color was developed at room temperature for 30 min, and the reaction was quenched by 50 μL of concentrated HCl.

Solid-phase peptide synthesis. Peptides were synthesized via the standard Fmoc solid-phase peptide synthesis (SPPS) chemistry on Rink Amide MBHA resin. All peptides were cleaved from the resin via TFA cocktail cleavage solution (95% TFA, 2.5% TIPS, 2.5% water). All peptides were purified on the RP-UPLC (DIONEX Ultimate 3000; Thermo Scientific, Germany) using a C18 reversed-phase preparative column (Kinetex. 5 μm EVO, 250 Å~ 21.2 mm) with an eluting gradient of 0/0/100/100/0% solvent B (0.1% TFA in acetonitrile) at 0/5/35/38/40 minute. The solvent A in the HPLC system is 0.1% TFA in water. The product was validated using MALDI-TOF MS (AB SCIEX TOF/TOF 5800, Framingham, MA) and lyophilized for long-term storage at -20 ºC.

3.3 Results and Discussion

Magnetic particles are widely used in affinity-based pull-down assay, cell sorting, and library screening processes.[24] We reasoned that, by proper design, magnetic particles could be utilized in the preclear process in our library screening, removing resins with strong non-specific interactions. We tested our hypothesis on a newly synthesized NT-1 library, a bicyclic peptide library prepared on TentaGel resin.[18] We carried out procedures similar to those of the colorimetric method. As shown in Figure 3.3, we incubated 200 mg of the NT-1 library with a scrambled peptide (Biotin-PEG5-D-P-G-F-P-K-L-I-A-D-A-W-N-A-K(N_3)-$CONH_2$) for 2 hours. After the incubation, we washed the library to remove the excessive amount of the scrambled peptides. Later, we introduced magnetic M280 streptavidin-coated Dynabeads to the mixture, which was incubated for 1 hour at room temperature. We expected that resins with strong non-specific interactions would adsorb the scrambled peptide and subsequently coated by the magnetic particles, which could be pulled out by a magnet. However, we did not observe any resin being moved by the magnet. Moreover, very few magnetic particles were attached to the resin (Figure 3.4).

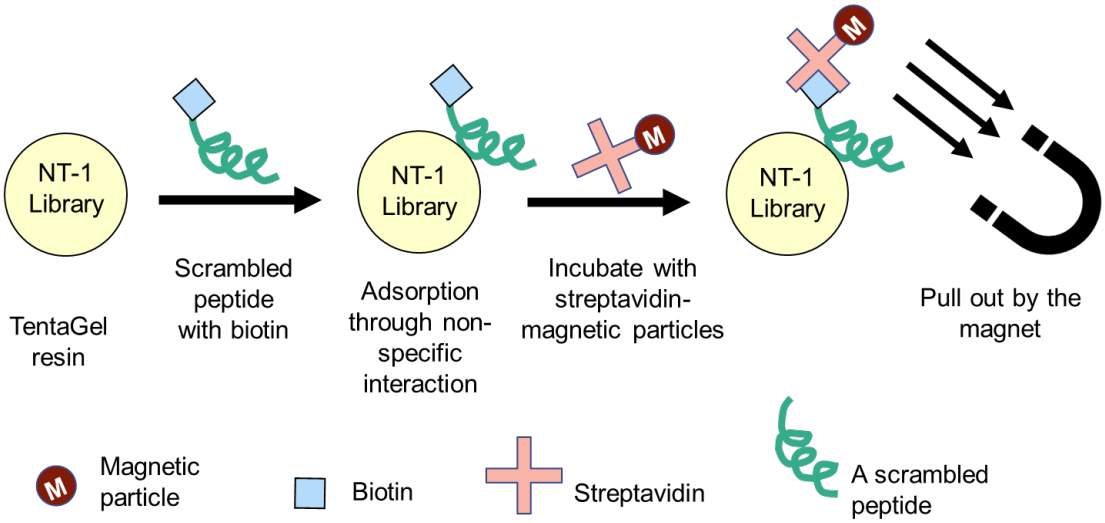

Figure 3.3 Proposed method to pull out the non-specific binding resins.

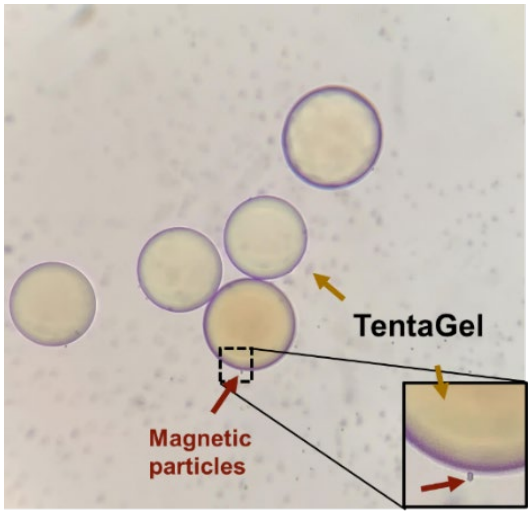

Figure 3.4 Very few magnetic particles adhere to the TentaGel resin. The TentaGel resins did not respond to the magnet.

We reasoned that the non-specific interaction between the scrambled peptide and the NT-1 library was too weak based on those results. In addition, the unique 3D bicyclic structure of the NT-1 library required stronger interactions to establish the binding. To optimize the preclear method, we resorted to starting with a positive control experiment. We modified the TentaGel resins with biotin residues and incubated them with the streptavidin-modified magnetic particles (Figure 3.5). To our surprise, we could not pull out any TentaGel resin by the magnet. It might be because that the biotin residues were too close to the surface, which made it difficult for the streptavidin molecules to adopt suitable orientations for binding.[25] Based on this hypothesis, we extend the gap between the biotin and the resin by adding a polyethylene glycol (PEG5) linker. Unfortunately, this attempt failed too.

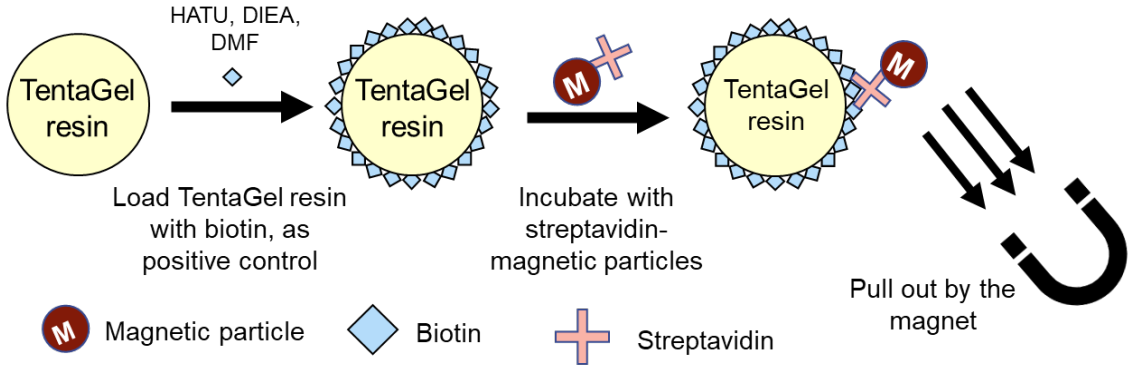

Figure 3.5 Efforts to pull out TentaGel resin loaded with biotin (positive control).

To further increase the distance between the two surfaces, we decided to use macromolecules as targets instead of peptides or small molecules like biotin. In this strategy, we utilized antibodies as targets, which significantly increased the gap between TentaGel and magnetic particles (Figure 3.6). We first incubate the library with an unconjugated rabbit polyclonal antibody (MAB1050 from R&D). After washing the resins, we introduced biotinylated anti-rabbit IgG to the system. Finally, we added streptavidin-coated magnetic particles. After these steps, we observed that the resins clustered together, and the cluster could be moved by the magnets (Figure 3.7).

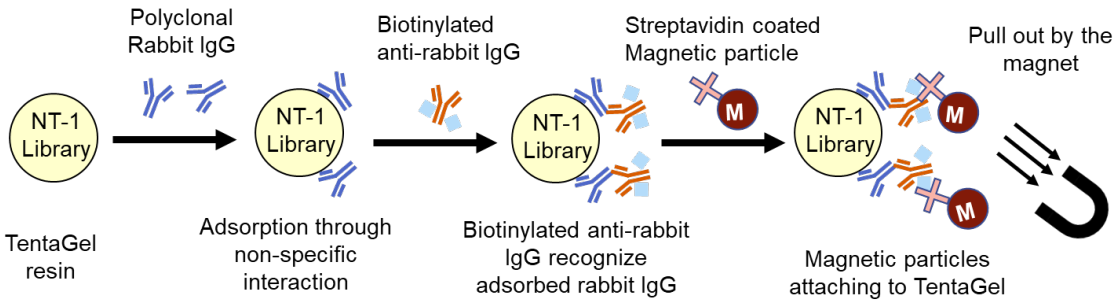

Figure 3.6 Pulling out high non-specific binding resins utilizing polyclonal antibodies to increase the distance between two surfaces.

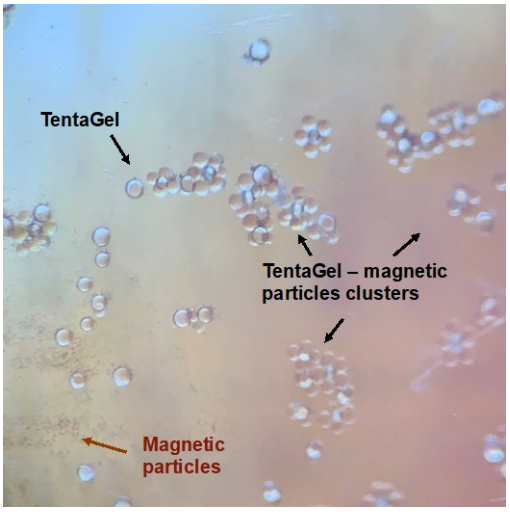

Figure 3.7 We observed that the TentaGel resins clustered together, and the clusters could be moved by the magnet.

When we checked the clusters under a microscope, we found that some resins were not coated with magnetic particles, yet still moved with the clusters. This would lead to false-negative results. To optimize the screening process, we tried to use the biotinylated bovine serum albumin (BSA-biotin) instead of two steps incubation (Figure 3.8). After incubation. We found that some TentaGel resins were nicely coated by the magnetic particles (Figure 3.9a), and they could be separated by the magnet (Figure 3.9b).

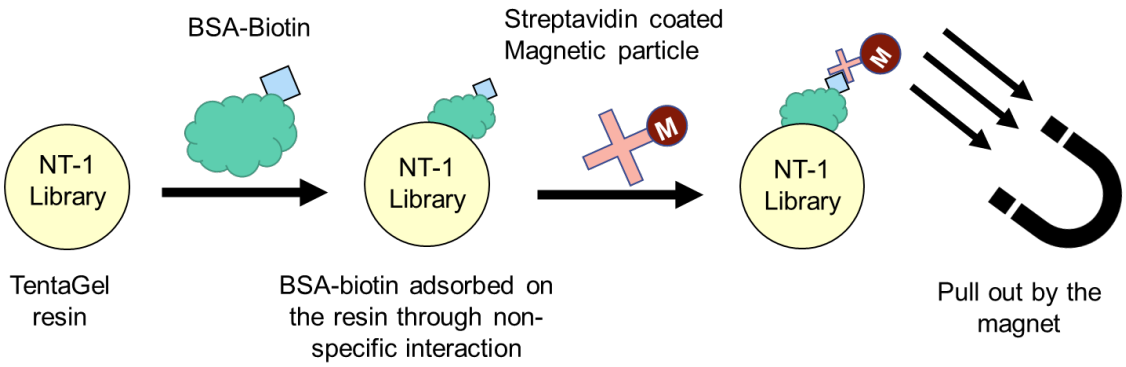

Figure 3.8 Magnetically pull out high non-specific binding resin utilizing BSA-biotin.

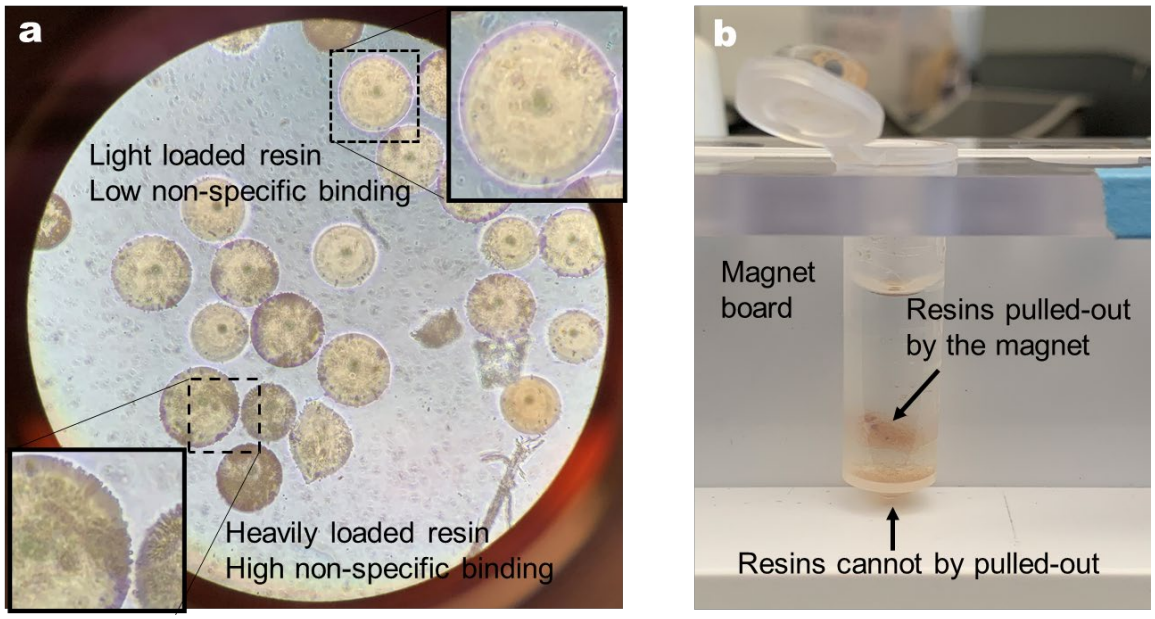

Figure 3.9 TentaGel resins with high and low non-specific binding can be clearly separated. (a) Under the microscope, some beads are heavily loaded with magnetic particles, while others are lightly loaded. (b) TentaGel resins with strong non-specific binding could be pulled out by the magnet board, while weak non-specific binding resins are enriched at the bottom of the 2 mL tube.

It is worth pointing out that other factors also affect the separation outcomes. For example, intensive mechanical agitation, such as vortex and centrifugation processes, are not preferred during the magnetic preclear screening process since the mechanical force will separate the magnetic particles and the TentaGel resin. Moreover, during the operation of the magnet separation, 1.5 mL conical tubes are not recommended because their steep slopes have less interaction surface with the magnet, leading to poor separation.

To validate the newly designed magnetic particle-based preclear process, we implemented the colorimetric method on the precleared and the magnetically pull-out beads (Figure 3.10a). We incubated the beads with avidin-alkaline phosphatase conjugates and added the 5-bromo-4-chloro-3-indolyl phosphate (BCIP) substrate. As a result, we found that the precleared resin did not become stained, while the magnetically pull-out beads were stained with light blue color (Figure 3.10b).

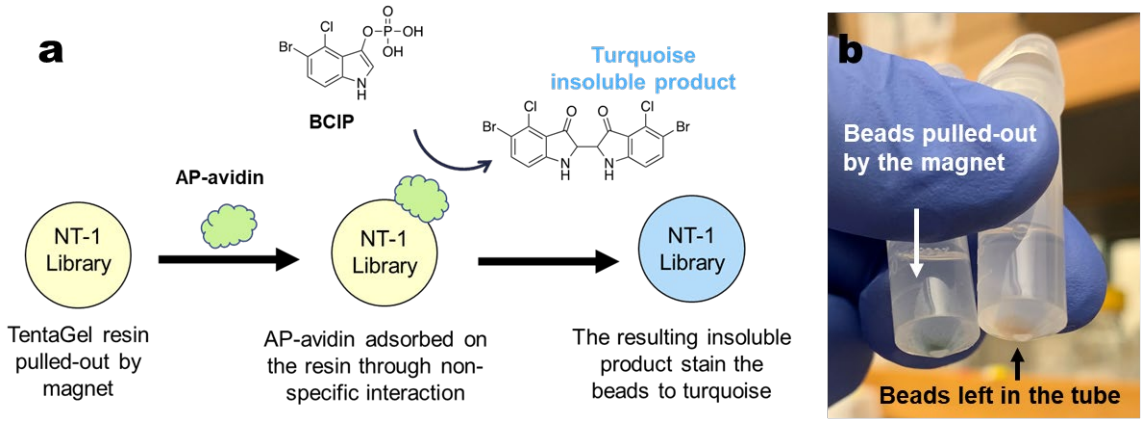

Figure 3.10 Validation of the magnetic particle-based preclear process. (a) standard colorimetric method for removing non-specific binding resins. (b) the resins that were pulled out by the magnet and the resins that were left in the tube were stained with AP-avidin and BCIP. The resins with a positive response to the magnet were stained to turquoise, while the beads with no response to the magnet remained clear.

3.4 Conclusion

In conclusion, we established a magnetic particle-based high throughput preclear screening method to remove the high non-specific interaction resins in a combinatory peptide library. We validated this method through the conventional enzymatic colorimetric pre-screening process. The method presented here can be implemented in the on-bead screening process with greatly improved efficiency and efficacy.

References

1. Goodnow, R. A.; Dumelin, C. E.; Keefe, A. D., DNA-encoded chemistry: enabling the deeper sampling of chemical space. Nature Reviews Drug Discovery **2017,** 16 (2), 131-147.

2. Martín, A.; Nicolaou, C. A.; Toledo, M. A., Navigating the DNA encoded libraries chemical space. Communications Chemistry **2020,** 3 (1).

3. Franzini, R. M.; Randolph, C., Chemical Space of DNA-Encoded Libraries. Journal of Medicinal Chemistry **2016,** 59 (14), 6629-6644.

4. Sohrabi, C.; Foster, A.; Tavassoli, A., Methods for generating and screening libraries of genetically encoded cyclic peptides in drug discovery. Nature Reviews Chemistry **2020,** 4 (2), 90-101.

5. Seelig, B., mRNA display for the selection and evolution of enzymes from in vitro-translated protein libraries. Nature Protocols **2011,** 6 (4), 540-552.

6. Pasqualini, R.; Ruoslahti, E., Organ targeting In vivo using phage display peptide libraries. Nature **1996,** 380 (6572), 364-366.

7. Smith, G. P., Phage Display: Simple Evolution in a Petri Dish (Nobel Lecture). Angewandte Chemie International Edition **2019,** 58 (41), 14428-14437.

8. Quartararo, A. J.; Gates, Z. P.; Somsen, B. A.; Hartrampf, N.; Ye, X.; Shimada, A.; Kajihara, Y.; Ottmann, C.; Pentelute, B. L., Ultra-large chemical libraries for the discovery of high-affinity peptide binders. Nat Commun **2020,** 11 (1).

9. Rohrbacher, F.; Deniau, G.; Luther, A.; Bode, J. W., Spontaneous head-to-tail cyclization of unprotected linear peptides with the KAHA ligation. Chemical Science **2015,** 6 (8), 4889-4896.

10. Walensky, L. D.; Bird, G. H., Hydrocarbon-Stapled Peptides: Principles, Practice, and Progress. Journal of Medicinal Chemistry **2014,** 57 (15), 6275-6288.

11. Anananuchatkul, T.; Chang, I. V.; Miki, T.; Tsutsumi, H.; Mihara, H., Construction of a Stapled α-Helix Peptide Library Displayed on Phage for the

Screening of Galectin-3-Binding Peptide Ligands. ACS Omega **2020,** 5 (11), 5666-5674.

12. Lau, Y. H.; De Andrade, P.; Wu, Y.; Spring, D. R., Peptide stapling techniques based on different macrocyclisation chemistries. Chemical Society Reviews **2015,** 44 (1), 91-102.

13. Lian, W.; Jiang, B.; Qian, Z.; Pei, D., Cell-Permeable Bicyclic Peptide Inhibitors against Intracellular Proteins. Journal of the American Chemical Society **2014,** 136 (28), 9830-9833.

14. Harker, E. A.; Daniels, D. S.; Guarracino, D. A.; Schepartz, A., β-Peptides with improved affinity for hDM2 and hDMX. Bioorganic & Medicinal Chemistry **2009,** 17 (5), 2038-2046.

15. Murrell, E.; Luyt, L. G., Incorporation of Fluorine into an OBOC Peptide Library by Copper-Free Click Chemistry toward the Discovery of PET Imaging Agents. ACS Combinatorial Science **2020,** 22 (3), 109-113.

16. Lian, W.; Upadhyaya, P.; Rhodes, C. A.; Liu, Y.; Pei, D., Screening Bicyclic Peptide Libraries for Protein–Protein Interaction Inhibitors: Discovery of a Tumor Necrosis Factor-α Antagonist. Journal of the American Chemical Society **2013,** 135 (32), 11990-11995.

17. Sarkar, P.; Li, Z.; Ren, W.; Wang, S.; Shao, S.; Sun, J.; Ren, X.; Perkins, N. G.; Guo, Z.; Chang, C.-E. A.; Song, J.; Xue, M., Inhibiting Matrix Metalloproteinase-2 Activation by Perturbing Protein–Protein Interactions Using a Cyclic Peptide. Journal of Medicinal Chemistry **2020,** 63 (13), 6979-6990.

18. Li, Z.; Shao, S.; Ren, X.; Sun, J.; Guo, Z.; Wang, S.; Song, M. M.; Chang, C.-E. A.; Xue, M., Construction of a Sequenceable Protein Mimetic Peptide Library with a True 3D Diversifiable Chemical Space. Journal of the American Chemical Society **2018,** 140 (44), 14552-14556.

19. Tamura, T.; Terada, T.; Tanaka, A., A Quantitative Analysis and Chemical Approach for the Reduction of Nonspecific Binding Proteins on Affinity Resins. Bioconjugate Chemistry **2003,** 14 (6), 1222-1230.

20. Chen, X.; Tan, P. H.; Zhang, Y.; Pei, D., On-Bead Screening of Combinatorial Libraries: Reduction of Nonspecific Binding by Decreasing Surface Ligand Density. Journal of Combinatorial Chemistry **2009,** 11 (4), 604-611.

21. Das, S.; Nag, A.; Liang, J.; Bunck, D. N.; Umeda, A.; Farrow, B.; Coppock, M. B.; Sarkes, D. A.; Finch, A. S.; Agnew, H. D.; Pitram, S.; Lai, B.; Yu, M. B.; Museth, A. K.; Deyle, K. M.; Lepe, B.; Rodriguez-Rivera, F. P.; McCarthy, A.; Alvarez-Villalonga, B.; Chen, A.; Heath, J.; Stratis-Cullum, D. N.; Heath, J. R., A General Synthetic Approach for Designing Epitope Targeted Macrocyclic Peptide Ligands. Angewandte Chemie International Edition **2015,** 54 (45), 13219-13224.

22. Shao, S.; Li, Z.; Cheng, H.; Wang, S.; Perkins, N. G.; Sarkar, P.; Wei, W.; Xue, M., A Chemical Approach for Profiling Intracellular AKT Signaling Dynamics from Single Cells. Journal of the American Chemical Society **2018,** 140 (42), 13586-13589.

23. Li, Z.; Cheng, H.; Shao, S.; Lu, X.; Mo, L.; Tsang, J.; Zeng, P.; Guo, Z.; Wang, S.; Nathanson, D. A.; Heath, J. R.; Wei, W.; Xue, M., Surface Immobilization of Redox-Labile Fluorescent Probes: Enabling Single-Cell Co-Profiling of Aerobic Glycolysis and Oncogenic Protein Signaling Activities. Angewandte Chemie International Edition **2018,** 57 (36), 11554-11558.

24. Hu, B.-H.; Jones, M. R.; Messersmith, P. B., Method for Screening and MALDI-TOF MS Sequencing of Encoded Combinatorial Libraries. Analytical Chemistry **2007,** 79 (19), 7275-7285.

25. Pezzi, H. M.; Niles, D. J.; Schehr, J. L.; Beebe, D. J.; Lang, J. M., Integration of Magnetic Bead-Based Cell Selection into Complex Isolations. ACS Omega **2018,** 3 (4), 3908-3917.

CHAPTER 4 Screening Metabolites-Binding Peptides from Peptide Libraries

4.1 Introduction

DNA stores the genetic information and passes it through RNA to proteins, which perform a vast array of functions within organisms, such as catalyzing metabolic reactions. Metabolites are the substrates and products of the metabolism, and their levels directly reflect the current bioactivities inside cells. Compared with DNA, RNA, and protein detection methods, the analytical tools for metabolites are underdeveloped. Amplification methods, such as the polymerase chain reaction (PCR), provide high sensitivity in nucleic acid detection. Similarly, amplification strategies for protein quantification are enabled by antibodies through enzymatic reactions or cascade immunorecognitions. As for metabolites, direct amplification methods like PCR are not available, and metabolite-specific antibodies are very rare. Therefore, the analytical tools to detect metabolites are very limited.

Currently, chemical probes are widely used to detect metabolites.[1, 2] Some chemoselective probes specifically react with specific functional groups, often resulting in optical output, for example, fluorescence readouts.[3-5] However, this method often suffers from low specificity because the probes target specific functional groups instead of whole molecules.[3, 6] Using molecular surrogates and labeled metabolites is another popular method to study metabolites. Nevertheless,

chemical tags, such as biotin and fluorophores, are big and may not faithfully represent metabolite bioactivities. Isotope tags like ^{13}C, ^{18}F are small,[7] but the related analytical methods (Mass spectrometry, NMR, and PET) are not sensitive enough to achieve high-resolution analysis.

An ideal analytical tool must exhibit high selectivity and specificity, as exemplified by antibodies. There are some metabolite-specific antibodies that exist. These antibodies are generated by eliciting immune responses from metabolite-antigen conjugates. For example, the immunogen for a commercially available anti-cAMP antibody (Abcam, EP8471) is cAMP-keyhole limpet hemocyanin conjugates. Such antibodies usually suffer from batch-to-batch inconsistency, low specificities, and affinities.

In the past two decades, aptamers emerge as a valuable tool for recognizing various chemical and biological targets, ranging from small molecules to a whole cell.[8-10] Compared with antibodies, aptamers have the advantage of easier production. However, aptamers also have limitations. For example, they are not stable in biological environments and prone to nuclease digestion. Another disadvantage of the aptamer is that the building block diversity is limited.

In biological systems, proteins are natural binding agents with high selectivity and specificity. Therefore, mimicking protein structures and getting similar functions are attractive to chemists.[11] Synthetic peptides are relatively small and can achieve a higher chemical diversity than aptamers of the same size. Many

peptides have been discovered to target specific proteins[12-14]. We reason that by proper design, peptides can be used to recognize metabolites. In this project, we tried to screen out peptide binders targeting metabolites from peptide libraries.

4.2 Materials and Methods

Materials:

2-Chlorotrityl chloride (CTC) resin and rink amide MBHA resin was purchased from Aapptec (Louisville, KY). TentaGel S-NH_2 resin (0.28 mmol/g) was purchased from Rapp Polymere GmbH (Tübingen, Germany). M280 streptavidin-coated Dynabeads was purchased from Thermo Fisher (Vilnius, LT). Biotinylated goat anti-rabbit IgG antibody and normal rabbit IgG control were purchase from Vector Laboratories and R&D system respectfully. All the Fmoc-protected amino acids were purchased from Anaspec (Fremont, CA) except Fmoc-Lys(N_3)-OH (Azido-lysine), which were purchased from Chem-Impex (Wood Dale, IL). Fmoc-Glu(OAll)-OH was purchased from Novabiochem (Latvia). Fmoc-L-propargylglycine was ordered from Matrix Scientific (Columbia, SC). Hoveyda-Grubbs Catalyst™ 2nd Generation (97%) was purchased from Sigma-Aldrich. Tetrakis(triphenylphosphine)palladium(0) (99%) was ordered from STREM CHEMICALS (Newburyport, MA). Cuprous Iodide (98.0%) was ordered from Spectrum (New Brunswick, NJ). The coupling reagent 2-(1H-benzotriazol-1-yl)-1,1,3,3-tetramethyluronium hexafluorophosphate (HBTU, 99.6%) was obtained from Chem-Impex (Wood Dale, IL). Diisopropylethylamine (DIEA) and cyanogen

bromide (CNBr) were purchased from ACROS (Pittsburg, PA). Triisopropylsilane (TIPS) was obtained from TCI (Portland, OR). 4-methylpiperidine was purchased from Alfa Aesar (Ward Hill, MA). α-cyano-4-hydroxycinnamic acid (CHCA) was obtained from Sigma-Aldrich (St. Louis, MO). Tris base, sodium phosphate dibasic anhydrous (Na_2HPO_4, 99.6%), sodium phosphate monobasic monohydrate (NaH_2PO_4, 99.4%), sodium chloride (NaCl), ascorbic acid, Tween 20, bovine serum albumin (BSA), acetonitrile (CH_3CN), diethyl ether (Et_2O), ethyl acetate (EA), N,N′-dimethylformamide (DMF), and dichloromethane (DCM) were purchased from Thermo Fisher Scientific (Waltham, MA).

Buffers:

1× TBS: 20 mM Tris and 150 mM NaCl, pH 7.6; 1× TBST: TBS, 0.05% Tween20; 1× PBS: 150 mM NaCl, 10mM phosphate buffer, pH 7.4; AP buffer: 100 mM Tris, 150 mM NaCl, 1 mM $MgCl_2$, pH 9.0.

Methods:

Construction of the monocyclic library. The monocyclic peptide library was synthesized as described in J. Am. Chem. Soc. 2018, 140, 42, 13586–13589.[15] Specifically, the linear peptide precursors were synthesized via solid-phase peptide synthesis (SPPS) protocols through a “split-and-pool” method on TentaGel resin, except for azido-lysine, which loading equivalents on the resin is only 80%, resulting in a linear one-bead-two-compounds linear peptide library. Cyclization of peptides was performed overnight at RT by treating the beads with five equivalents of CuI and 15 equivalents of L-ascorbic acid in a solution of 20%

2,6-lutidine in DMF. After the cyclization, the absorbed copper catalyst was then removed by washing the beads extensively with washing solution (5% w/v sodium diethyldithiocarbamate and 5% v/v DIEA in DMF). After cyclization, a click handle L-propargylglycine was appended to the library. Before the screening, all protection groups were removed by a TFA cleavage solution (TFA: TIPS: ddH_2O; 95:2.5:2.5).

Synthesis of GSH screening target. The GSH screening target was synthesized on CTC resin. Fmoc-Cys(Trt)-OH, Fmoc-Gly-OH were attached to the CTC resin via Fmoc SPPS. Fmoc-Glu-OAll was appended to the sequence via the side chain. Fmoc-Lys(N_3)-OH, secondary linker and Rhodamine B were attached the peptide sequentially. The beads were agitated with a mixture of $Pd(PPh_3)_4$ (65 mg, 55 μmol), $PhSiH_3$ (555 uL, 6.5 mmol) in DCM (5 mL) at rt for 2 hours to remove ally protection group. After DMF wash, the GSH screening target was cleaved from the resin via a TFA cleavage solution (TFA: TIPS: ddH_2O; 95:2.5:2.5). The peptide was purified via a preparative UPLC system, and characterized by MALSI-TOP-MS.

Construction of NT-1 library. The NT-1 library was synthesized as described in J. Am. Chem. Soc. 2018, 140, 44, 14552–14556.[16] Specifically, three stages were involved in NT-A library synthesis, including linear peptide precursor synthesis, Cu(I)-catalyzed azide-alkyne cycloaddition CuAAC click reaction, and ring-closing metathesis (RCM) reaction, and global deprotection.

Monocyclic peptide screening. The monocyclic peptide library screening process involved two parts, preclear screening and target screening.

For the preclear screening process, 500 mg of resin from the library was swelled in TBS (25 mM Tris, 150 mM NaCl, pH = 7.5) for 2 hours and blocked in 1% BSA/TBST overnight at 4 °C. After washed with 0.1% BSA/TBST (TBS with 0.05% Tween 20) at 4°C (5 min × 3), the beads were incubated with 10 μM linker-Rhodamine B conjugate in 0.1% BSA/TBST for 5 – 6 hours at RT. Afterwards, the library was washed with Guanidine HCl buffer, MilliQ H_2O stringently and decolorized in DMF overnight at RT. Following washes with water, the colored beads were manually picked out under a microscope in TBST.

For the target screening process, the beads were incubated with the 10 uM GSH-Rhodamine in 0.1% BSA/TBST for 5 – 6 hours at RT. Following washes with 0.1% BSA/TBST (5 min × 3), TBST (5 min × 3) and TBS (5 min × 3), the beads were treated with 7.5 M guanidine-HCl (pH 2.0) for 2 h. After washing with water, the beads were washed with DMF overnight to remove all noncovalent binding. Later the beads were swelled in TBST, and the colored beads were picked out under a microscope. Finally, the hit beads were pipetted and washed successively with water, DMF, and DCM. After air-drying, the beads were subjected to Edman degradation and cleavage for sequencing.

Monocyclic peptide linearization and cleavage. Edman degradation steps were adapted from the literature.[17] Cycle 1 (to remove the Az4 click handle): Hit beads were transferred into an autosampler vial. The coupling reaction was

initiated by adding 50 μL of PhNCS solution (2.5% in 1:1 pyridine/H_2O). The vial was flushed with N_2 for 10 s, sealed with a stopper and put in a 50 °C water bath for 30 min. Afterward, the solution was removed, and the vial was carefully washed with EA 3 times. After air-drying, the vial was added with 100 μL of TFA, flushed with N_2 for 10 s, sealed with a stopper, and allowed to react for 10 min at 50 °C. The solution was then diluted with 200 μL of EA and removed. The beads were washed carefully with EA twice and air-dried. Cycle 2 (to open the ring): The coupling and cleavage reactions were performed again following the same procedures as in Cycle 1. The resulting beads containing the linear anilinothiazolinone (ATZ)-peptide were treated in 20% TFA solution and heated to 80 °C for 5 min. Following the removal of the solution, the beads were washed carefully with EA and dried.

Following the manual Edman degradation, each hit bead was transferred to a microcentrifuge tube containing pure water (10 μL). After the addition of CNBr (10 μL, 0.50 M in 0.2 N HCl solution) the reaction vessel was purged with argon and then placed under microwave for 1 min. The resulting solution was concentrated under a centrifugal vacuum for 2 hours at 45 °C.

Bicyclic peptide library screening. The library was precleared through the magnetic particle preclear process as described in chapter 2. The precleared process was validated through colorimetric assay as described in chapter 2. The colored beads were manually picked out under a microscope.

We use the colorimetric method to screen the small molecule binders. The precleared library was swelled in TBS buffer for 2 hours and incubated with biotinylated cAMP/cGMP (10 μM in 1× TBS) overnight at 4 °C. Later, the library was washed with 1× TBS (3 × 3 mL) and incubated with Avidin-AP (1/10000 dilution) at 4 °C for 1 hour. Finally, 10 μL BCIP substrate (50 mg/mL) was introduced to the systems with 1 mL of AP buffer. The color was developed at room temperature for 30 min, and the reaction was quenched by 50 μL of concentrated HCl. The colored bead was picked out manually under a microscope. Later the hit beads were treated with 7.5 M guanidine-HCl (pH 8.0) for 2 h, washed successively with water, DMF, and DCM. After air-drying, the beads were subjected to linearization and cleavage for sequencing.

Linearization and cleavage of bicyclic peptide library. The hit beads (color stripped already) were incubated with phenyl isothiocyanate (2.5% v/v) in pyridine: water (1:1) and heated to 50 °C for 30 min. The solution was drained, and the beads were washed with DMF ×3, EtOAc ×3 and dried. The beads were agitated with a mixture of Pd(PPh3)4 (13 mg, 11 μmol), $PhSiH_3$ (111 uL, 1.3 mmol) in DCM (1 mL) at rt for 2 hours. The resulting dark solution was removed, and the beads were washed with a) DMF ×3, b) chelating solution (Sodium diethyldithiocarbamate (5% w/v), DIEA (5% v/v) in DMF) ×3, c) DMF ×3, d) 50% DMF in H_2O ×3, e) DMF ×3, f) EtOAc ×3 and dried. Then the beads were treated with TFA (degassed with argon) and heated to 50 °C for 10 min; after removal of

the TFA, 20% TFA in H_2O (v/v) was added and heated to 80 °C for 10 min. The beads were washed with DMF, EtOAc and dried.

For the photocleavage, 50 uL THF (degassed with argon) was added in a 1.5 mL centrifuge tube with a single bead inside. The tube was irradiated under a UV lamp (Llak-Ray B-100A high intensity UV lamp, 100 W, 365 nm) at rt for 30 min. The resulting solution was evacuated by SpeedVac concentrator (Savant SPD121P) and ready for MALDI-TOP-MS sequencing.

Solid-phase peptide synthesis. Peptides were synthesized on Rink Amide MBHA resin via the standard Fmoc solid-phase peptide synthesis (SPPS) chemistry. For Fmoc deprotection, the resin was agitated with piperidine (20%v/v in DMF, 3x5 min) and washed with DMF 5 times. To couple amino acids to the resin, a DMF solution of Fmoc-AA(protection group)-OH (5 eq.), HBTU (4.75 eq), and DIEA (15 eq.) was mixed for 3 minutes. Then the mixture was added to the resin and agitated at room temperature for 1 hour. For peptide side-chain global deprotection and cleavage, the resin was washed with DCM and dried with compressed airflow. The beads were then cleaved in a TFA cleavage solution (TFA: TIPS: ddH_2O; 95:2.5:2.5) for 2 hours. Before the RP-HPLC cleavage, the peptides were precipitated out by cold ether. All peptides were purified on the RP-HPLC (DIONEX Ultimate 3000; Thermo Scientific, Germany) using a C18 reversed-phase preparative column (Kinetex. 5 μm EVO, 250 Å~ 21.2 mm) or a C18 reversed-phase semi-preparative column (Kinetex. 5 μm EVO, 250 Å~ 10

mm). The product was validated using MALDI-TOF MS (AB SCIEX TOF/TOF 5800, Framingham, MA) and lyophilized for long-term storage at -20 ºC.

4.3 Results and discussions

We first chose to screen glutathione (GSH) against a cyclic peptide library as a proof of concept. GSH is very important for scavenging reactive oxygen species (ROS) and maintaining the redox balance in cancer cells[18-23], which is crucial to support tumor progression.

Because linear peptides are flexible, their binding with targets accompanies a decrease in entropy. As a result, the entropic penalties often lead to a weak binder. To overcome this issue, we pay the entropic loss beforehand by cyclizing the peptides, expecting peptide binders with higher affinities.

We constructed a one-bead-two-compound monocyclic/linear peptide library (Figure 4.1) using 18 amino acids as building blocks. The 20% linear peptides on the resin aid the sequencing process. This library was built on the TentaGel resins using the split-and-pool method. A methionine was installed at the C-terminus of the library, allowing the cyanogen bromide cleavage, releasing peptides from resins after screening. We incorporated azido-lysine and propargylglycine in the sequences and cyclized the peptides by CuAAC. Lastly, we capped the N-terminus with an extra propargylglycine, which was critical to the screening process.

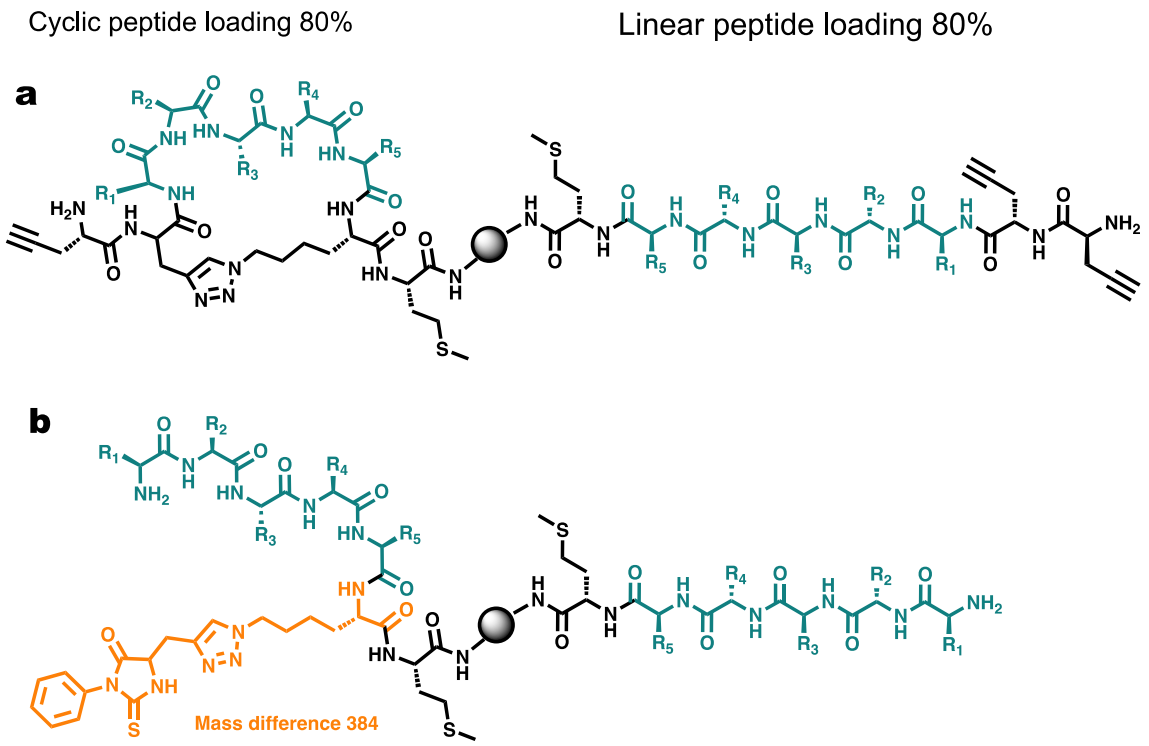

Figure 4.1 a) The design of the one-bead-two-compounds monocyclic peptide library. R_1-R_5 are the 18 natural L-amino acids side chains, excluding Cys and Met. b) After two rounds of Edman degradation, the cyclic peptides contain a PTH group, resulting in a 384 mass difference compared to linear peptides.

We synthesized a rhodamine-tagged GSH as the screening target (Figure 4.2 a). This molecule was prepared on the 2-chlorotrityl chloride (CTC) resins, yielding an uncapped C-terminus. After attaching glycine and cysteine through SPPS, we appended a glutamic acid using the side chain of Fmoc-Glu-OAll. Later, we added a secondary amine linker and Rhodamine B to the structure. Finally, we performed a de-allylation reaction and global deprotection to release the targets from the resins (Figure 4.2 b). We also prepared a linker-Rhodamine b (Figure 4.2 c) for the preclear process.

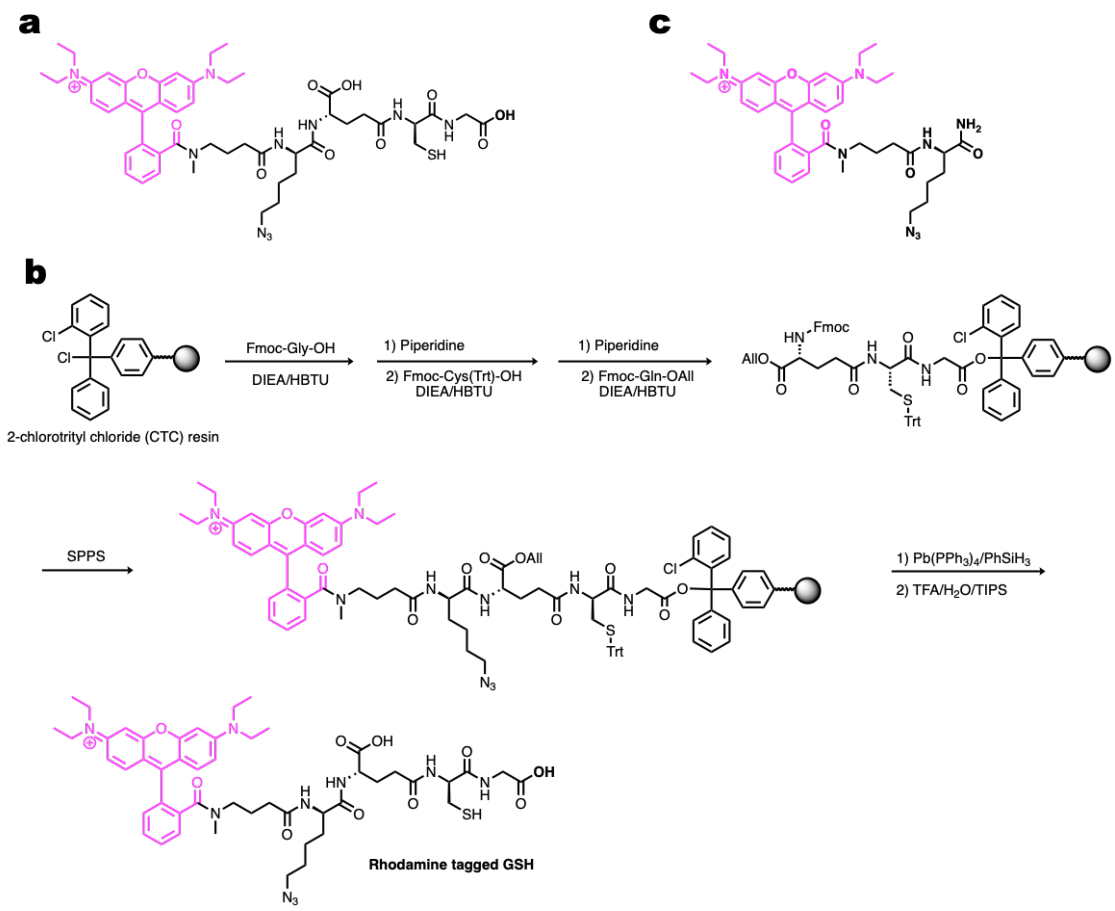

Figure 4.2 The design of the GSH screening target. a) The structure of the Rhodamine-tagged GSH for target screening. b) The synthesis of the Rhodamine-tagged GSH on the CTC resin. c) the structure of linker-Rhodamine conjugate as a preclear screening agent.

To identify peptides that bind to GSH, we performed a high-throughput screening on the one-bead-two-compound monocyclic/linear peptide library (Figure 4.3). To remove the non-specific binding beads, we incubated the library with the linker-Rhodamine conjugate. After washing the library, we picked out beads that were colored in red. Then, we incubated the library with the Rhodamine-tagged GSH target. A proximity-based *in situ* click reaction would covalently link the Rhodamine-tagged GSH to the beads upon a binding event. After stringent washing steps, we manually picked out the colored beads under a microscope and subjected them to linearization and sequencing.

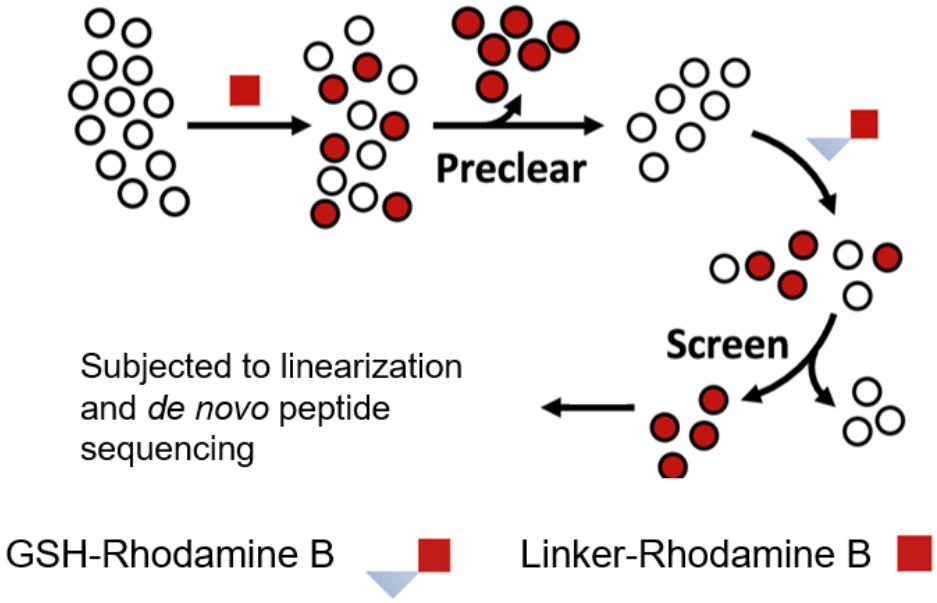

Figure 4.3 The screening process of GSH. The library was precleared by GSH-Rhodamine conjugate, and the colored beads were manually picked out. Then the precleared library was incubated with the screening agent Rhodamine tagged GSH. The hits were isolated and subjected to MS sequencing.

The primary method to identify the sequence of peptides is *de novo* peptide sequencing by mass spectrometry. However, peptides have to be in a linear conformation to be fragmented, generating b ions and y ions. We performed two rounds of Edman degradation (Figure 4.4) to open the ring of the monocyclic peptides. The first round of Edman degradation released the bounded structures from the proximity-based *in situ* click reaction. The second round of Edman degradation opened the ring formed by CuAAC. After linearization, we released the peptides from the library through a cyanogen bromide cleavage. Finally, we submitted peptides for MALDI-TOF MS sequencing.

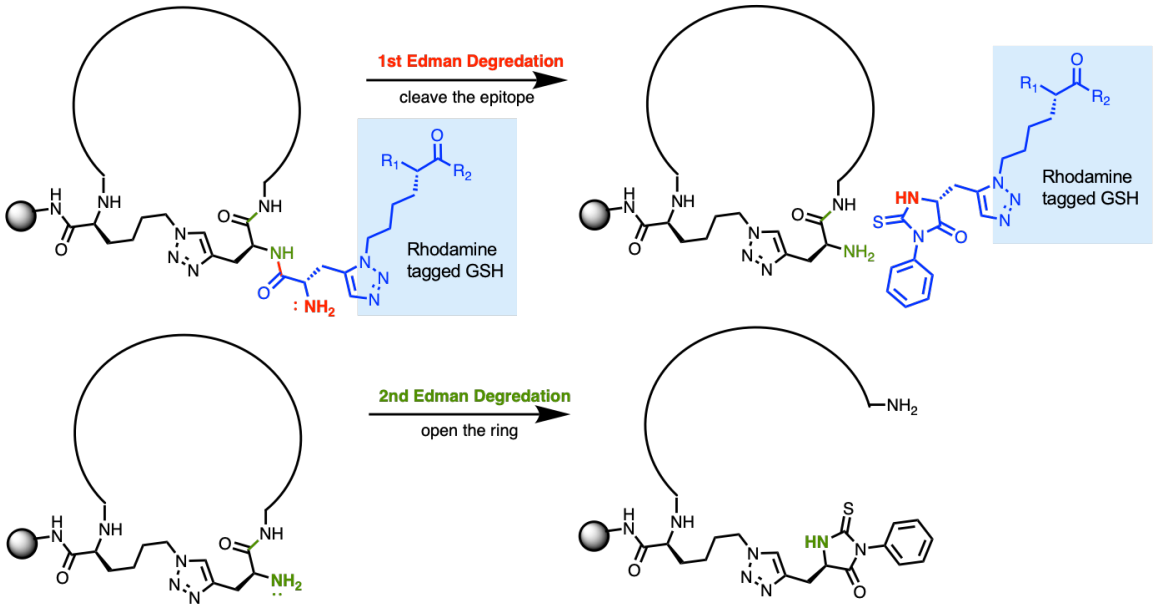

Figure 4.4 The linearization of monocyclic peptides. The first round of Edman degradation removed the screening agent, and the second round of Edman degradation opened the ring.

After screening, we solved one hit, cy(VFRYR) (Figure 4.5a). We used isothermal titration calorimetry (ITC) to measure the binding affinity of the cy(VFRYR) and GSH. ITC experiment allows us to access the thermodynamic parameters of a binding interaction and calculate the binding affinity. The binding affinity resulting from the ITC was not good (Figure 4.5b). We reasoned that it was rooted in the design of the library. The monocyclic peptide structure is sufficient when targeting proteins. However, compared with protein surfaces, metabolites are too small and have fewer interacting sites. In this case, peptides did not serve as classical ligands but molecular hosts binding with the small molecules. Therefore, we reasoned that a topological complex structure is needed to develop the metabolite binders.

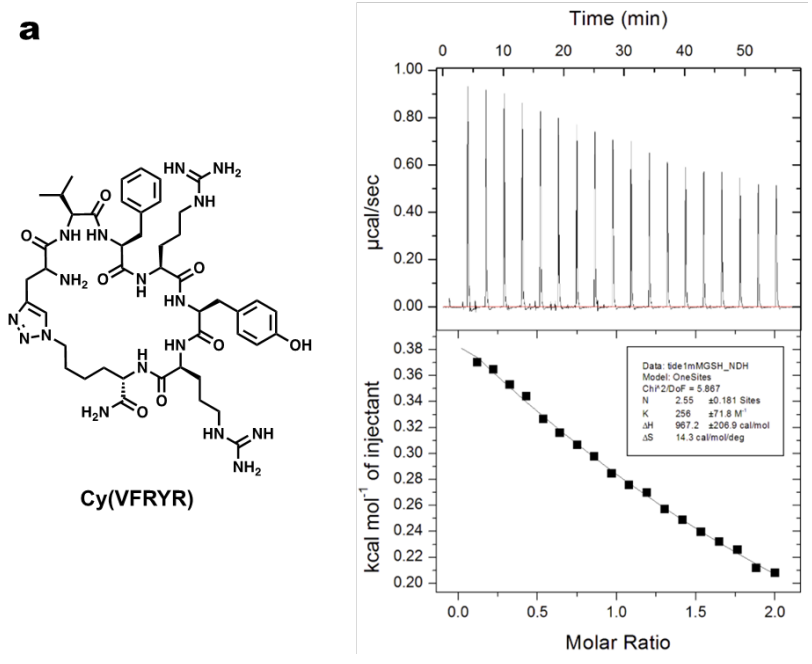

Figure 4.5 (a) The structure of the hit cy(VFRYR), which potentially binds with GSH. (b) ITC experiment results showed poor binding affinities.

We decided to apply the newly designed bicyclic peptide libraries (Figure 4.6) to achieve this goal. This bicyclic peptide library provides access to a 3D-diversifiable chemical space. Moreover, the bicyclic structures are more rigid than the monocyclic structures, further reducing the entropic penalty.

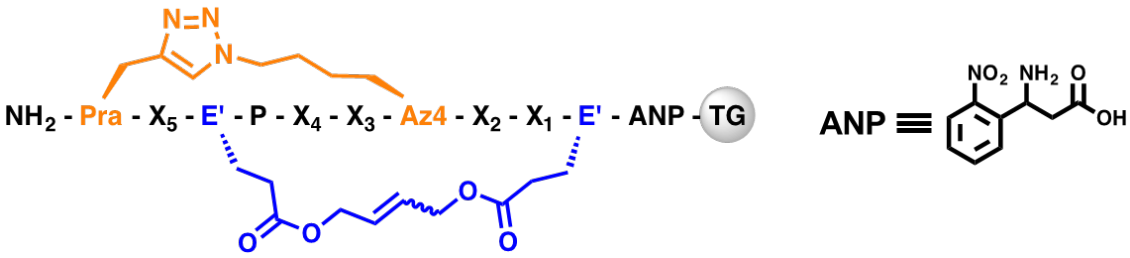

Figure 4.6 The design of the bicyclic peptide library.

We constructed two bicyclic peptide libraries, named NT-1 and NT-2. The only difference between these two peptide libraries was the stereo conformation of the azido-lysine. In NT-1 library, the azido-lysine was L-configuration, while in NT-2 library, it was D-configuration. We prepared these libraries according to the literature[16] (Figure 4.7). Specifically, we constructed linear peptide precursors on the TentaGel resins, with a photocleavable linker 3-amino-3-(2-nitrophenyl)propionic acid (ANP) attached to the resins. We closed the first ring using a CuAAC click reaction and removed the Cu catalyst with sodium diethyldithiocarbamate (NaDTC). We cyclized the second ring with a ring-closing metathesis (RCM) reaction and later removed the catalyst by tris(hydroxymethyl)phosphine (THP) solution. Lastly, after Fmoc removal by piperidine, we uncapped all the side chains by a global deprotection process.

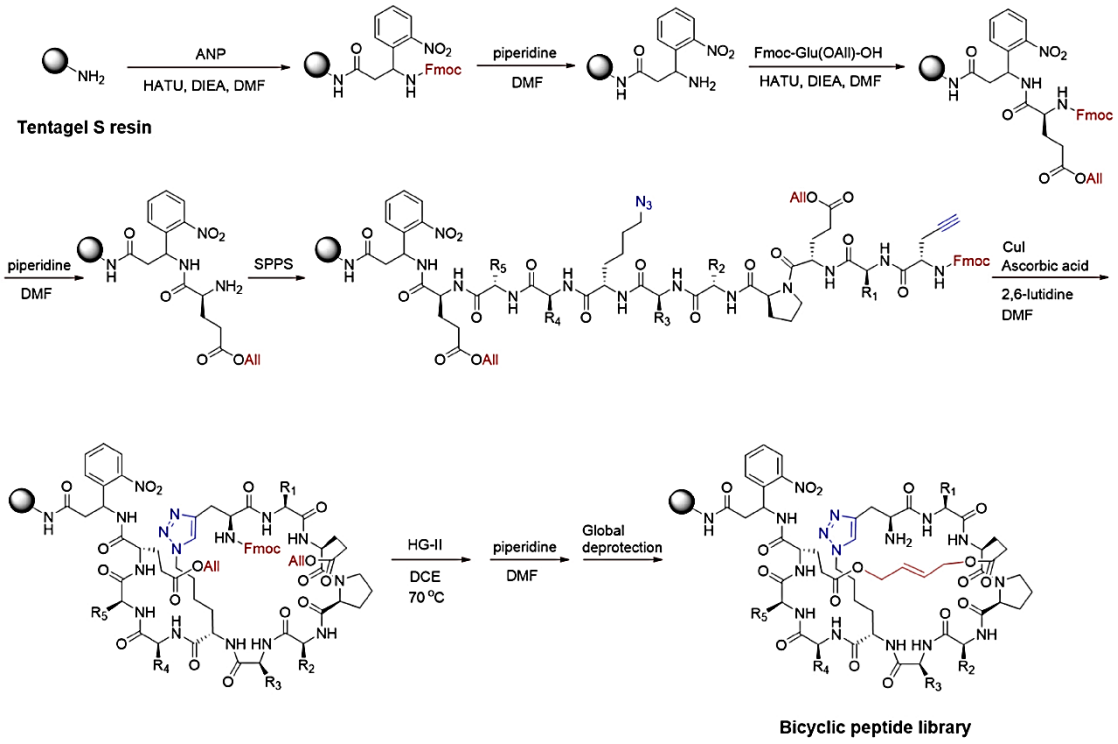

Figure 4.7 Synthesis of the bicyclic peptide library.

As a proof of concept of bicyclic peptide library screening, we chose cyclic adenosine monophosphate (cAMP) and cyclic guanosine monophosphate (cGMP) as targets (Figure 4.8 a). cAMP is a key second messenger that plays an essential role in intracellular signaling transduction. It is synthesized by adenylate cyclase upon activation of the G-protein coupled receptors (GPCR). cAMP transfers extracellular signals into the cells and involves the activation of protein kinases. Like cAMP, cGMP is also a second messenger, activating intracellular protein kinases in response to extracellular ligands binding to the cell surfaces. We chose these two metabolites as the targets to test the specificity of the screened-out small molecule binders. We use cAMP-biotin and cGMP-biotin conjugates (Figure 4.8 b) as screening agents.

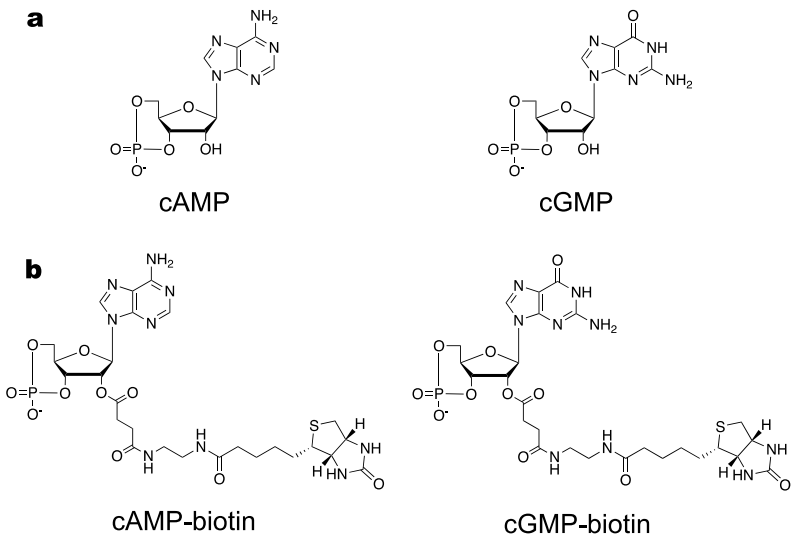

Figure 4.8 Structures of (a) cAMP, cGMP, and (b) cAMP-biotin and cGMP-biotin

In the screening process (Figure 4.9), we used magnetic particles to remove the beads with strong non-specific interactions, as described in chapter 2. We incubated the screening targets (cAMP/cGMP-biotin) with the libraries for the target screening process. After washing the library, removing the unbounded screening targets, we incubated the library with avidin-alkaline phosphatase (avidin-AP) and its substrate 5-bromo-4-chloro-3-indolyl phosphate (BCIP). Binding interactions between cAMP/cGMP and the peptides anchored the alkaline phosphatase through the biotin-avidin interaction. As a result, the resins with hit sequences were colored in light blue. We manually picked out around 40 blue beads and submitted them to the sequencing process.

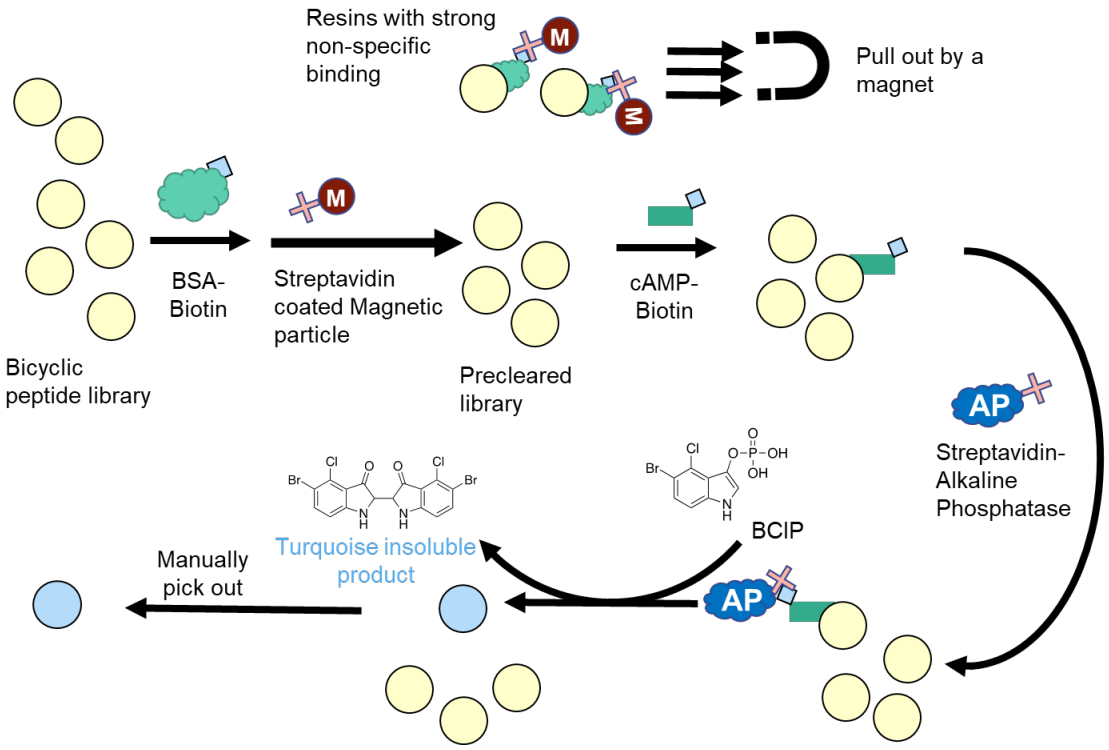

Figure 4.9 Screening procedure for cAMP and cGMP.

We isolated the NT-1 and NT-2 library hits and removed all non-covalent binding molecules with stringent wash. We linearized the bicyclic structure to get the sequence information from tandem mass spectrometry. We removed the extra propargylglycine at the N-terminus by Edman degradation. The first ring was opened by partial Edman degradation, leaving all primary amine groups protected by the phenyl thiohydantoin (PTH) group. The second RCM ring was opened by a de-allylation reaction using the palladium catalyst. And finally, we finished the partial Edman degradation process, resulting in a linear conformation. The peptide was released from the resin by photocleaving and submitted to MS/MS analysis to get the sequence information.

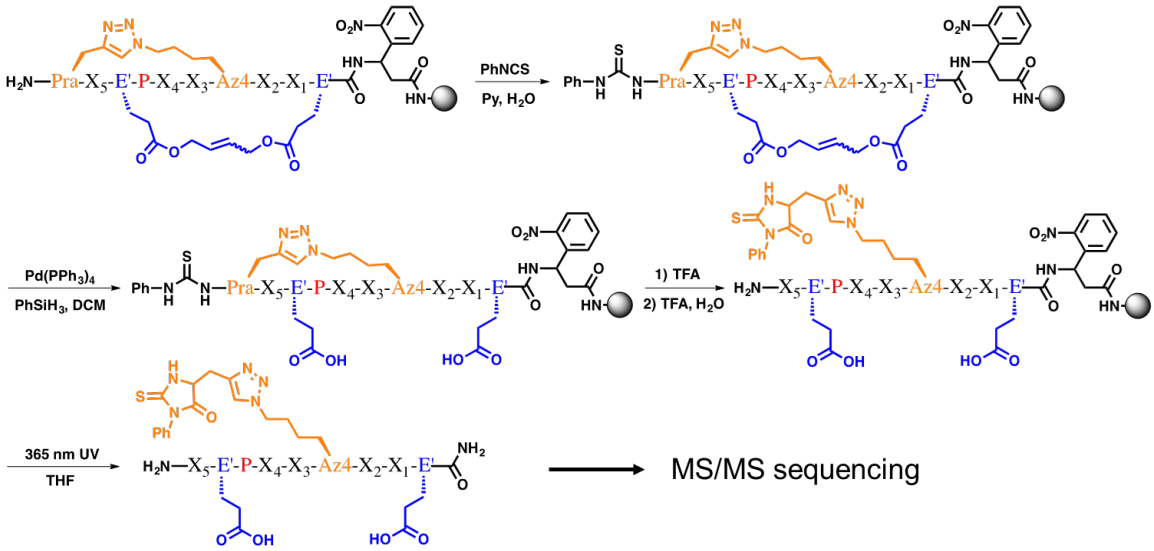

Figure 4.10 Linearization procedure for the bicyclic peptide libraries.

We identified eight sequences and six sequences that potentially bind with cAMP and cGMP respectfully (Table 4.1 - 4.2, Figure 4.12-4.20 in section 4.5). These sequences are rich in arginine and tyrosine residues. We hypothesized that the positive charges on the arginine and the aromatic structures on the tyrosine contributed to the binding with cAMP and cGMP.

Table 4.1 List of cAMP binding hits. Pra, L-propargylglycine; E(alloc), alloc-protected glutamic acid; Az4(D), D-azidolysine; Az4(L), L-azidolysine.

name	**cAMP binding hits**
D24	**Pra – R – E(alloc) – P – Y – Y – Az4(D) – N – R – E(alloc)**
H13L	**Pra – R – E(alloc) – P – L – Y – Az4(L) – R – R – E(alloc)**
H13I	**Pra – R – E(alloc) – P – I – Y – Az4(L) – R – R – E(alloc)**
H18L	**Pra – Y – E(alloc) – P – L – R – Az4(L) – Q – R – E(alloc)**
H18I	**Pra – Y – E(alloc) – P – I – R – Az4(L) – Q – R – E(alloc)**
H19	**Pra – N – E(alloc) – P – Y – F – Az4(L) – R – R – E(alloc)**
H7PR	**Pra – R – E(alloc) – P – P – R – Az4(L) – Q – R – E(alloc)**
H7RP	**Pra – R – E(alloc) – P – R – P – Az4(L) – Q – R – E(alloc)**

Table 4.2 List of cGMP binding hits. Pra, L-propargylglycine; E(alloc), alloc-protected glutamic acid; Az4(D), D-azidolysine; Az4(L), L-azidolysine.

name	**cGMP binding hits**
J6	**Pra – N – E(alloc) – P – R – Y – Az4(D) – Y – R – E(alloc)**
J11	**Pra – R – E(alloc) – P – R – Y – Az4(L) – Q – R – E(alloc)**
J23	**Pra – Y – E(alloc) – P – R – R – Az4(L) – R – Y – E(alloc)**
K8L	**Pra – R – E(alloc) – P – L – R – Az4(L) – Y – R – E(alloc)**
K8I	**Pra – R – E(alloc) – P – I – R – Az4(L) – Y – R – E(alloc)**

We resynthesized and purified the hit sequences at the milligram scale to get access to the binding properties. Since the peptide binders and metabolites are small molecules, any modification may change the binding behaviors. Thus, label-free methods are highly desired to get access to the binding affinities. We started with the ITC test for the binding affinity between peptides (D24, H13L, H18L) and cAMP. However, the heat change upon binding may be too little to be detected by ITC, and we cannot measure the binding affinity through it. We reason that it might cause by the buffer difference in syringes and the cells. Unlike standard ITC experiments, we cannot dialysis our sample to make the buffer system the same. Another approach to get the binding affinity is titrating cAMP with the hits peptides and measuring the UV-Vis absorbance change. We observed UV-Vis change when titrating D24 to cAMP, which hints at a potential binding of D24 with cAMP (Figure 3.20). Yet, these results need to be further validated.

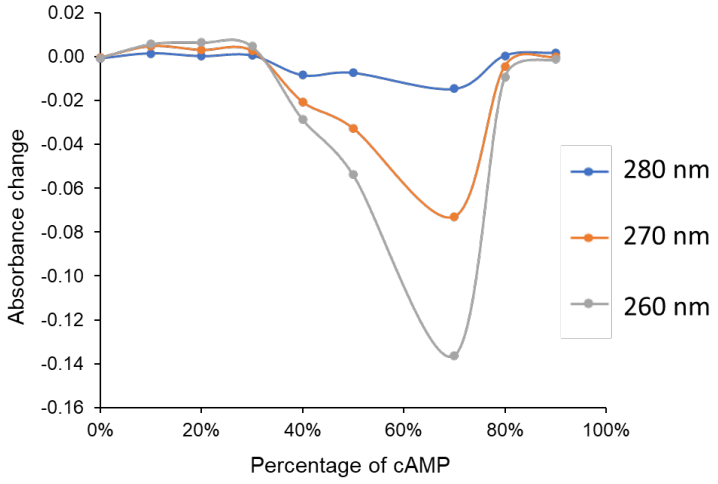

Figure 4.11 Job plot of cAMP and D24 binding. The total concentration of cAMP and D24 is 0.4 mM. We observed UV-Vis absorbance decrease up when cAMP mixed with D24.

4.4 Conclusion

In conclusion, we constructed monocyclic peptide and bicyclic peptide libraries and screened peptides against small molecules, including GSH, cAMP, and cGMP. We expect to find peptide binders to small molecules. After the screening, linearization, and MS/MS sequencing processes, we found one hit from the monocyclic peptide library that may bind with GSH, and fourteen hits from the bicyclic peptide libraries that may bind with cAMP and cGMP respectfully.

4.5 Mass spectroscopy data for hit sequences

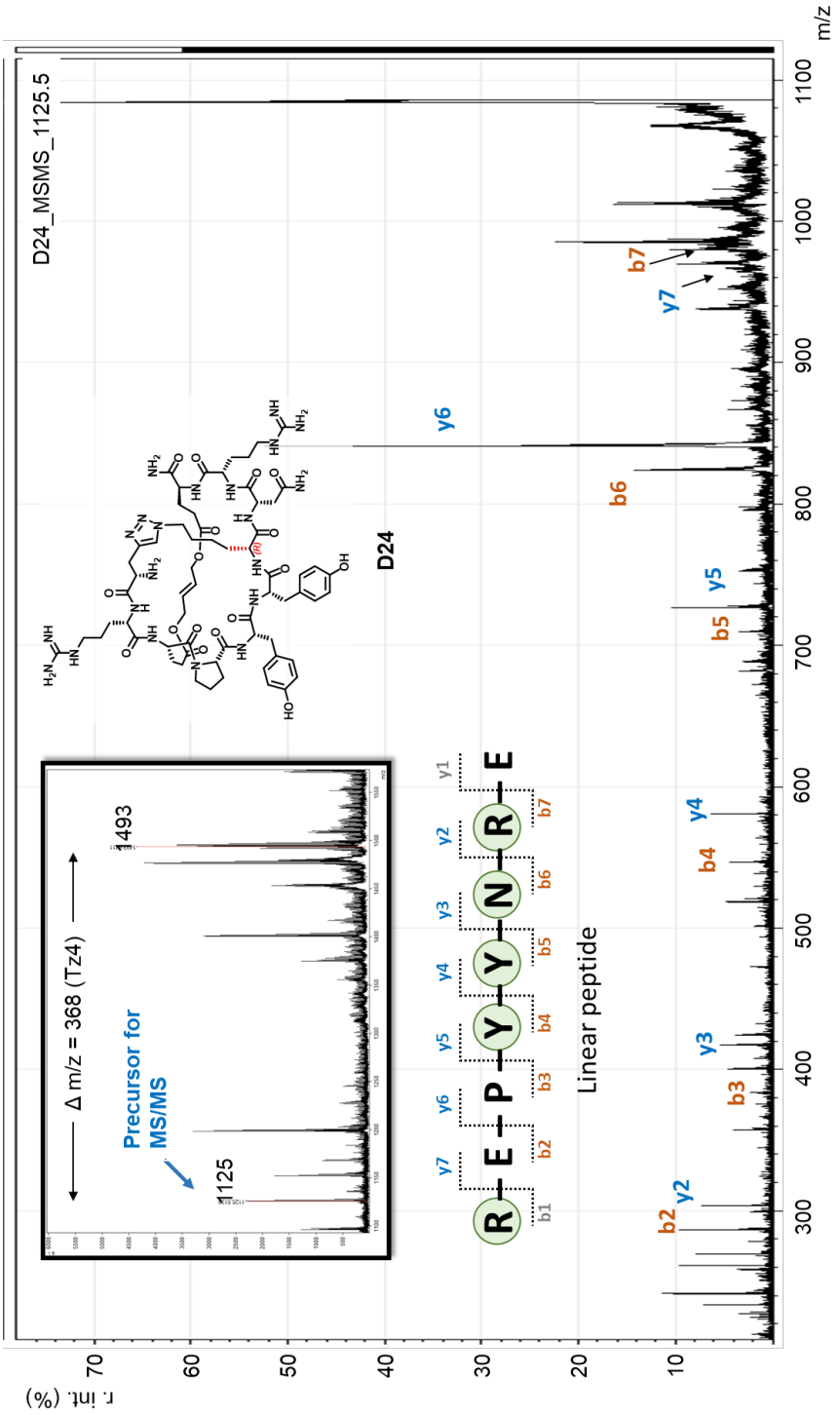

Figure 4.12 Mass spectrum for D24. MS1 is shown on upper left panel and MS /MS data is shown on the bottom. Y ions are shown in blue and b ions are shown in orange. Not founded ion are shown in grey.

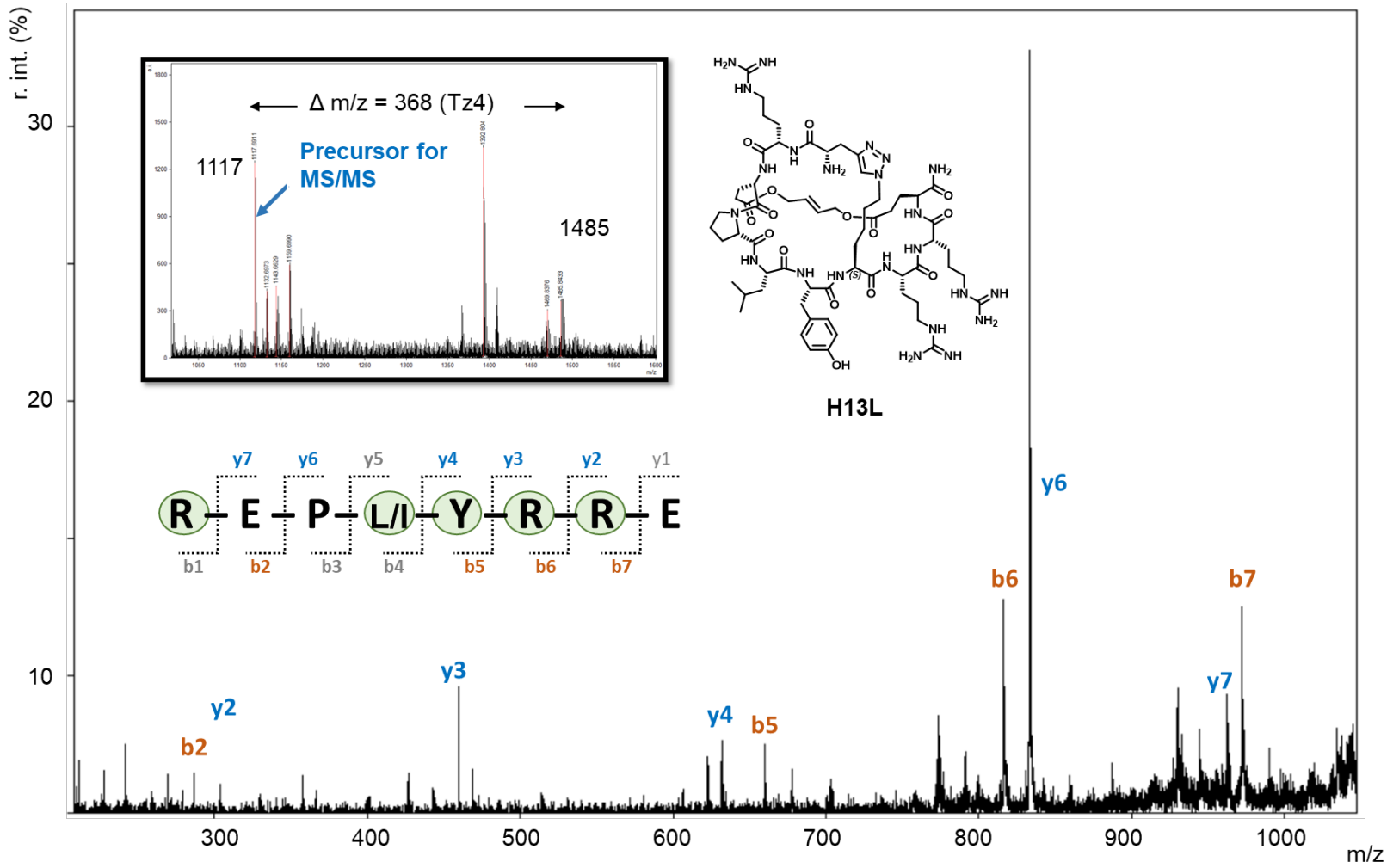

Figure 4.13 Mass spectrum for H13L. MS1 is shown on upper left panel and MS /MS data is shown on the bottom. Y ions are shown in blue and b ions are shown in orange. Not founded ion are shown in grey.

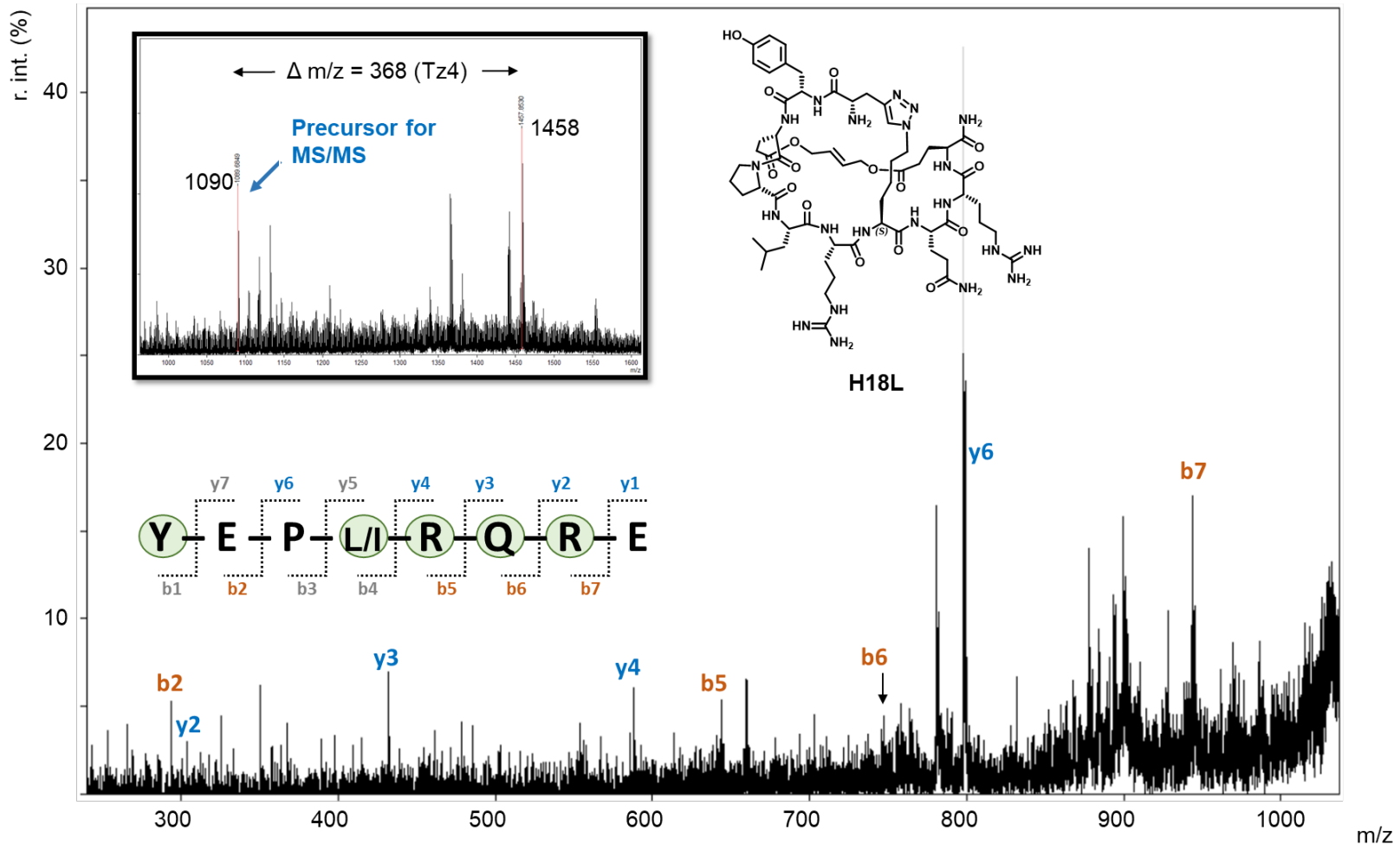

Figure 4.14 Mass spectrum for H18L. MS1 is shown on upper left panel and MS /MS data is shown on the bottom. Y ions are shown in blue and b ions are shown in orange. Not founded ion are shown in grey.

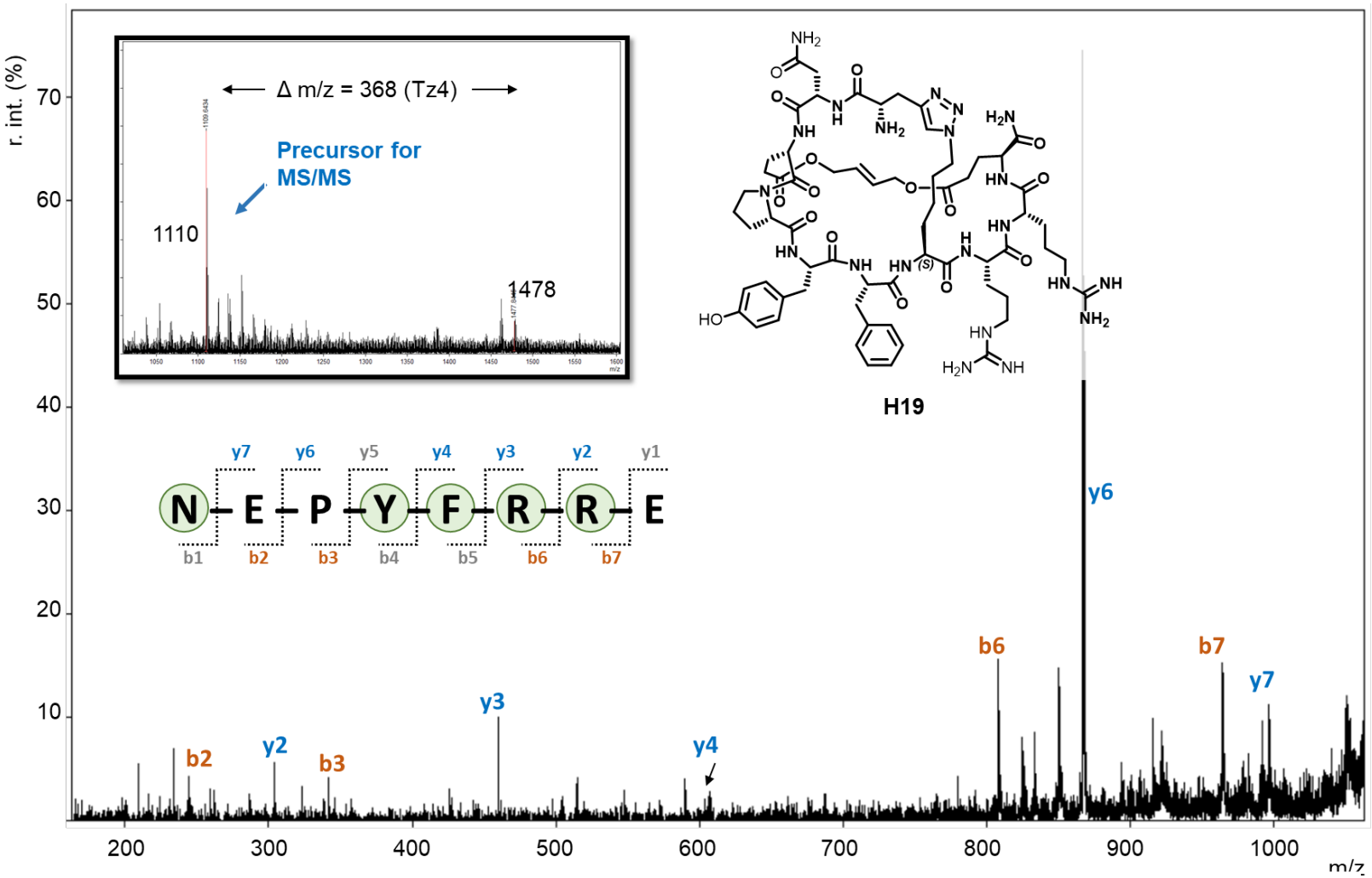

Figure 4.15 Mass spectrum for H19. MS1 is shown on upper left panel and MS /MS data is shown on the bottom. Y ions are shown in blue and b ions are shown in orange. Not founded ion are shown in grey.

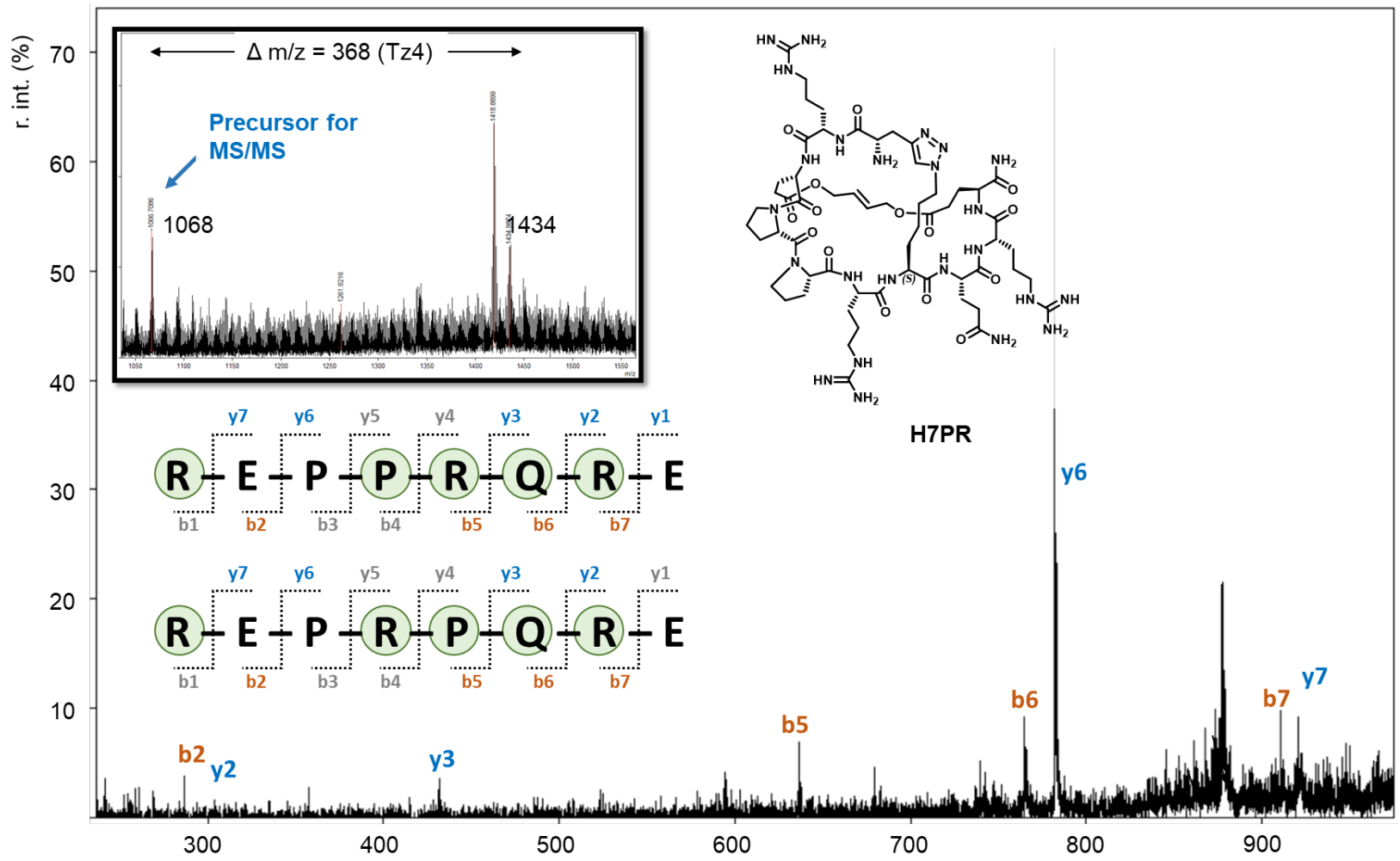

Figure 4.16 Mass spectrum for H7. MS1 is shown on upper left panel and MS /MS data is shown on the bottom. Y ions are shown in blue and b ions are shown in orange. Not founded ion are shown in grey.

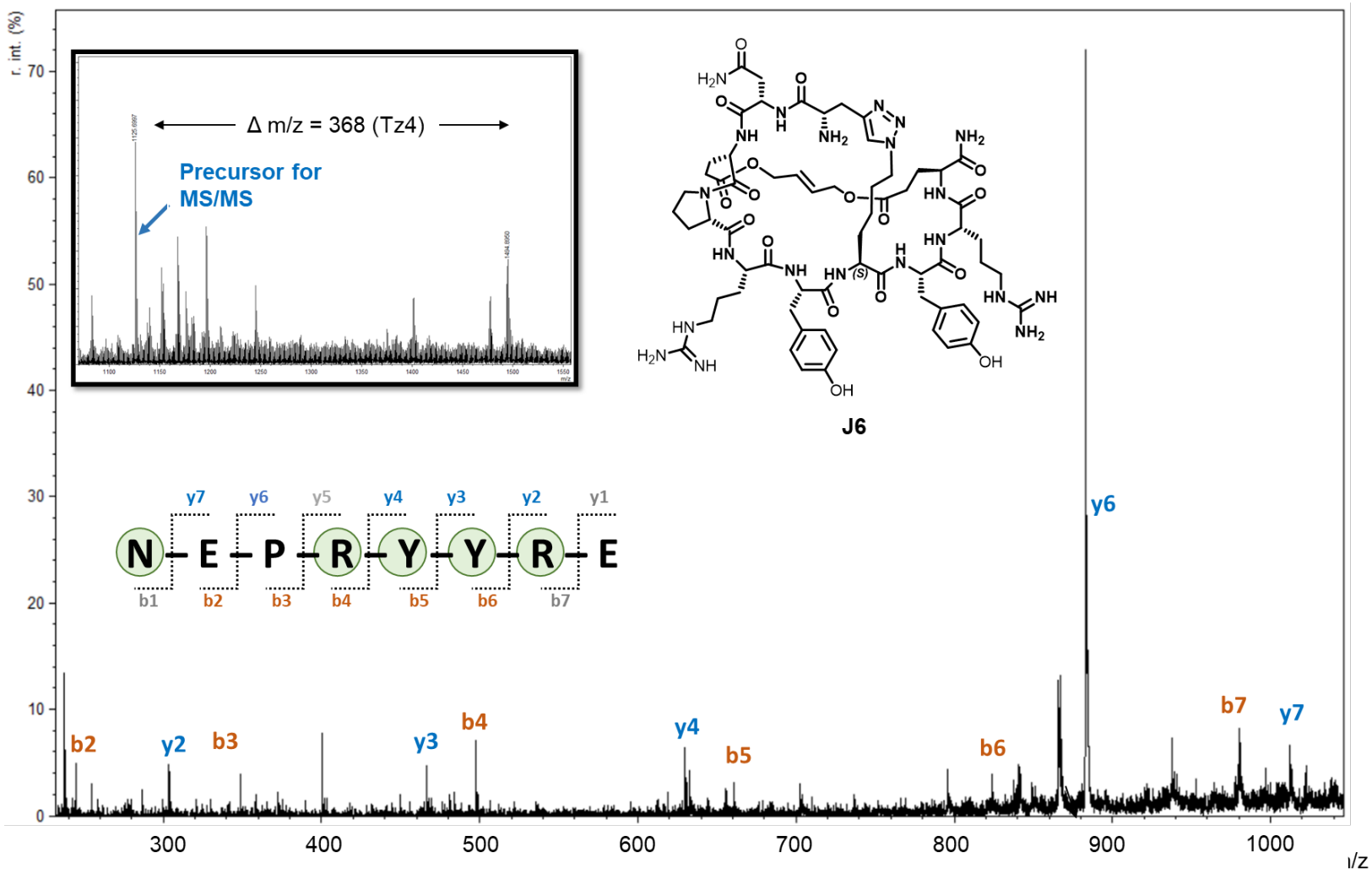

Figure 4.17 Mass spectrum for J6. MS1 is shown on upper left panel and MS /MS data is shown on the bottom. Y ions are shown in blue and b ions are shown in orange. Not founded ion are shown in grey.

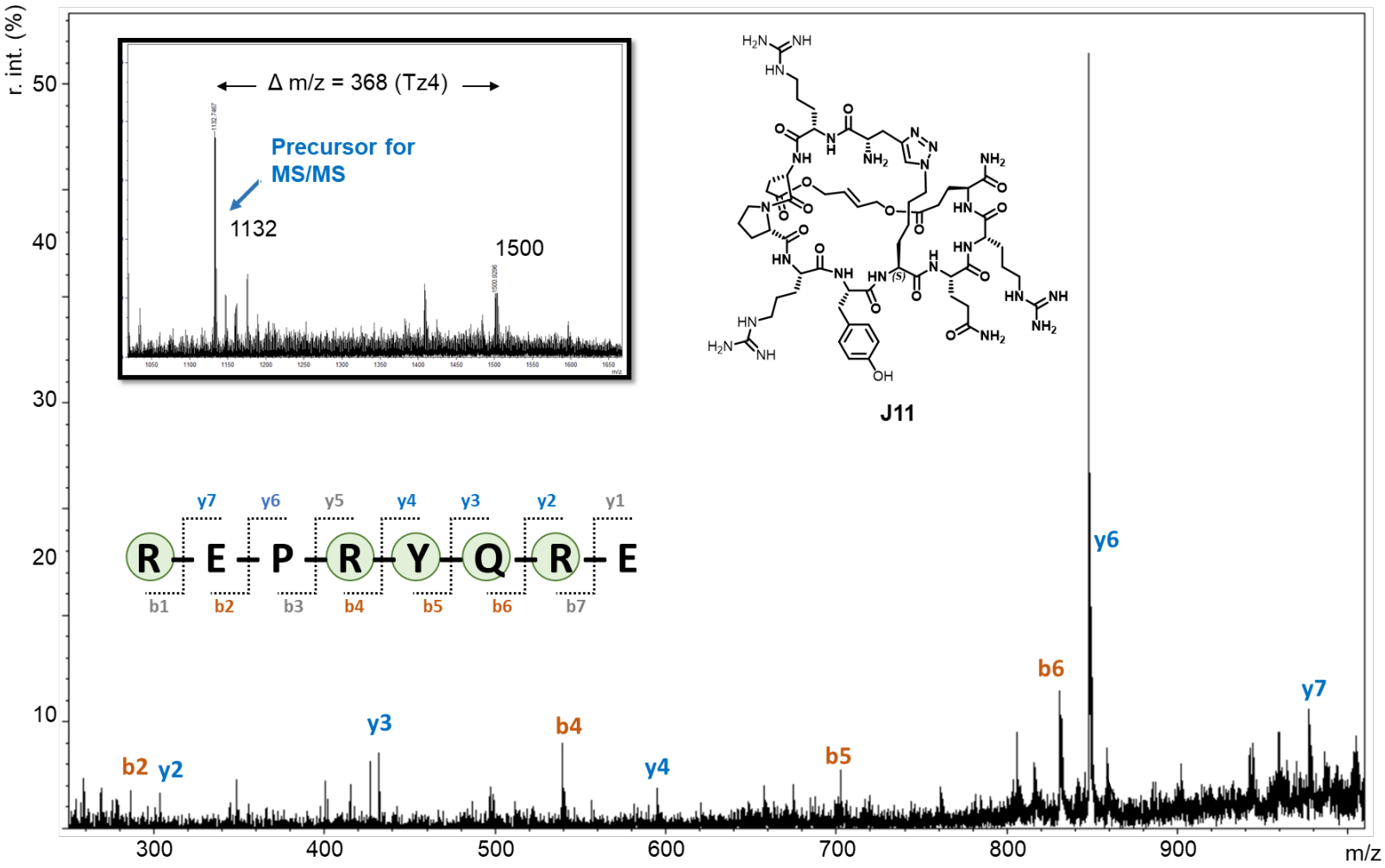

Figure 4.18 Mass spectrum for J11. MS1 is shown on upper left panel and MS /MS data is shown on the bottom. Y ions are shown in blue and b ions are shown in orange. Not founded ion are shown in grey.

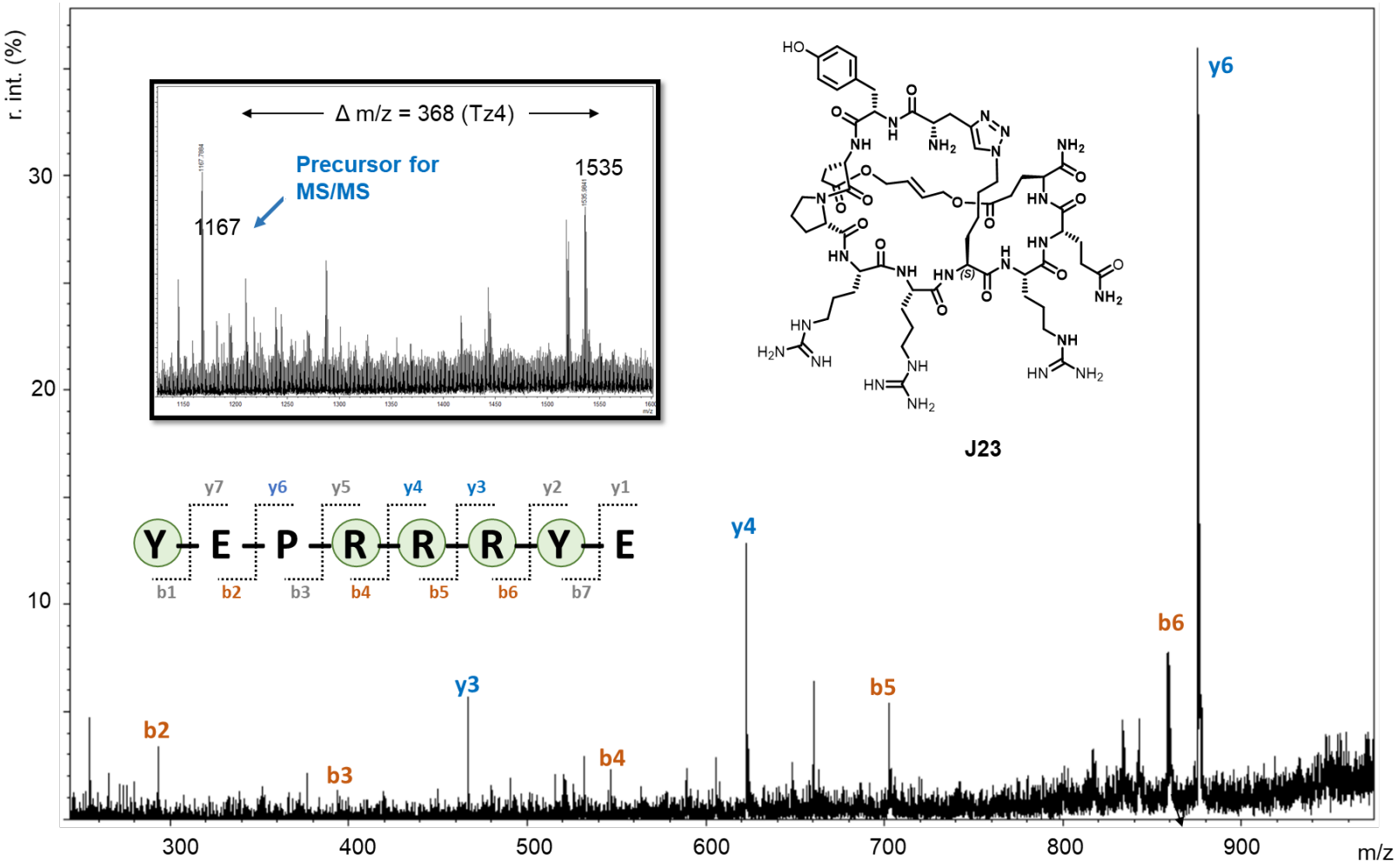

Figure 4.19 Mass spectrum for J23. MS1 is shown on upper left panel and MS /MS data is shown on the bottom. Y ions are shown in blue and b ions are shown in orange. Not founded ion are shown in grey.

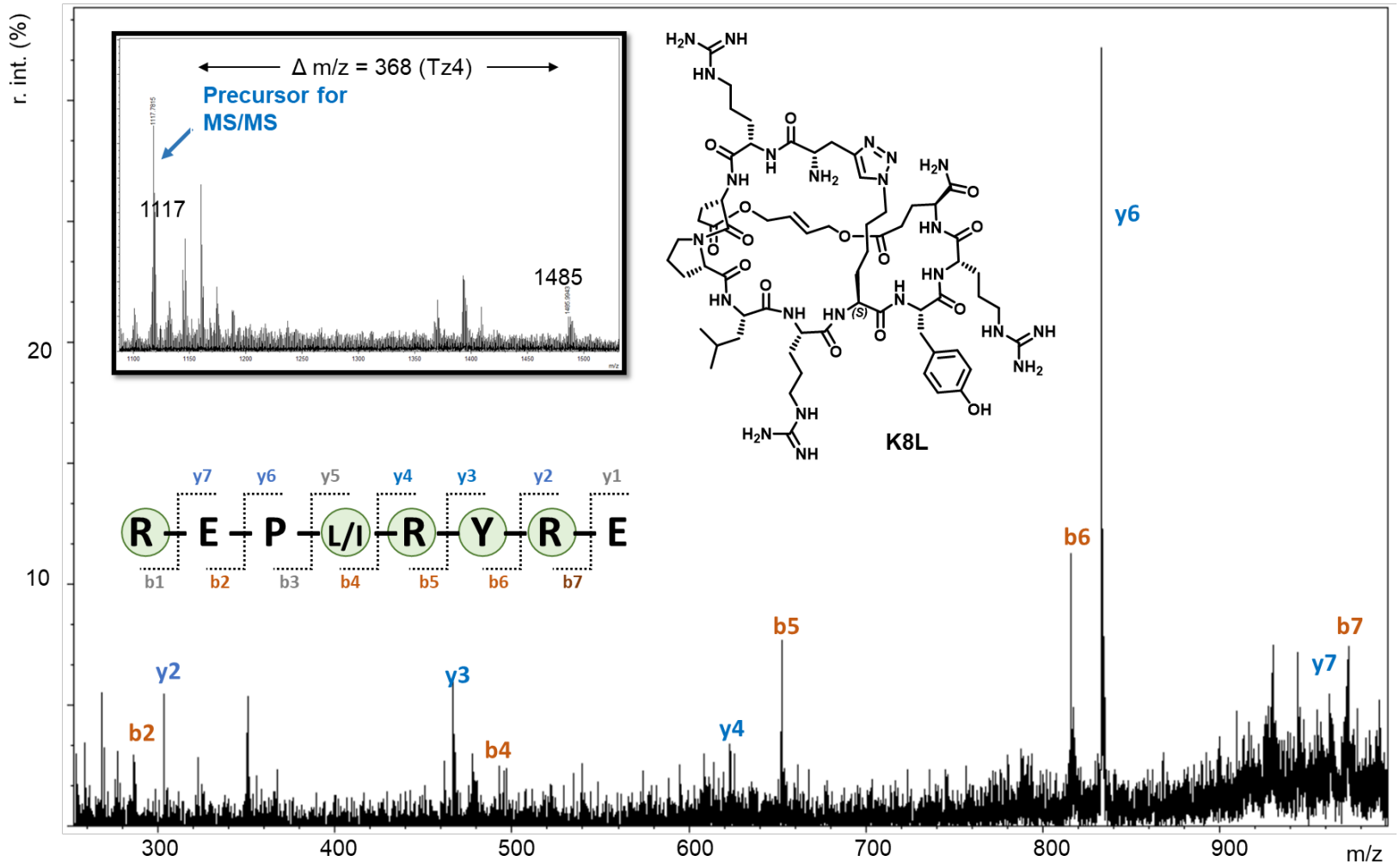

Figure 4.20 Mass spectrum for K18. MS1 is shown on upper left panel and MS /MS data is shown on the bottom. Y ions are shown in blue and b ions are shown in orange. Not founded ion are shown in grey.

References

1. Chen, X.; Zhou, Y.; Peng, X.; Yoon, J., Fluorescent and colorimetric probes for detection of thiols. *Chemical Society Reviews* **2010,** *39* (6), 2120-2135.

2. Jung, H. S.; Chen, X.; Kim, J. S.; Yoon, J., Recent progress in luminescent and colorimetric chemosensors for detection of thiols. *Chemical Society Reviews* **2013,** *42* (14), 6019-6031.

3. Yin, J.; Kwon, Y.; Kim, D.; Lee, D.; Kim, G.; Hu, Y.; Ryu, J.-H.; Yoon, J., Cyanine-Based Fluorescent Probe for Highly Selective Detection of Glutathione in Cell Cultures and Live Mouse Tissues. *Journal of the American Chemical Society* **2014,** *136* (14), 5351-5358.

4. Liu, Z.; Zhou, X.; Miao, Y.; Hu, Y.; Kwon, N.; Wu, X.; Yoon, J., A Reversible Fluorescent Probe for Real-Time Quantitative Monitoring of Cellular Glutathione. *Angewandte Chemie International Edition* **2017,** *56* (21), 5812-5816.

5. Wang, F.; Zhou, L.; Zhao, C.; Wang, R.; Fei, Q.; Luo, S.; Guo, Z.; Tian, H.; Zhu, W.-H., A dual-response BODIPY-based fluorescent probe for the discrimination of glutathione from cystein and homocystein. *Chemical Science* **2015,** *6* (4), 2584-2589.

6. Yin, J.; Kwon, Y.; Kim, D.; Lee, D.; Kim, G.; Hu, Y.; Ryu, J.-H.; Yoon, J., Preparation of a cyanine-based fluorescent probe for highly selective detection of glutathione and its use in living cells and tissues of mice. *Nature protocols* **2015,** *10* (11), 1742.

7. Buescher, J. M.; Antoniewicz, M. R.; Boros, L. G.; Burgess, S. C.; Brunengraber, H.; Clish, C. B.; DeBerardinis, R. J.; Feron, O.; Frezza, C.; Ghesquiere, B., A roadmap for interpreting 13 C metabolite labeling patterns from cells. *Current opinion in biotechnology* **2015,** *34*, 189-201.

8. Sazani, P. L.; Larralde, R.; Szostak, J. W., A Small Aptamer with Strong and Specific Recognition of the Triphosphate of ATP. *Journal of the American Chemical Society* **2004,** *126* (27), 8370-8371.

9. Wang, J.; Jiang, Y.; Zhou, C.; Fang, X., Aptamer-Based ATP Assay Using a Luminescent Light Switching Complex. *Analytical Chemistry* **2005,** *77* (11), 3542-3546.

10. Ying, Y.-L.; Wang, H.-Y.; Sutherland, T. C.; Long, Y.-T., Monitoring of an ATP-Binding Aptamer and its Conformational Changes Using an α-Hemolysin Nanopore. *Small* **2011,** *7* (1), 87-94.

11. Lam, K. S.; Lehman, A. L.; Song, A.; Doan, N.; Enstrom, A. M.; Maxwell, J.; Liu, R., Synthesis and screening of “one-bead one-compound” combinatorial peptide libraries. *Methods in enzymology* **2003,** *369*, 298-322.

12. Das, S.; Nag, A.; Liang, J.; Bunck, D. N.; Umeda, A.; Farrow, B.; Coppock, M. B.; Sarkes, D. A.; Finch, A. S.; Agnew, H. D., A general synthetic approach for designing epitope targeted macrocyclic peptide ligands. *Angewandte Chemie International Edition* **2015,** *54* (45), 13219-13224.

13. Sarkar, P.; Li, Z.; Ren, W.; Wang, S.; Shao, S.; Sun, J.; Ren, X.; Perkins, N. G.; Guo, Z.; Chang, C.-E. A.; Song, J.; Xue, M., Inhibiting Matrix Metalloproteinase-2 Activation by Perturbing Protein–Protein Interactions Using a Cyclic Peptide. *Journal of Medicinal Chemistry* **2020,** *63* (13), 6979-6990.

14. Lian, W.; Upadhyaya, P.; Rhodes, C. A.; Liu, Y.; Pei, D., Screening Bicyclic Peptide Libraries for Protein–Protein Interaction Inhibitors: Discovery of a Tumor Necrosis Factor-α Antagonist. *Journal of the American Chemical Society* **2013,** *135* (32), 11990-11995.

15. Shao, S.; Li, Z.; Cheng, H.; Wang, S.; Perkins, N. G.; Sarkar, P.; Wei, W.; Xue, M., A Chemical Approach for Profiling Intracellular AKT Signaling Dynamics from Single Cells. *Journal of the American Chemical Society* **2018,** *140* (42), 13586-13589.

16. Li, Z.; Shao, S.; Ren, X.; Sun, J.; Guo, Z.; Wang, S.; Song, M. M.; Chang, C.-E. A.; Xue, M., Construction of a Sequenceable Protein Mimetic Peptide Library with a True 3D Diversifiable Chemical Space. *Journal of the American Chemical Society* **2018,** *140* (44), 14552-14556.

17. Klemm, P., Manual Edman Degradation of Proteins and Peptides. Humana Press: pp 243-254.

18. Boroughs, L. K.; DeBerardinis, R. J., Metabolic pathways promoting cancer cell survival and growth. *Nature cell biology* **2015,** *17* (4), 351.

19. Cairns, R. A.; Harris, I. S.; Mak, T. W., Regulation of cancer cell metabolism. *Nature Reviews Cancer* **2011,** *11* (2), 85-95.

20. DeBerardinis, R. J.; Chandel, N. S., Fundamentals of cancer metabolism. *Science advances* **2016,** *2* (5), e1600200.

21. Hanahan, D.; Weinberg, R. A., Hallmarks of cancer: the next generation. *Cell* **2011,** *144* (5), 646-674.

22. Martinez-Outschoorn, U. E.; Peiris-Pagès, M.; Pestell, R. G.; Sotgia, F.; Lisanti, M. P., Cancer metabolism: a therapeutic perspective. *Nat Rev Clin Oncol* **2016,** *14* (1), 11-31.

23. Sabharwal, S. S.; Schumacker, P. T., Mitochondrial ROS in cancer: initiators, amplifiers or an Achilles' heel? *Nature reviews. Cancer* **2014,** *14* (11), 709.